Role of Oncogene-Induced Senescence in Thyroid Carcinogenesis

Thesis

UNRESTRICTED

ROLE OF ONCOGENE-INDUCED SENESCENCE IN THYROID CARCINOGENESIS

Maria Grazia Vizioli
Degree in Medical Biotechnology

This thesis is presented to

The Open University for the Degree of Doctor of Philosophy

Discipline: Life and Biomolecular Sciences

Date of submission: 30th June 2012

Affiliated Research Centre:
Fondazione IRCCS Istituto Nazionale dei Tumori, Milan (Italy)

Date of Submission: 26 June 2012
Date of Award: 20 November 2012

Table of Contents

List of Figures and Tables

Abbreviations

AC	acethylated
ARF	alternative reading frame gene
ATC	anaplastic thyroid carcinoma
ATM	ataxia telangectasia mutated
ATR	ataxia telangectasia and Rad3 related
ATP	adenosine tri-phosphate
5'Aza-dc	5-Aza-2'Deoxycitidine
bp	base pair
BrdU	5-bromo-2-deoxyuridine
cAMP	cyclic adenosine monophosphate
CAV	caveolin
CDK	cyclin dependent kinase
CDKI	cyclin dependent kinase inhibitor
CDKN1	cyclin dependent kinase inhibitor, family 1
CDKN2	cyclin dependent kinase inhibitor, family 2
cDNA	complementary DNA
CHK	checkpoint kinases
CLDN10	claudin10
CR	conserved region
CRD	cysteine rich domain
CXCL	CXC chemokine ligand
DAPI	4,6-diamidino-2-phenylindole
DAPK	death-associated protein kinase
DDR	DNA damage response
DMEM	Dulbecco's modified Eagle's medium
dNTP	deoxyribonucleotide triphosphate
DNA	deoxyribonucleic acid
DNMT	DNA methyltransferase
DSB	double strand break
DTT	dihiothreitol
EMT	epithelial-mesenchymal transition
FBS	foetal bovine serum
FRS	fibroblast growth factor receptor substrate

FTC	follicular papillary carcinoma
GDNF	glial derived neutrophic factor
GDP	guanosine diphosphate
GDS	guanine dissociation stimulator
GFR	glycosyl-phosphadylinositol receptor
GFP	green fluorescent protein
GLB1	galactosidase, beta 1
GTP	guanosine-5'-triphosphate
H	histone
HAT	histone acetyltransferase
γH2AX	phosphorylated histone 2, variant X
H3K9me3	histone 3 lysine 9 trimethylation
H3K9Ac	histone 3 lysine 9 acethylation
HCA	high content analysis
HCC	hurthle cell carcinoma
HDAC	histone deacetylase
HMGA	high mobility group A
HP1	heterochromatin protein 1
HRAS	Harvey rat sarcoma gene
IF	immunofluorescence
IGF	insulin growth factor
IGFBP	insulin growth factor binding protein
IL	interleukin
INK4	inhibitor of CDK4
IRS	insulin receptor substrate
LAMB3	laminin beta 3
LGALS3	lectin galactoside-binding soluble, 3
K	lysine
kb	kilobase
kDa	kiloDalton
MAPK	mitogen-activated protein kinases
Me3	trimethylated
MEN2	multiple endocrine neoplasia type 2
mRNA	messanger RNA
miRNA	microRNas

MYC	myelocytomatosis gene
MTC	medullary thyroid cancer
NFG	nerve growth factor
NIS	sodium iodine symporter
NOS	not otherwise specified
NTRK1	neurotrophic tyrosine kinase receptor type 1
OIS	oncogene-induced senescence
PBS	phosphate buffered saline
PCNA	proliferating cell nuclear antigen
PCR	polymerase chain reaction
PDTC	poorly differentiated thyroid carcinoma
PEI	polyethylenimine
PFA	paraformaldehyde
PI	propidium iodine
PI3-K	phosphoinositide 3'-kinase
PKC	protein kinase C
PLC	phospholipase C
PML	promyelocitic leukemia nuclear
PTC	papillary thyroid carcinoma
PTMC	papillary thyroid microcarcinoma
qPCR	quantitative PCR
RB	retinoblastoma
RBD	RAS binding region
RET	rearranged during transfection
RNA	ribonucleic acid
ROS	reactive oxygen species
rpm	rotations per minute
SA-β-gal	senescence-associated β-galactosidase
SAHF	senescence-associated heterochromatic foci
SASP	senescence associated secretory phenotype
SH2	sequence homology 2
shRNA	small hairpin RNA
SOX2	SRY(sex determining region Y)-box 2
SOS	son of sevenless
TC	tall cell

TFG	TRK fused gene
TGF	tumour growth factor
TIMP	tissue inhibitor of metalloproteinases
TMP3	tropomyosin 3
TPR	translocated promoter region
THS	thyroid stimulating hormone
UTR	untranslated region
VEGF	vascular endothelial growth factor

Abstract

Oncogene-induced senescence (OIS) is an irreversible G1 cell cycle arrest triggered by aberrant expression of oncogenes. The arrest observed during senescence is implemented mainly through activation of p53 and the upregulation of the cyclin-dependent kinase (CDK) inhibitors, $p16^{INK4a}$ and $p21^{CIP1}$. *In vivo* OIS may act as a barrier to neoplastic transformation, and bypass of OIS is a prerequisite for tumorigenesis.

In this work the role of OIS in thyroid carcinogenesis was investigated by in combination of *in vitro* and *in vivo* approaches.

We found that the expression of different thyroid tumour-associated oncogenes (BRAF, RAS, RET and TRK) in human primary thyrocytes triggers senescence, as demonstrated by the presence of OIS hallmarks. For instance, cells appeared flatted and enlarged; they displayed senescence-associated β-galactosidase activity (SA-β-Gal), senescence associated heterochromatic foci (SAHF), and high expression levels of the CDK inhibitors $p16^{INK4a}$ and $p21^{CIP1}$ and p53. Additionally, using RNA-interference strategy we directly assessed the individual contribution of $p16^{INK4a}$ in $BRAF^{V600E}$-induced senescence. In our experimental setting the inactivation of $p16^{INK4a}$ did not have any impact on oncogene-induced senescence suggesting the possibility that $p16^{INK4a}$ may cooperate with other factors in triggering senescence.

A major consequence of oncogene activation is the secretion of a plethora of proteins including growth factors, cytokines, and chemokines. Some of these secreted proteins are known to be regulators of OIS. For example, IGFBP7 is recently proposed as a mediator of $BRAF^{V600E}$-induced senescence in melanocytes.

We showed that IGFBP7 gene is frequently downregulated in Papillary thyroid tumour (PTC); restoration of its expression in a PTC-derived, IGFBP7-negative cell line affects

growth properties, migration and invasion, and this is associated to the induction of apoptosis. Thus, our results implicate IGFBP7 as a tumour suppressor protein in thyroid tumours. Additionally, we investigated the possible involvement of IGFBP7 in our cellular senescence model. Our data indicate that IGFBP7 expression is not changed during OIS.

We also established and characterized OIS inducible system in our cellular model; we transduced human primary thyrocytes with a retroviral vector carrying an activated form of RAS oncogene coupled to the ligand binding domain of the estrogen receptor. Upon addition of 4-hydroxytamoxifen (4-OHT), we observed a robust induction of senescence, including significantly reduced incorporation of BrdU and high levels of $p16^{INK4a}$, $p21^{CIP1}$, and p53. Moreover, we assessed the relative importance of tumour suppressor proteins, $p16^{INK4a}$ and p53 in mediating OIS in H-RAS^{G12V} transfected thyrocytes. Surprisingly, silencing of p53 expression did not alter the growth arrest induced by H-RAS^{G12V}, whereas $p16^{INK4a}$ seems to be the dominant effector of senescence in this experimental setting, as its specific inactivation delays the onset of senescence.

We also found that senescence induced by H-RAS^{G12V} is associated with activation of inflammatory transcriptome including IL8 and its receptor CXCR2. We reported that knocking down the chemokine receptor CXCR2 either IL8 prevents H-RAS^{G12V} cells from undergoing OIS.

To translate information from *in vitro* experiments to a clinic setting, senescence markers identified in cultured cells were used to detect OIS in a panel of thyroid tumours characterized by different aggressiveness. Our immunohistochemical analysis showed that the expression of OIS markers is upregulated at early stages of the thyroid tumour and lost during tumour progression. These evidences support the notion that

OIS may counteract oncogenic activity in thyroid tumours, and its escape allows thyroid tumour progression.

CHAPTER 1

Chapter 1 – Introduction

1.1 Thyroid cancer

Thyroid cancer is the most common malignant tumour of endocrine system, accounting for approximately 1% of all newly diagnosed cancer cases. Its worldwide incidence has increased significantly over the last few decades, albeit it is limited to the papillary type of thyroid cancer and is mostly due to tumours of small size (less than 1 cm, termed microcarcinoma) (Davies and Welch, 2006; Albores-Saavedrea et al., 2007). It is not yet clear if such increase is a true biological issue or if it is a result of improvement in the diagnostic tools, for example increased access to high resolution imaging (particularly ultrasonography) and increased use of fine-needle aspiration biopsy. However, it has been proposed that other factors also contribute to the fast-growing number of new thyroid cancer cases, including the exposure to radiation during medical procedures (Mettler et al., 2007), the obesity (Kitahara et al., 2011) as well as the increase in pathological detection of incidental papillary thyroid cancer (Grodski et al., 2008). Mortality rates, in contrast to incidence rates, are stable or decreasing (Davies et al., 2002; La Vecchia et al., 2010). The 10-year relative survival rate is very good, ranging from 90% in differentiated thyroid cancer (Hundahl et al.,1998) to 74% in medullary thyroid cancer while it is dramatically short, less than 1 year, in case of anaplastic thyroid cancer which represents one of the most aggressive malignant tumours.

Patients with differentiated thyroid cancer are cured by surgery, adjuvant radioactive iodine therapy and THS suppression (Samaan et al., 1992). However, some of these patients cannot be cured because tumours are unresctable, or fail to absorb radioiodine, or, in rare cases, they progress from differentiated to poorly differentiated carcinoma.

Anaplastic thyroid carcinomas are very difficult to treat; surgery is not often technically feasible due to the local invasion of the contiguous anatomic structures (Hag et al., 2005).

Thyroid cancer is a unique and fascinating model that includes several histotypes characterized by peculiar biological and clinical features.

Significant knowledge in molecular mechanisms of thyroid carcinogenesis has been achieved in the past few years. This improved knowledge has provided new insights into thyroid cancer aetiology and has offered novel diagnostic tools and prognostic markers that could improve the management of patients with thyroid cancer.

1.1.1 Histological classification

The vast majority of thyroid tumours arise from thyroid follicular epithelial cells, whereas 3-5% of cancers derive from parafollicular or C cells. The follicular cell-derived cancers comprise papillary carcinoma (about 80% of the cases), follicular carcinoma (10%), poorly differentiated carcinoma (4-6%), and anaplastic carcinoma (2-5%). Tumours, originating from C cells, are known as medullary carcinomas (5-10%). Papillary and follicular histotypes are also referred as differentiated thyroid carcinomas. Poorly differentiated carcinoma and anaplastic carcinoma, much less frequent, can develop *de novo* or derive through the process of stepwise dedifferentiation of papillary and follicular carcinoma (Nikiforov and Nikiforova, 2011) (Figure 1.1).

Papillary thyroid carcinoma (PTC)

PTC is the most frequent thyroid tumour type and the most common paediatric thyroid malignancy (Davies and Welch, 2006). It is associated with external radiations; an increased incidence has been observed after nuclear Chernobyl accident, overall in children, who are much more sensitive to the tumorigenic effect of external irradiation, because of the high degree of replication of thyroid cells (Nikiforov, 2006).

PTCs characteristically spread to regional lymph nodes, in fact cervical lymph node metastases are very frequent at the time of diagnosis.

Classic PTC is microscopically characterized by a papillary architecture and a population of follicular cells with "ground glass" nuclei and irregularities of nuclear contours, including grooves and nuclear pseudoinclusions. Psammona bodies, which represent a typical PTC feature, are found in at least 50% of cases: they are rounded and concentrically laminated calcifications, which can be present within the tumour stroma, in the tip of the papillae or in lymphatic spaces.

The prognosis of classic PTC is excellent and influenced by patient age, tumour size and presence of distance metastasis.

In addition to classic PTC, also known as not otherwise specified (NOS), several histological variants, differing in morphological pattern as well as in prognosis have been described. The most common are papillary thyroid microcarcinoma, follicular, oncocytic, clear cells, diffuse sclerosing, tall cell, columnar cell, solid and cribriform (Sherman, 2003). For most of them the prognosis is similar to classic PTC, whereas for some histotypes such as tall cell, columnar cell and solid variant, the outcome is worse. These rare variants are characterized by an aggressive behaviour, with the primary tumour often presenting with extrathyroid extension and vascular invasion. Papillary thyroid microcarcinoma (PTMC) represents a particular variant of papillary thyroid carcinoma and it is very common in the general population, accounting for up to 30% of all papillary carcinoma. It is defined as a tumour measuring <1cm in diameter and it is considered the early stage of PTC, exhibiting architectural, cytological and behavioural features of papillary lesions, often found incidentally. It has an indolent course and very favourable prognosis despite the presence of multifocality within the thyroid and synchronous nodal local-regional spread (Sakorafas et al., 2005).

Follicular thyroid carcinoma (FTC)

FTC is characterized by evidence of follicular cell differentiation but lacking the diagnostic features of PTC. It is usually encapsulated and solitary (Sobrinho Simoes et al., 2004). FTC is more common in regions of iodine insufficiency and metastasizes almost exclusively via the blood stream (Delellis et al., 2004). Compared to PTC, cervical lymph nodes involvement is less common at diagnosis while distant metastases can be found in 20% of the cases, lung and bone being the most involved sites. Invasiveness of the capsule and vascular invasion are the microscopic characteristics of FTC.

Hurthle cell carcinoma (HCC) is a rare variant of FTC. It differs from conventional FTC in biological and clinical behaviour, leading some groups to classify HCC as a distinct pathologic entity. It is defined as a tumour composed of 75% or greater Hurthle cells with complete capsular-or vascular-invasion (Rosai et al., 1992). The tumour cells are typically characterized by an abundant granular, eosinophilic cytoplasm derived from the presence of a large number of mitochondria. Moreover, HCC presents cervical lymph node in 30% of the cases, and distant metastases can also occur.

FTC is generally considered a more aggressive disease with a poorer prognosis when compared with PTC; 50% of patients with a widely invasive FTC die, whereas patients with a minimally invasive FTC have a survival expectance similar to that of a normal population matched for age and sex (Sobrinho-Simoes et al., 2011).

Poorly differentiated thyroid carcinoma (PDTC)

PDTC is a rare tumour with higher incidence in areas having iodine deficiency. It behaves intermediately between differentiated (PTC and FTC) and anaplastic carcinoma. It can be the terminal stage of the dedifferentiation process of PTC or FTC or can grow *ex novo* (Pilotti et al., 1997). PDTC can appear as a unique rapidly growing thyroid with or without cervical node involvement. Distant metastases can be also

present. Three different histological patterns have been described: insular, trabecular and solid (Sobrinho-Simoes, 1996). They are similar for features including increased mitotic activity, necrosis, and capsular and vascular invasion. The mean 5-year survival of FTC patients is less than 50% (Sobrinho-Simoes et al., 2005).

Anaplastic thyroid carcinoma (ATC)

ATC is the most aggressive and lethal form of thyroid cancer. It carries a dismal prognosis, with a median survival of 4 to 12 months from the time of diagnosis. ATC can arise *de novo* or from preexisting differentiated thyroid cancer. At the clinical level, it is characterized by a large thyroid mass, rapidly growing and infiltrating surrounding tissues and muscles. The larynx (13%), oesophagus (44%) and trachea (46%) may also be involved in up to 70% of the patients. Systemic metastases disease can also occur at presentation or during the course of the illness with lung being the most common site (80%), followed by bone (6-15%) and brain (5-13%) (Mclever et al., 2001). The clinical course of the disease can be so rapid that surgical procedures performed are often useless.

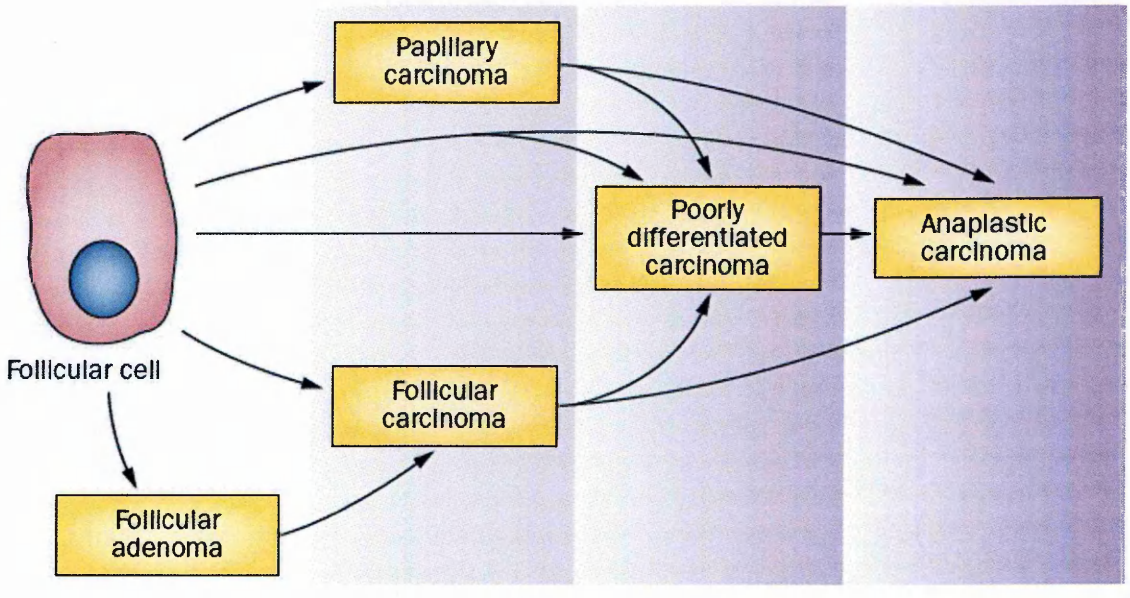

Figure 1.1 Multistep oncogenesis in thyroid cancer. The follicular cells give rise to a broad spectrum of tumours which display very distinctive phenotypic, biological and clinical features. (Adapted from Nikiforov and Nikiforova, 2011)

Medullary thyroid cancer (MTC)

MTC arises from parafollicular or C cells that produce calcitonin, and predominately develops as a sporadic tumour in about 60% of the cases, whereas it is hereditary in 40% of the cases. MTC is the principal disease feature of multiple endocrine neoplasia type 2 (MEN2), an autosomal dominantly inherited cancer syndrome caused by activating germ-line mutations in the RET proto-oncogene (Ball et al., 2000).

MTC is typically located at the junction of the upper third and the lower two-thirds of the thyroid lobes. On histological examination, MTC consists in sheets of spindle-shaped, round or polygonal cells separated by fibrous stroma. The nuclei are usually uniform in shape with rare mitotic figures. The cytoplasm is eosinophilic with a finely granular appearance (Hedinger et al., 1988; Rosai et al., 1992).

Metastatic dissemination to both central and latero-cervical lymph nodes occurs at similar high frequencies. Distant metastases are the main cause of MTC-related death. They are usually diffuse and multiple in involved organs and simultaneously affect multiple organs, such as the liver, lungs and bones (Moley and DeBenedetti, 1999; Guignat et al., 2001).

The survival of MTC patients strongly correlates with stage at diagnosis. The 10-year survival rate is approximately 65%. Some clinical features are related to a lower survival. These include older age, male gender, extent of local tumour and presence of distant metastases (Bhattacharyya, 2003).

1.1.2 Genetic alterations in thyroid cancer

Thyroid cancer initiation and progression occur through gradual accumulation of various genetic and epigenetic alterations, including activating and inactivating somatic mutations, alteration in gene expression patterns.

Moreover, thyroid cancer represents a type of neoplasia in which critical genes are frequently mutated via two distinct molecular mechanisms: point mutation or chromosomal rearrangement. The former is a result of single nucleotide change within the DNA chain, whereas the latter represents a genetic abnormality with breakage and fusion of parts of the same or different chromosomes.

Most mutations in thyroid cancer involve the effectors of the MAPK and PI3K-AKT pathways (Figure 1.2). The mutated genes that affect these signalling networks encode cell membrane receptor tyrosine kinases RET and NTRK1 and intracellular signal transducers BRAF and RAS. These typically mutually exclusive mutations occur in approximately 70% of patients with PTC (Kimura et al., 2003). In FTC, in addition to mutation of RAS, another common event is PAX8/PPARγ rearrangement (Dwight et al., 2003) (Figure 1.7). Thyroid cancer progression and dedifferentiation involve a number of additional mutations that affect the PI3K-AKT pathway and other cell signalling pathways.

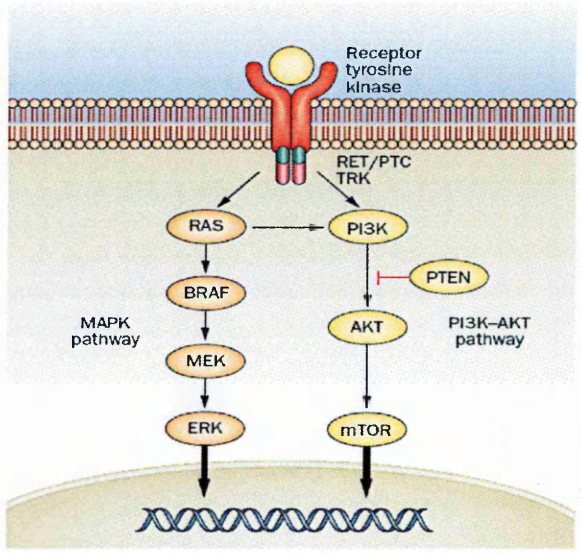

Figure 1.2 The main signalling pathways involving in thyroid cancer. MAPK and PI3K-AKT pathways are involved in propagation of signals from various cell membrane receptor tyrosine kinase into the nucleus, and they regulate multiple cell process including proliferation, differentiation and survival. (Adapted from Nikiforov and Nikiforova, 2011)

1.1.2.1 RET

The RET prooncongene is located in the pericentromeric region of chromosome 10q11.2 and comprises 21 exons (Pasini et al., 1995). RET encodes a receptor tyrosine kinase, which is expressed in neuroendocrine cells (including thyroid C cells and adrenal medullary cells), neural cells, urogenital tract cells and testis germ cells. RET protein is structured with an extracellular portion (which contains four cadherin-like repeats, a calcium binding site, and a cysteine-rich region), a transmembrane portion, and an intracellular portion, which two tyrosine kinase subdomains that are involved in the activation of several intracellular signal transduction pathways (Ishizaka et al., 1989) (Figure 1.3).

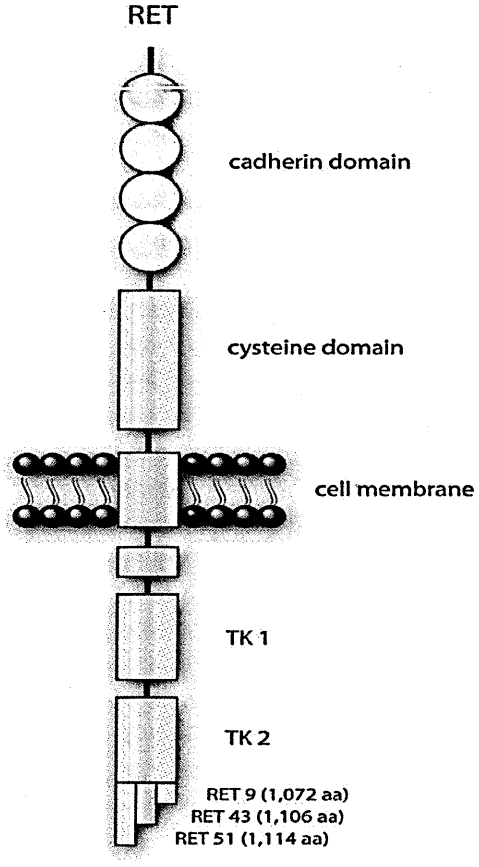

Figure 1.3 Schematic representation of the RET tyrosine kinase. The extracellular region comprises four cadherin domains and a cysteine-rich domain. A single transmembrane region spans the cell membrane, and the two tyrosine kinase domains (TK1 and TK2) are located in the intracellular region. The three isoforms of RET are indicated. (Adapted from de Groot JW, 2006)

A tripartite cell-surface complex is necessary for RET signalling. One of four glial derived neurotrophic factor (GDNF) family ligands, GDNF, neurturin, artemin, or persephin, binds RET in conjunction with one of four glycosylphosphadylinositol-linked co-receptors designated as GFRα 1, 2, 3, and 4. It has been demonstrated that GDFN interacts with GFRα1, whereas neurturin, artemin, and persephin preferentially bind GFRα2, GFRα3, or GFRα4, respectively (Airaksinen et al., 1999). Ligand stimulation leads to activation of the RET receptor with dimerization and subsequent autophosphorylation of intracellular thyrosine residues, which serve as docking sites for adaptor proteins that link the signal from the receptor to the main signal transduction pathways (Santoro et al., 2004). At least 18 of these specific phosphorylation sites have been identified. For example, phosphorylated Y981 constitutes the major binding site of v-src sarcoma viral oncogene homolog (Src), which is essential for neuronal survival. Src is also necessary for RET signalling through focal adhesion kinase (FAK), an important mediator of tumour cell migration and metastases. Tyrosine 1015 is a binding site for phospholipase C (PLC)-γ, which activates protein kinase C (PKC) enzymes (Andreozzi et al., 2003). PCK enzymes, in turn, cause RET phosphorylation but also down-regulate RET and its downstream signalling, thus functioning as a negative feedback loop to modulate RET activity. Phosphorylation of Y1062 is crucial for activation of major intracellular signalling pathways such as RAS/ERK, PI3K/AKT, p38MAPK, and Rac/JNK pathways. Y1062 is a docking site for various adaptor proteins, including Src-homology collagen (Shc), ShcC, insulin receptor substrate (IRS) 1/2, fibroblast growth factor receptor substrate 2 (FRS2), downstream of kinase (DOK) 1/4/5 and Enigma (Iwashita et al., 1996).

In 1990, a chimeric gene generated by the fusion of the RET tyrosine kinase domain and the 5' terminal region of a new gene was reported as the first oncogene in PTC and

was therefore denominated RET/PTC (Grieco et al., 1990) (Figure 1.5). These chromosomal aberrations occur in 2 to 40% of cases and are the result of double-stranded DNA breaks with erroneous rearrangements involving the C-terminal portion of RET and the promoter and coding region of the N terminus of a constitutively expressed unrelated gene from chromosome 10 or a different chromosome (Santoro et al., 2006). Interestingly, all breakpoints of the RET gene occur within intron 11. All partner genes have in common constitutive expression in thyroid follicular cells and dimerization and is no longer an integral membrane protein due to the lack of a transmembrane domain like RET. The intact tyrosine kinase domain of RET allows the RET/PTC protein to bind SHC via Y1062 and thus activates the MAPK pathway. To date, 12 different fusion partner genes are reported to form at least 17 different RET hybrid oncogenes (Tallini and Asa, 2001; Saenko et al., 2003). The most prevalent variants of these chimeric oncogenes are RET/PTC1 (60 to 70%) and RET/PTC3 (20 to 30%) in which RET is fused to either CCDC6 (also known as H4) or NCOA4 (also known as ELE1), respectively (Nikiforov, 2002). Both of these rearrangement types are paracentric, intrachromosomal inversions, as all fusion partners reside on the long arm of chromosome 10.

Several studies reported an increase in the prevalence of RET/PTC rearrangements in PTC from patients with a radiation history (Fagin et al., 2004; Nikiforova et al., 2000). After Chernobyl accident the majority of PTCs carry RET/PTC3 and are associated with the solid/follicular variant of PTC, while the less frequent RET/PTC1 is associated with the classical and diffuse sclerosing variant (Williams, 2002).

Besides the association with ionizing radiation, there are several lines of evidence that indicate RET/PTC as a causative factor in the pathogenesis of PTC. RET/PTC transforms thyroid follicular cells *in vitro* (Santoro et al., 1993), and overexpression of RET/PTC1 and RET/PTC3 in the thyroid of transgenic mice leads to the development

of tumours that resemble PTC (Powell et al., 1998; Santoro et al., 1996). Interestingly, not all transgenic mice developed thyroid tumours, suggesting that the expression of the oncoprotein is necessary but not sufficient for tumorigenesis. Furthermore, in microscopic PTC, RET/PTC expression is highly prevalent, indicating that RET/PTC is activated at early stages of the tumour (Sugg et al., 1998).

Although several studies failed to demonstrate correlation of RET/PTC rearrangements with clinicopathological features of increased mortality (Puxeddu et al., 2003; Santoro et al., 2002; Tallini et al., 1998), different types of RET/PTC rearrangement with variation in biological behaviour were described. Patients with RET/PTC1 usually show an indolent behaviour, whereas RET/PTC3 is associated with a more aggressive tumour phenotype (Basolo et al., 2002; Bongarzone et al., 1998). These observations are in keeping with transgenic mouse models expressing RET/PTC. Mice harbouring RET/PTC1 develop thyroid lesions with morphological features of PTC that do not metastasize, whereas mice carrying RET/PTC3 are associated with tumour growth and metastases (Powell et al., 1998; Santoro et al., 1993).

RET gene is also crucial in MTC being mutated in more than 95% of MEN2 families and in 30-50% of sporadic MTCs (Nikiforova and Nikiforov, 2008). A spectrum of RET mutations has been identified in MEN2 families. In 98% of MEN2A, the mutations affect one of the five cysteines in the extracellular cysteine-rich domain of RET: codons 609, 611, 618, 629 (exon 10), and 634 (exon 11) (Eng et al., 1996). These mutations result in receptor dimerization and constitutive activation. The "gain function" mutations associated with familial MTC (FMTC) involve a broad range of codons including some associated with MEN2A, particularly, 609, 618, and 620, as well as others: 768, 790, and 791 (exon 13), 804 and 844 (exon 14), or 891 (exon 15) (Niccoli-Sire et al., 2001; Kouvaraki et al., 2005). Most MEN2B patients (95% of cases) carry the M918T mutation in RET kinase domain, causing receptor auto-

phosphorylation and activation, resulting in a shift in substrate specificity (Hansford and Mulligan, 2000).

Besides mutations, other RET genetic alterations must occur at the somatic level and act in concert with RET mutations for the tumour to develop: duplication of the mutant allele or deletion of wild type allele have been reported (Huang et al., 2000).

1.1.2.2 NTRK1

NTRK1 (also named TrkA) is a tyrosine kinase receptor for the nerve growth factor (NGF) and is a member of the neurotrophin receptor family which also includes NTRK2 and NTRK3, binding to BDNF and NT3, respectively (Kaplan and Miller, 2000).

NTRK1 regulates growth, differentiation, and programmed cell death of neurons in both the peripheral and central nervous system. The NTRK1 gene is located on chromosome 1q21-22 and consists of 17 exons distributed within a 25-kb region (Greco et al., 1998). The NTRK1 receptor is a glycosylated protein of 140 KDa, comprising an extracellular portion containing Ig-like and leucine rich domains for ligand binding, a single transmembrane region made of 25 hydrophobic, a juxta-membrane domain, a catalytic domain responsible for the kinase activity and a C-terminal tail of about 15 amino acids (Figure 1.4). Following NGF binding, NTRK1 undergoes dimerization and autophorylation of five tyrosine residues (Y490, Y670, Y675, and Y785) (Figure 1.5). Activated receptor initiates several signal transduction cascades, including MAPK, PI3K, and the PLC-γ pathways. These signalling networks culminate in the activation of transcription factors that alter gene expression (Kaplan and Miller, 2000).

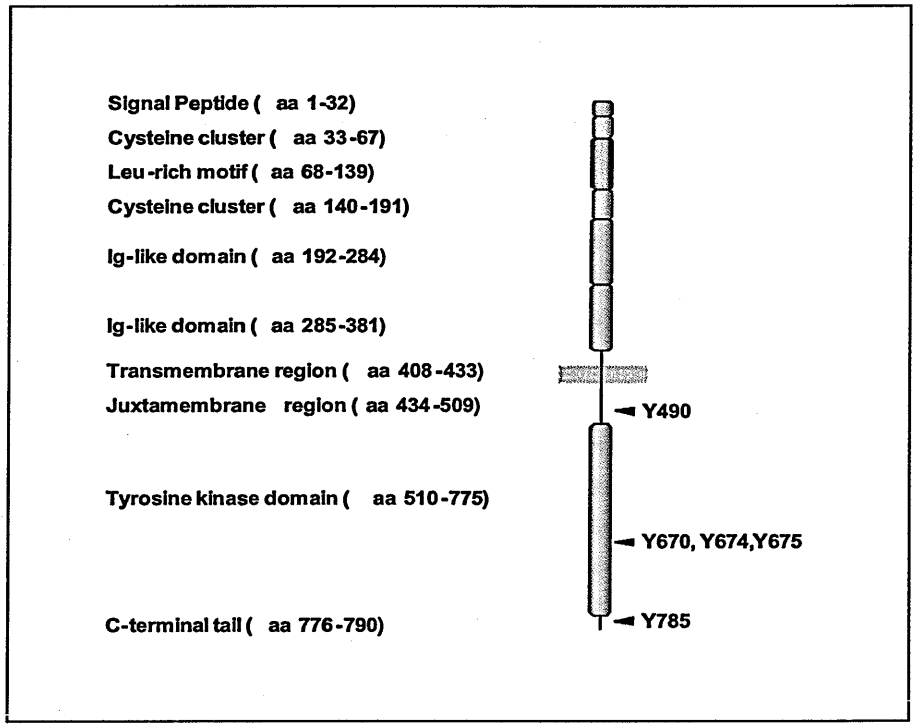

Figure 1.4 Schematic representation of NTRK1 receptor. The domains and the main tyrosine residues of the NTRK1 receptor are indicated.

Deregulation of NTRK1 activity is associated with several human diseases. Mutations affecting NTRK1 have been found in CIPA, Congenital Insensitivity to Pain with Anhidrosis, a rare recessive genetic characterized by loss of pain and temperature sensation, defects in thermal regulation and occasionally mental retardation (Indo et al., 1996; Pierotti and Greco, 2006).

A mutation in the NTRK1 gene was identified in a patient with acute myeloid leukaemia. This deletion removes 75 amino acids in the extracellular domain of NTRK1 receptor resulting *in vitro* transforming activity (Reuther et al., 2000).

NTRK1 was also shown to play a role in regulating neurogenic neoplasms such as neuroblastoma (NBL). High levels of NTRK1 are expressed in NBL with good prognosis which often spontaneous regression (Nakagawara et al., 1992). On the other

hand, down regulation of NTRK1 was found in NBL with aggressive behaviour (Borrello et al., 1993; Nakagawara et al., 1992).

Deregulation of NGF/NTRK1 pathway, may also lead to prostate and breast cancer (Weeraratna et al., 2001; Descamps et al., 1998).

Several TRK oncogenes, arising from rearrangements of NTRK1 gene, have been isolated in PTC. The NTRK1 gene joins to TMP3 (Martin-Zanca et al., 1986), TPR (Greco et al., 1992) or TFG (Greco et al., 1995) generating chimeric oncogenes TRK, TRK-T1, TRK-T2 and TRK-T3, respectively. TRK-T1 and TRK-T2 are two fusion variants of TPR-NTRK1 (Greco et al., 1997).

In TRK the NTRK1 TK domain is fused to the sequences of one isoform of the non-muscle tropomyosin gene, TMP3, localized on chromosome 1q22-q23 (Wilton et al., 1995).

TRK-T1 oncogene contains sequences belonging to the translocated promoter region (TPR) gene, encoding a filamentous protein of the nuclear protein pore complex implicated in nuclear protein transport (Byrd et al., 1994). TPR locus is located on chromosome 1q25 and the mechanism leading to the formation of TRK-T1 oncogene is an intrachromosomal inversion inv(1)(q21-22q25) (Miranda et al., 1994). TRK-T1 encodes a 55 kDa protein, consisting of 192 amino acids of TPR preceding the NTRK1 portion (Greco et al., 1997).

In addition, TPR is involved in generating TRK-T2 oncogene, which contains a TPR portion longer by 737 amino acids than in TRK-T1 (Greco et al., 1997).

The TRK-T3 oncogene is activated by TFG (TRK Fused Gene), a novel gene localized on chromosome 3 (3q11-12) (Greco et al., 1995). Differently from the other TRK oncogenes, TRK-T3 is produced by a translocation involving chromosomes 1 and 3

t(1;3)(q21-22;q11-12). The TRK-T3 protein has a molecular weight of 68 kDa and is made of 592 amino acids.

Somatic rearrangements of NTRK1 gene in PTC occur with a significantly lower prevalence than RET/PTC rearrangements; they are present in about 11% of PTC and are rare (3.3%) in post-Chernobyl thyroid tumours (Bongarzone et al., 1998). Experimental evidence indicates that TRK oncogenes play a direct role and represent an early event in the thyroid carcinogenesis. Transgenic mice carrying TRK-T1 oncogene under the control of thyroglobulin promoter (Tg-TRK-T1 mice) develop thyroid hyperplasia and PTC (Russell et al., 2000).

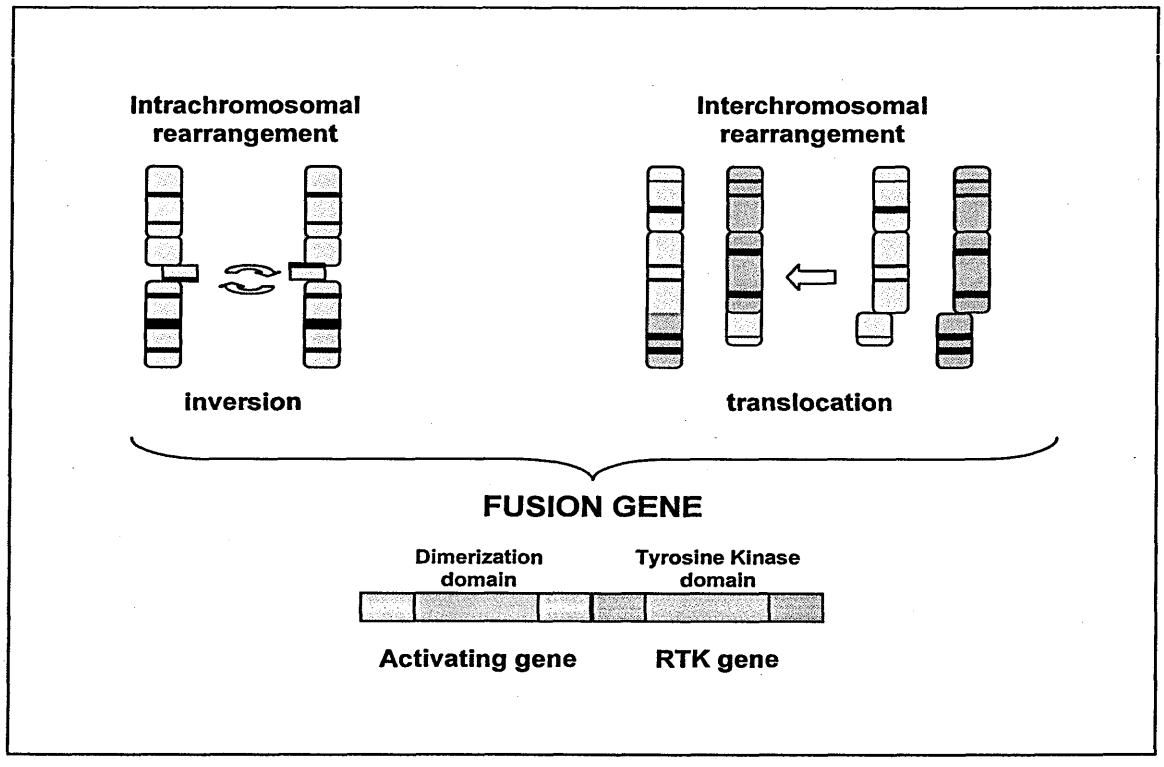

Figure 1.5 Mechanism of chromosomal rearrangements generating fusion transforming gene in PTC. Inversion between genes localized on the same chromosome or translocation between genes on two different chromosomes generate chimeric fusion gene made of the thyrosine kinase domain of RTK gene preceded by the N-terminal portion of the activating gene, containing the dimerization domain.

1.1.2.3 Molecular mechanisms underlying chromosomal rearrangements in PTC

Chromosomal rearrangements involving either RET or NTRK1 genes are a frequent event in tumours originating from follicular epithelial cells (up to 60% of the cases in PTC). This peculiarity of thyroid epithelium sets it apart from other epithelial cells considering that chromosomal rearrangements leading the formation of fusion oncoproteins are a future usually associated with mesenchymal and hematopoietic cells (Pierotti et al., 2001). However, the molecular mechanisms underlying the predisposition of thyrocytes to undergo chromosomal rearrangements are not completely understood.

Some reports have suggested that the spatial proximity of translocation-prone gene loci may favour gene rearrangements. In particular, two studies used two-colour FISH analysis and three-dimensional microscopy investigated in the thyrocytes nucleus the proximity of loci undergoing rearrangements such as RET and H4 genes forming RET/PTC1 (Nikiforova et al., 2000) or the NTRK1 and TPR genes forming TRK-T1 (Roccato et al., 2004). They compared interphase nuclei of thyrocytes and B-cell lymphoma and found that in their respective normal cells both translocation-prone gene loci were positioned close to their translocation partner genes suggesting that this spatial contiguity may facilitate the specific translocation. Another model system considered that the high frequency of chromosomal rearrangements in thyroid tumours might reflect the thyrocyte intrinsic capability to repair DNA DSBs, either spontaneous or induced. In particular, *in vitro* irradiation failed to induce apoptosis in human thyroid cells, but increased a DNA end-joining enzymatic activity. Therefore, following DNA damage, thyrocytes would more prone to DNA repair than to apoptosis, and this would increase the likelihood of gene rearrangements (Yang et al., 1997).

1.1.2.4 RAS

The RAS gene product is a monomeric membrane-bound guanosine triphosphate (GTP)/guanosine diphosphate (GDP)-binding (G) protein that serves as a "molecular switch," converting signals from the cell membrane to the nucleus. These chemical signals lead to protein synthesis and regulation of cell survival, proliferation, and differentiation. The human RAS gene family includes HRAS, KRAS, and NRAS.

Each RAS protein consists of about 190-amino-acid residues that are highly conserved in the N and C termini. Most of the differences between these proteins occur in the near C-terminal hypervariable domain of about 25 amino acids, which is presumed to be responsible for their different functions.

RAS cycles between the GDP-bound inactive form and the GTP-bound active form. In the quiescent state, RAS exists in the GDP-bound form. After binding of an external ligand to its receptor, dimerization of the receptor occurs, and the intrinsic receptor tyrosine kinase is activated. This is followed by autophosphorylation of specific tyrosine residues on the intracellular portion of the receptor. These phosphorylated tyrosine residues then bind the sequence homology 2 (SH2) domains of adaptor proteins such as Grb2. These adaptor proteins contain not only an SH2 domain(s) but also an SH3 domain(s) that binds proline-rich motifs of other proteins, such as son of sevenless (SOS), a guanine dissociation stimulator (GDS) of RAS. The key adaptor molecule for RAS is Grb-2 that consists solely of one SH2 and two SH3 domains and links the activated receptor to SOS. Such a complex formation recruits SOS, a cytosolic protein, into close proximity to RAS on the plasma membrane. The binding of SOS to RAS causes a change in the RAS conformation and leads to the dissociation of GDP, which allows RAS to bind GTP and become active. Activated RAS activates several distinct effectors, such as the serine–threonine kinase raf-1, phosphoinositide 3′-kinase (PI3-K). These downstream effectors activate several distinct signalling cascades, leading to

either activation of certain genes, such as those encoding growth factors transforming growth factor-α and vascular endothelial growth factor (VEGF), or changes in actin cytoskeleton by activating Rho family G proteins. Normally, these Ras-signaling cascades are only transiently activated because each normal RAS has low intrinsic guanine triphosphatase (GTPase) activity that gradually inactivates its own signalling function by hydrolyzing the bound GTP. More importantly, several distinct cytoplasmic GTPase-activating proteins (GAPs) stimulate the intrinsic GTPase activity of RAS, rapidly converting RAS from the active GTP form to the inactive GDP form.

A high frequency of RAS mutations has been found in a variety of tumour types. Identified mutations are limited to a very small number of sites (amino acids 12, 13, 59, and 61), all of which abolish GAP-induced GTP hydrolysis of the RAS proteins. Such single-point mutations can lead to its constitutive activation of RAS protein, with an impaired GTPase activity. Although they still bind GAP, there is no "off" sign, since GTPase is no longer activated. This results in continuous stimulation of cellular proliferation. Mutations are frequently limited to only one of the RAS genes, and frequency is dependent on tissue and tumour type. Thus, RAS gene mutations are rare in cancers of the breast, ovary, stomach, oesophagus, and prostate; however, they are present in almost all adenocarcinomas of the pancreas and in 50% of colon and thyroid cancers. Mutations in colon and pancreatic cancers are found only in the KRAS gene. In cancers of the urinary tract and bladder, mutations are primarily in the HRAS gene; mutations are in the NRAS gene in leukaemia. Thyroid carcinomas are unique in having mutations in all three RAS genes.

In thyroid cancer, NRAS codon 61 and HRAS codon 61 mutations are most common. RAS mutations are found in a variety of thyroid tumours, including 10-20% of PTC, 40-50% of FTC and 20-40% of PDTC and ATC (Suarez et al., 1990). Among papillary

carcinoma, all tumours that harbour a RAS mutation grow forming neoplastic follicles and no papillary structures and are, therefore, diagnosed as the follicular variant of papillary carcinoma (Motoi et al., 2000). RAS mutations are also reported in 20-40% of benign follicular adenomas. The finding of this mutation in benign adenomas as well as in follicular-patterned carcinomas suggests that RAS may serve as a precursor for RAS-positive follicular carcinomas and the follicular variant of PTC (Namba et al., 2000). Furthermore, RAS mutations may predispose differentiated cancers to dedifferentiation and anaplastic transformation (Basolo et al., 2000; Garcia-Rostan et al., 2003). The close relationship between RAS mutations and the loss of tumour differentiation is also supported by studies in transgenic mice showing that the expression of NRAS-Q61K in thyrocytes can drive the formation of tumours that undergo differentiation and neoplastic progression (Vitagliano et al., 2006).

Remarkably, oncogenic RAS not only correlates with the loss of tumour differentiation but also with the presence of distant metastases and poor prognosis (Garcia-Rostan et al., 2003; Manenti et al., 1994). It is conceivable that RAS activation may be insufficient to induce malignant growth but may predispose to acquire further genetic or epigenetic alteration leading to a fully transformed phenotype.

1.1.2.5 BRAF

The BRAF gene is located on human chromosome 7q24 and encodes a cytosolic serine-threonine protein kinase that is expressed in many human cells, including thyroid follicular cells (Kondo et al., 2007). The wild-type (wt) BRAF is activated at the plasma membrane through a complex process that involves RAS activity, phosphorylation events, and protein-lipid interactions resulting the most potent activator of MAPK signalling pathway. Upon activation by RAS binding and recruitment to the cell membrane, BRAF activates the protein kinase MEK, which, in turn, activates the

protein kinase ERK and consequent effectors of MAPK cascade. All together they form a molecular axis crucial in the regulation of gene expression, cell proliferation, and differentiation (Leicht et al., 2007; Raman et al., 2007).

BRAF is comprised of three homologous regions, CR1, CR2 and CR3. CR1 has all the elements for BRAF membrane recruitment. These include a RAS binding domain (RBD) that binds to the active RAS-GTP, and a cysteine rich domain (CRD) that stabilizes its interaction with RAS. CR2, the N-terminal regulatory domain, contains a conserved phosphorylation site at S259 that serves as a regulatory binding site for protein 14-3-3, an essential dimeric cofactor for BRAF kinase activity. The N-terminal domain also acts as autoinhibitor of the C-terminal kinase domain and helps to maintain BRAF in an inactive state in the absence of extracellular stimuli. CR3, the C-terminal kinase catalytic domain, serves as the catalytic portion of the BRAF kinase domain (Leicht et al., 2007). BRAF exhibits a characteristics bilobar structure (McKay and Morrison, 2007). The inactive conformation of BRAF involves the simultaneous binding of 14-3-3 to phosphorylated sites S365 and S729 (Dhillon and Kolch, 2004). The activated wt BRAF is phosphorylated at site S446, leading to a maximally negatively charged amino region. Extracellular signals act on RAS-GTP to induce a thyrosine kinase receptor and initiate the activation sequence. Pre-activated BRAF is recruited to the plasma membrane where it is fully activated, first as two protein phosphatases (PP1 and PP2A) dephosphorylate the N-terminal 14-3-3-binding sites, and second by phosphorylation of the BRAF kinase domain, converting it to its active form (Dhillon and Kolch, 2004; Ikenoue et al., 2003). Importantly, oncogenic RAS phosphorylates two conserved sites of BRAF (T598 and S601) (Zhang and Guan, 2000). This event not only renders BRAF constitutively active, but also induces ERK1/2 activation, causing cell transformation (Figure 1.6).

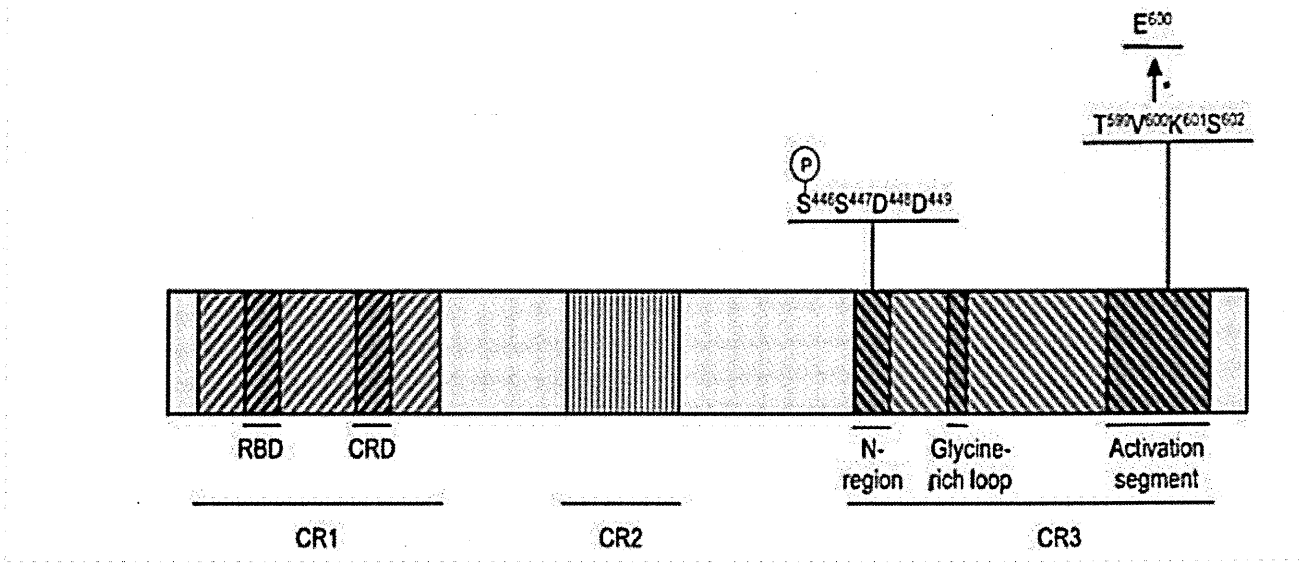

Figure 1.6 Schematic representation of the BRAF protein kinase. The three conserved regions CR1, 2, 3 are highlighted. CR1 and CR2 are regulatory domains and CR3 is the catalytic domain. The Ras-binding domain (RBD) and Cystein-rich domain (CRD) are located in CR1. The N-region, Glycine-rich loop and activation segment are located in CR3. S^{446} in the SSDD motif is constitutively phosphorylated. Phosphorylation of residues T^{599} and S^{602} results in BRAF activation. (Adapted from Michaloglou et al., 2007)

Constitutive activation of RAS-ERK signalling pathway is common to numerous cancers. More than 30 mutations of the BRAF gene associated with human cancers have been described. In 2002 Davies et al. identified an oncogene widespread amongst human cancers, mutant $BRAF^{V600E}$. This BRAF point mutation involves a thymine to adenine substitution at nucleotide position 1799, which results in a valine-to-glutamate replacement at residue 600 (Val600Glu). The V600E mutation strongly enhances BRAF kinase activity that over-activates the MAP kinase pathway (Davies et al., 2002). $BRAF^{V600E}$ is expressed in different human cancer cell lines including melanoma (Tuveson et al., 2003), colorectal cancer (Ikenoue et al., 2003), and thyroid cancer (Xing, 2007).

$BRAF^{V600E}$ is the most common genetic lesion in PTC, being detected in about 29 to 69% of cases and is highly prelevant in PTC with classical histology and in tall cell

variant tumours (69-71%) (Xing, 2007). Controversial relationship between $BRAF^{V600E}$ and the potential aggressiveness of PTCs has been described. Some studies show a positive correlation between $BRAF^{V600E}$ and advanced PTCs, characterized by poorer outcomes, extrathyroidal extension, and lymph nodal metastasis, while others do not. PTCs carrying $BRAF^{V600E}$ mutation exhibit decreased expression of genes involved in thyroid hormone biosynthesis, including sodium iodine symporter (NIS), decreased ability to trap radioiodine and consequent treatment failure (Frasca et al., 2008).

Furthermore, $BRAF^{V600E}$ is also found in PDTC and ATC, suggesting that this mutation may be involved in progression of thyroid cancer from PTCs to poorly differentiated and undifferentiated phenotypes (Nikiforova and Nikiforov, 2008).

Interestingly, $BRAF^{V600E}$ is also the most common genetic alteration in PTMC which is generally considered to have a very low risk of progression and/or recurrence (Kim et al., 2005; Trovisco et al., 2005). Recent studies showed that even in PTMC, $BRAF^{V600E}$ was significantly associated with extrathyroidal extension, high tumour stage, and lack of tumour capsule (Lupi et al., 2007). These results suggest that $BRAF^{V600E}$ may also confer a higher risk of tumour progression and invasiveness versus the wild-type in PTMC, potentially serving as a predictive indicator of aggressive behaviour in PTMC.

Transgenic mice with thyroid-specific expression of $BRAF^{V600E}$ developed PTC closely recapitulating those seen in human tumours, thus supporting the role of mutant BRAF in tumour initiation and differentiation, as well as its correlation with tumour characteristics (Knauf et al., 2005). It has been recently demonstrated that $BRAF^{V600E}$ localizes to mitochondria and exerts an antiapoptotic effect, independent from kinase activity, which is not abrogated by BRAF inhibitors (Lee et al., 2011).

Recently, another mechanism of BRAF oncogene activation has been reported in post-Chernobyl thyroid carcinomas. This new BRAF alteration derives from a fusion of the first eight exons of the A-kinase anchor protein 9 (Akap9) gene with the c-terminal-

encoding region of BRAF (Ciampi et al., 2005). The Akap9 fusion gene of this rearrangement is intriguing since it is interacting with the type II regulatory subunit of the cAMP-dependent protein kinase A.

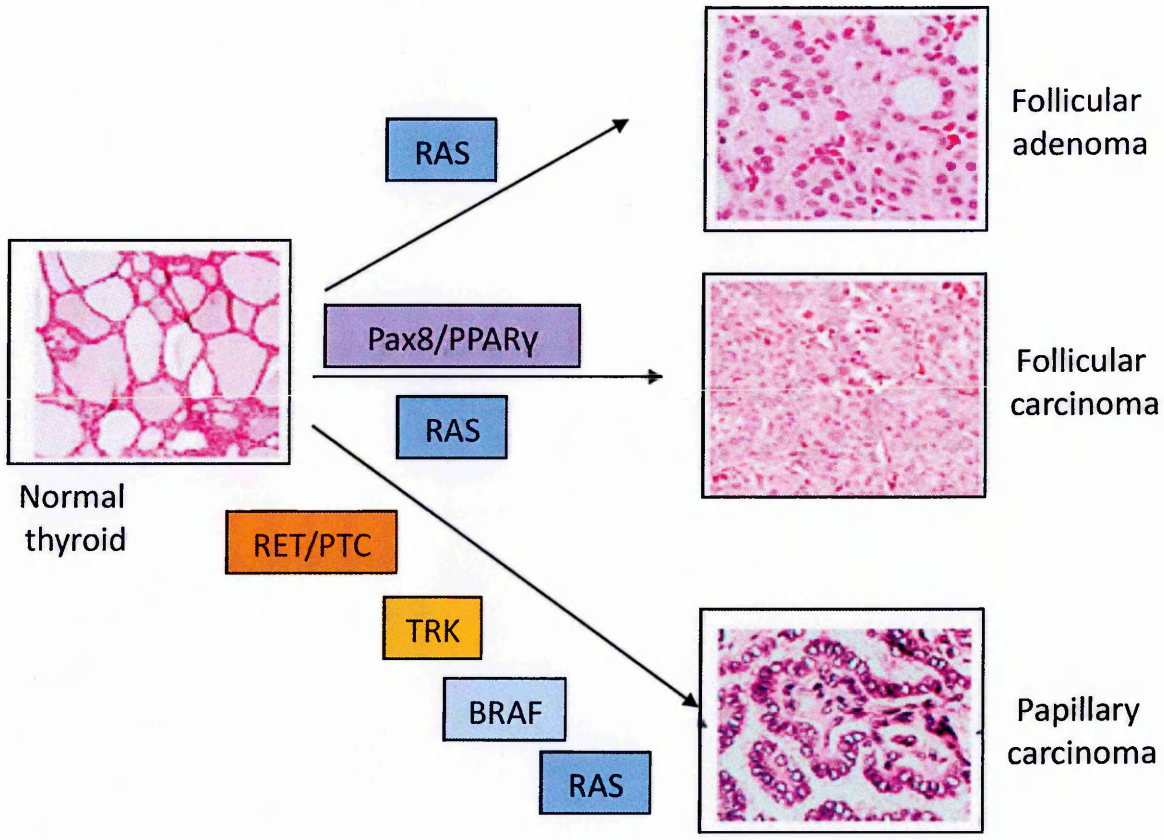

Figure 1.7 Genetic alterations in thyroid cancer. Common mutational mechanisms in thyroid cancer are point mutations, such as those in the RAS and BRAF genes, and chromosomal rearrangements, such us RET/PTC, TRK and PAX8/PPARγ. Genetic alterations and association with the different histological types of thyroid tumours are shown.

1.1.2.6 Other molecular events

In the last few years gene expression analysis studies have identified several genes, involved in different cellular processes, which might be important in the molecular pathogenesis and the malignant progression of thyroid cancer. Distinct alterations in gene expression have been observed in PTC and others types of thyroid cancer. For instance, Huang et al. undertook the first study of PTC gene expression profile. Respect to normal thyroid tissue they observed upregulation of many genes involved in cell adhesion, motility and cell-cell interaction, including MET, TIMP1, LAMB3, CITED1, LGALS3. Conversely, they found downregulated genes responsible for specialized thyroid function such as thyroid hormone synthesis (Huang et al., 2001). These results are consistent with the fact that most malignant thyroid tumours are hypofunctioning in trapping iodine and producing thyroid hormone. Genes underexpressed in PTC also included tumour suppressor and fatty acid binding proteins. Therefore, despite its clinical heterogeneity, PTC is characterized by consistent and specific molecular changes and behaves as a homogeneous group in terms of gene expression (Frattini et al., 2004; Huang et al., 2001). Moreover, some of the differentially expressed genes have been proposed as useful PTC markers (Huang et., 2001).

Different gene expression profiles have been observed between PTC and FTC: a combination of five genes was proposed to distinguish PTC from FTC. PTCs showed overexpression of CITED1, IGFBP6 and CLDN10, whereas FTCs did not express CLDN10 and displayed a decreased expression of IGFBP6, CAV1 and CAV2 (Aldred et al., 2004).

The relationship between the presence of thyroid cancer histotype-specific mutations and gene expression profiles of tumours is complex. However, several studies described the gene expression profile changes with the presence of different mutations that contribute to thyroid cell carcinogenesis. As mentioned above, PTC is associated with

well defined genetic lesions i.e. BRAF mutations and RTK rearrangements. Independent expression studies showed differences in gene expression between BRAF-positive PTCs and those with RTK rearrangements (Frattini et al., 2001; Giordano et al., 2005). These results could suggest that although RTK and BRAF act along the same signal transduction pathway, their activity occurs at different levels, leading to the regulation of different gene sets.

Alteration in gene expression as result of aberrant methylation of gene promoter regions or histone modification also occurs in thyroid cancer (Xing et al., 2007). These epigenetic events can alter the function of tumour suppressor genes and thus contribute to activation of important signalling pathways, such as PI3K-AKT and MAPK cascades. Changes in epigenetic regulation might also result in downregulation of thyroid-specific genes during tumour progression and dedifferentiation. Hypermethylation of tumour suppressor genes, including TIMP3, DAPK, SLC5A8, was associated with tumour aggressiveness and BRAF mutation in PTC (Hu et al., 2006).

Despite the numerous gene expression studies, validated by different approaches, only a few data addressing the role of differentially expressed genes in the pathogenesis of thyroid tumours have been produced yet. Nevertheless, such studies are important for a deeper understanding of molecular mechanisms underlying thyroid carcinogenesis, and they could also identify possible new strategies for therapeutic intervention.

1.1.3 Thyroid cancer and inflammation

The relationship between inflammation and thyroid cancer is not yet completely understood. Like others tumours, thyroid cancer is influenced by and modulates inflammation. For instance, thyroid cancer often has an inflammatory cell infiltrate including lymphocytes, macrophages, dendritic cells and mast cells. The role of these cells is complex and the effect can be either pro- or anti-tumorigenic, depending on the

specific cell population, as demonstrated by several studies. Specifically, the presence of lymphocytes, which belong to the adaptive branch of immunity, is significantly higher in neoplastic than in non-neoplastic lesions (Okayasu, 1997). However, lymphocytic infiltration seems to confer protection against cancer progression. In fact, numerous studies indicate that PTC with high number of infiltrating and proliferating lymphocytes are associated with less extensive disease at diagnosis and improved disease free-survival. Conversely, thyroid carcinomas with poor prognosis, such as PDTCs and ATCs, are characterized by a strongly reduced lymphocytic infiltration compared with PTCs, thus suggesting that these cells may play a protective role in thyroid cancer (Ugolini et al., 2007). On the other hand, the presence of macrophages and mast cells, belonging to innate immunity, correlates with tumour progression and poor prognosis (Scarpino et al., 2000). In particular, the macrophage component termed "tumour-associated-macrophages (TAMs), which is closely mixed with cancer cells plays a key role in thyroid tumour progression. In fact, studies show that ATCs display a very dense network of interconnected TAMs characterized by elongated thin ramified cytoplasmic extensions in direct contact with intermingled cancer cells (Caillou et al., 2011).

Oncoproteins typically express in PCTs, such as RET/PTC, RAS, and BRAF, trigger a proinflammatory program in thyrocytes including the expression of cytokines, chemokines and their receptors (Borrello et al., 2005; Melillo et al., 2005). These molecules have a dual effect in thyroid cancer. By acting in an autocrine way, they can enhance proliferation, survival and invasiveness of thyroid cells. But, they can also induce, in a paracrine manner, remodelling of the tumoral stroma by recruiting inflammatory, immune, endothelial cells. For instance, several studies have demonstrated that activated RET, in its different forms, leads to expression of a number of inflammatory mediators in different cell environments. For example, RET/PTC1

oncogene, when exogenously expressed in primary normal human thyrocytes, induces the expression of a large set of genes involved in inflammation and invasion, including those encoding chemokines (CCL2, CCL20, CXCL8, and CXCL12), chemokine receptors (CXCR4), cytokines (IL1B, CSF-1, GM-CSF, and G-CSF), matrix-degrading enzymes (metalloproteases and uroki-nase-type plasminogen activator and its receptor), and adhesion molecules (L-selectin) (Borrello et al., 2005). These RET/PTC1-induced genes were also expressed in specimens of PTC suggesting a direct link between a transforming oncogene involved in the pathogenesis of a human tumour and the activation of a proinflammatory network in the primary human cells originating that tumour. Molecules activated by RET/PTC1 in human thyrocytes is likely to contribute to the tumour. This is in line with another work showing the up-regulation of some chemokines (CXCL1, CXCL10, and CCL2) and of CXCR4 in a rat thyroid cell line expressing RET/PTC and suggesting a chemokine role in proliferation and invasion (Melillo et al., 2005). As a consequence, not only oncoproteins, but also inflammatory molecules are promising targets for novel thyroid cancer therapeutical strategies.

1.2 The limited lifespan of normal somatic cells

Cellular senescence was formally described more than 40 years ago when Hayflick and Moorhead showed that normal cells had a limited ability to proliferate in culture. In fact, they observed that human primary fibroblasts, isolated from embryonic lung tissue, initially exhibited robust proliferation and after many population doublings (PDs), they underwent a gradual decline in proliferate rate. Eventually, all cells lost the ability to divide (after 50-80 PDs), despite the abundance of growth and nutrients and ample room for expansion. This finite proliferative lifespan is known as the "Hayflick limit". The process, which describes this cellular condition of ceased proliferation, is termed cellular senescence (Hayflick, 1965).

Subsequent studies showed that senescence was not specific to human fibroblasts, it was described in cultures established human mammalian species and in a variety of cell types including keratinocytes (Rheinwald and Green, 1975), vascular smooth muscle cells (Bierman, 1978), lens cells (Tassin et al., 1979) and lymphocytes (Tice et al., 1979).

The work by Hayflick gave birth to the idea that normal somatic cells possessed a "mitotic clock" that dictates their maximum lifespan, which constitute a protective mechanism against unlimited cell proliferation essential for tumorigenesis. Nowadays, cellular senescence is an important mechanism for preventing the proliferation of potential cancer cells. In addition to suppressing tumorigenesis, cellular senescence might also promote tissue repair and fuel inflammation associated with the ageing and cancer progression (Campisi et al., 2001).

1.2.1 Characteristics of senescent cells

Senescent cells display important and unique properties that distinguish them from cells undergoing other types of proliferative arrest.

In contrast to quiescence, a form of cell cycle arrest that can be reverted in the presence of appropriate physiological signals, the hallmark of cellular senescence is its irreversible nature. Once senescent cells arrested growth, they cannot re-enter the cell cycle despite adequate growth conditions (Campisi and d'Adda di Fagagna, 2007). Although cells reach a state in which they can no longer initiate replication, this happens asynchronously so that at any given moment in mitotic cultures, the population is a heterogeneous mixture of senescent and non-senescent cells, that are at various stages in their proliferative life (Cristofalo and Sharf, 1973). Early passage cultures consist primarily of cells that exhibit short cell cycle periods. With successive subcultivations, the percentage of cells in the population that exhibit longer generation times and those unable to proliferate, increases. Successful progression through the cell cycle involves the synthesis of the new DNA that can be quantified by 5-bromodeoxyuridine (BrdU) incorporation assay. Senescent cells fail to incorporate BrdU because they are arrested predominantly at G1 phase and do not progress to S phase for DNA synthesis. However, senescent cells remain metabolically active, as evidenced by changes in the pH of the growth medium.

Senescence, like apoptosis, is a cellular response to stress, and plays an important role in suppressing tumorigenesis. But, whereas senescence prevents the growth of damaged or stressed cells, apoptosis quickly eliminates them. Interestingly, senescent cells acquire resistance to apoptosis induced by several stimuli (Chen et al., 2000; Hampel et al., 2004).

It is not clear which factors direct the choice of cells between apoptosis and senescence; it may depend on cell type and on the intensity, duration and nature of the damage.

Moreover, the balance between proapoptotic and antiapoptotic proteins may also be important (Rebbaa et al., 2003; Seluanov et al., 2001). The mechanisms by which senescent cells resist apoptosis are not completely understood. They are most probably related to their common regulator, the p53 tumour suppressor protein. This resistance, in some cells, might be associated with the expression changes in proteins, which are key executioners for committing apoptotic death (Marcotte et al., 2005). In others, p53 might transactivate genes that arrest proliferation rather than those that induce apoptosis (Jackson and Pereira-Smith, 2006). This could partly explain why senescent cells are so stable in culture, and why they increase with age *in vivo*.

Cellular senescence is also accompanied by morphological and structural changes. Upon entering the state of senescence, cells become large and flat (Serrano et al., 1997). Moreover, they exhibit an increase in the number of lysosomes and Golgi, appearance of vacuoles in the cytoplasm and endoplasmic microfilaments and an increase in the size of the nucleus and nucleoli. However, the molecular mechanisms underlying such morphological alterations in senescent cells have not been elucidated.

Senescence associated β-galactosidase activity detectable at pH 6.0 is the most frequently used senescence marker (Dimri et al., 1995). Its induction in senescent cells is due to an increase in GLB1 expression, the gene encoding lysosomal β-D-galactosidase. Fibroblasts, obtained from patients with autosomal recessive G_{m1}-gangliosidosis, which have defective lysosomal β-galactosidase, fail to express SA-β-Gal even though they undergo senescence. These results confirmed that SA-β-Gal activity is an outcome rather than a cause of the senescent cells and is due to an expansion of the lysosomal compartment. Importantly, this activity can be uncoupled from senescence (Lee et al., 2006). For instance, SA-β-Gal activity increases also in non-senescent cells following serum starvation, oxidative treatment with H_2O_2 or contact inhibition (Severino et al., 2000). For these reasons, SA-β-Gal is not

senescence-specific; therefore it must be used in conjunction with additional markers (Cristofalo, 2005).

Another common feature of senescence is the widespread nuclear heterochromatization; senescence is accompanied by profound chromosome condensation, so that each chromosome forms a punctate heterochromatic domain, called a senescence-associated heterochromatin focus (SAHF) that is detectable by DNA staining dye, 4',6-diamidino-2-phenylindole (DAPI). When stained with DAPI normal human cells exhibit a relatively diffuse distribution of DNA through the nucleus. The chromatin from cells with SAHF appears much more compact than the chromatin in normal interphase growing cells. Moreover, these foci are enriched in markers of heterochromatin such as heterochromatin protein 1 (HP1) and Lys 9 tri-methyl on histone H3 (H3K9me3) and exclude euchromatic markers, such acetylation of histone H3 on lysine 9 (H3K9Ac) or tri-methylation on lysine 4 (H3K4me3). SAHFs are also characterized by depletion of histone H1 and enrichment in at least two other proteins, namely the histone variant macroH2A and high mobility group A (HMGA) proteins. Paradoxically, the presence of HMGA proteins in chromatin is normally associated with gene activation, cell proliferation and cell transformation. Thus, it was a surprise when SAHFs were shown to be enriched in HMGA proteins and that these proteins contribute to senescence (Narita et al., 2003).

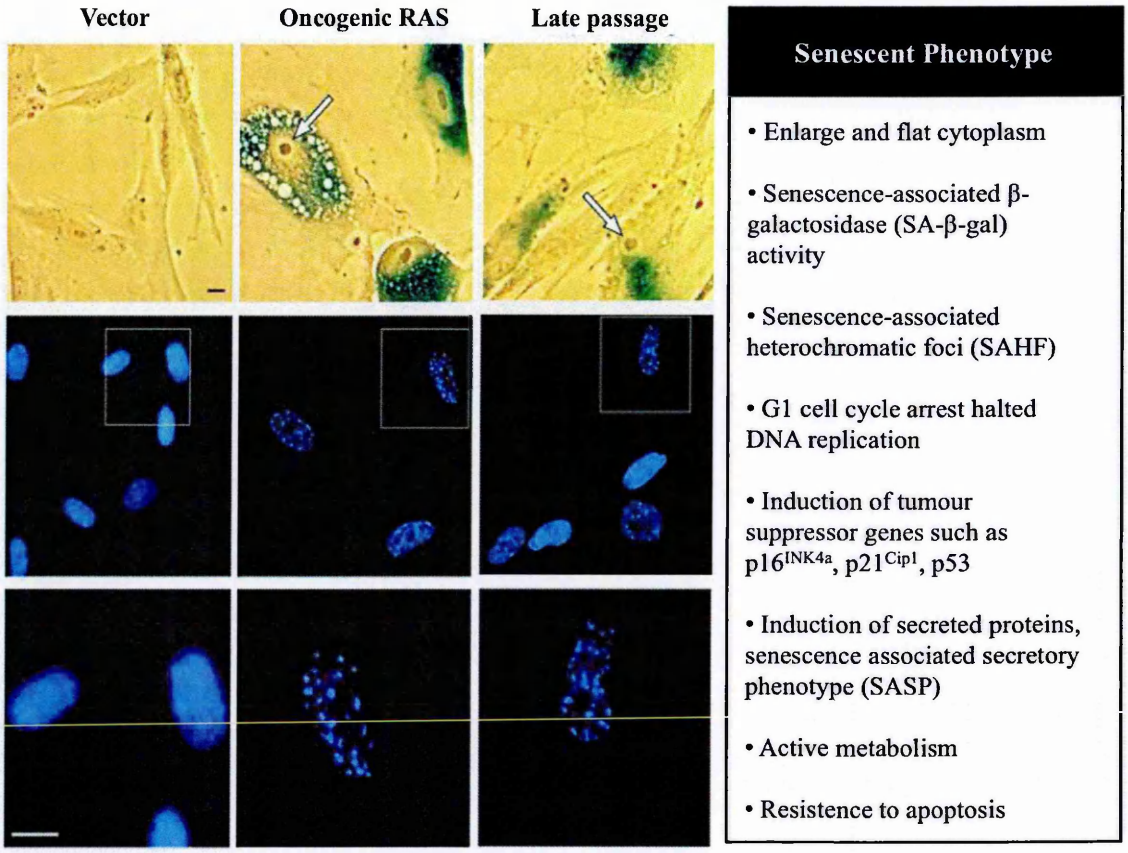

Figure 1.8 The senescent phenotype. Premature senescence can be observed in young cells under a number of physiological stresses including expression of oncogenes (oncogene-induced senescence). Replicative senescence is described as the growth arrest in response to prolonged passaging. Both lead to a senescent phenotype with morphologic and functional characteristics, which are listed in the right box. SA-β-Gal activity (upper panel) and SAHF formation (middle panel) of IMR90 fibroblasts transfected with empty vector or RAS oncogene, as well as cells in late passage, are shown. Enlarged image of DAPI stained chromatin foci is shown in the lower panel. (Adapted from Narita et al., 2003)

As transcription in heterochromatin is generally low, the idea was launched that the senescence-associated heterochromatization contributes to shutting down transcription of proliferation-associated genes. Consistent with this, the promoters of several E2F target genes acquire increased binding of heterochromatin-associated proteins (Narita et al., 2003).

Since the discovery of SAHF, several studies have dissected the events that eventually culminate in the formation of SAHF observed in senescent cells (Adams, 2007). An essential step in the initiation phase of chromosome condensation is the translocation of

HIRA (histone chaperon) and HP1 to promyelocytic leukaemia nuclear bodies (PML bodies), another senescence effector. Currently, the exact function of PML bodies, and how PML bodies are involved in senescence program are not clear; it has been suggested that PML bodies are sites for macromolecular assembly and posttranslational modifications of proteins. These subnuclear organelles are thought to serve as a staging ground for formation of histone chaperones complex, HIRA/ASF1A, which are incorporated into chromatin and play an essential role in SAHF formation (Zhang et al., 2005).

Senescence phenotype exhibits a specific gene expression profile, including changes in cell-cycle regulators (Mason et al., 2004; Shelton et al., 1999; Trougakos et al., 2006; Yoon et al., 2004). Two cell-cycle inhibitors that are often expressed by senescent cells are the cyclin-dependent kinase inhibitors (CDKIs) p21 (also termed CDKN1a, $p21^{CIP1}$, Waf1) and p16 (also termed CDKN2a or $p16^{INK4a}$). Senescent cells also repress genes that encode proteins involved in cell cycle; some of them are E2F targets (for example, replication-dependent histones, c-FOS, cyclin A, cyclin B and PCNA) (Pang and Chen, 1994; Seshandri and Campisi, 1990). Interestingly, amongst the genes whose expression is upregulated during senescence there are a myriad of secreted proteins, which are the basis of the so-called senescence-associated secretory phetotype (SASP) (Coppé et al., 2008; Rodier et al., 2009) or senescence-messaging secretome (SMS) (Kuilman and Peeper, 2009). Many of these factors contribute to reinforce senescence: the plasminogen activator inhibitor (PAI)-1 is necessary and sufficient for the induction of senescence (Kortlever et al., 2006); insulin-like growth factor binding 7 (IGFBP7) was shown to mediate senescence induced by oncogenic BRAF (Wajapeyee et al., 2008). Equally, pro-inflammatory cytokines and chemokines such as IL-8, CXCL1, IL-6 and their receptors have an indispensable role in the establishment and maintenance of the senescence arrest (Acosta et al., 2008; Kuilman et al., 2008). In addition to these

tumour-suppressing functions, increasing evidence also points to a tumour-promoting role of these secreted factors. SASP factors can boost up cancer progression by stimulating proliferation (Krtolica et al., 2001; Coppé et al., 2008), inducing epithelial to mesenchymal transition (EMT) and promoting angiogenesis (Nickoloff et al., 2004). These two opposing effects of SASP can be reconciled: the tumour-suppressing role generally functions in a cell-autonomous manner (by enforcing senescence), whereas its tumour-promoting actions are mediated by cell-non-cell-autonomous mechanisms, altering the microenvironment. Thus, secreted factors affect not only the cells producing them (autocrine effect), but also the neighbouring cells (paracrine effect) (Kuilman and Peeper, 2009) (Figure 1.8).

1.2.2 Causes of cellular senescence

1.2.2.1 Replicative Senescence

Induction of cellular senescence by prolonged *in vitro* culturing has been termed replicative senescence, reflecting its onset after a defined number of cell divisions. The timed nature of this cell cycle arrest suggests the existence of a counting mechanism, and this is indeed the case. The extreme ends of chromosomes, i.e. telomeres, are subject to attrition due the fact that DNA polymerase fails to completely replicate the lagging strands, a phenomenon called the end-replication problem that is a major reason why normal cells do not proliferate indefinitely (Olavnikon, 1971; Watson, 1972). Telomere erosion can be prevented or even reverted by telomerase. This enzyme contains a catalytic protein component (telomerase reverse transcriptase; TERT) and a template RNA component, and adds telomeric DNA repeats directly to the chromosome ends (Collins and Mitchell, 2002). Its activity is low or absent in most human somatic cells, so telomeres become progressively shorter with every round of cell division (Masutomi et al., 2003). It is thought that telomere shortening triggers DNA damage

response, thereby activating a checkpoint mediated by the p53 pathway that contributes to either senescence or apoptosis (D'Adda di Fagagna et al., 2003; Takai et al., 2003). Telomere length therefore functions as a mitotic clock, counting the number of cell divisions that human somatic cells undergo (Harley et al., 1990). In this regard, introduction of telomerase extends the replicative life span of normal human cells (Bodnar et al., 1998). Although telomerese expression is strictly regulated in normal human somatic cells, in tumour cells its expression is frequently deregulated (Neumann and Reddel, 2002). Since telomerase is specifically required for most human cancer cells to bypass senescence, it is clear that telomere maintenance is essential for cellular immortality and thus telomerase offers a possible therapeutic target in human cancer. However, some immortalized cell lines and tumours can also elongate their telomere through another mechanism termed alternative lengthening of telomeres (ALT). It was discovered in some cancer cell lines in which telomere lengths were maintained in the absence of telomerase activity. The ALT mechanism seems to depend on recombination in which single-stranded telomere ends invade double-stranded telomeric DNA, use it a template for synthesis of new telomeric DNA and thereby elongate themselves (Cesare and Reddel, 2010).

1.2.2.2 Oncogene-induced senescence

Not only prolonged passaging in culture, but also other types of imposed stress can lead to the induction of cellular senescence. For instance, oxidative stress, DNA damage and chromosome perturbation can all induce this response, in different cell types (Campisi and D'Adda di Fagagna, 2007). Somewhat counterintuitively, senescence can be implemented in primary cells also upon expression of an activated oncogene and this process has been termed oncogene-induced senescence (OIS) (Figure 1.9). It was first observed when an oncogenic form of RAS, a cytoplasmic transducer of mitogenic

signals, was expressed in normal human fibroblasts (Serrano et al., 1997). Subsequently, other members of the RAS signalling pathway such as RAF, MEK, MOS and BRAF can induce cellular senescence (Dimri et al., 2000; Lin et al., 1998; Michaloglou et al., 2005). Conversely, the loss of PTEN, which is an inhibitor of the same pathway, also leads to senescence establishment (Chen et al., 2005). Since RAS transduction pathways relay their signals to the nucleus to regulate proliferation, the activation of several pro-proliferative nuclear proteins also induces senescence: increased expression of E2F transcription factors, key regulators of G1/S cell-cycle transition triggers cellular senescence.

Time-course studies have revealed that the expression of the oncogenic form of H-RAS (H-RAS^{G12V}) in normal fibroblasts leads to a biphasic response. RAS drives an initial hyperproliferation phase in which cells proliferate faster than the control cells. This in keeping with the mitogenic functions of this signal transducer molecule. However, this burst of proliferation is transient and is quickly followed by a proliferation slow down and the eventual establishment of cellular senescence (D'Adda di Fagagna, 2008).

In this context, OIS is therefore a tumour suppressor mechanism that restricts the proliferation of a cell that expresses high levels of an aggressive oncogene.

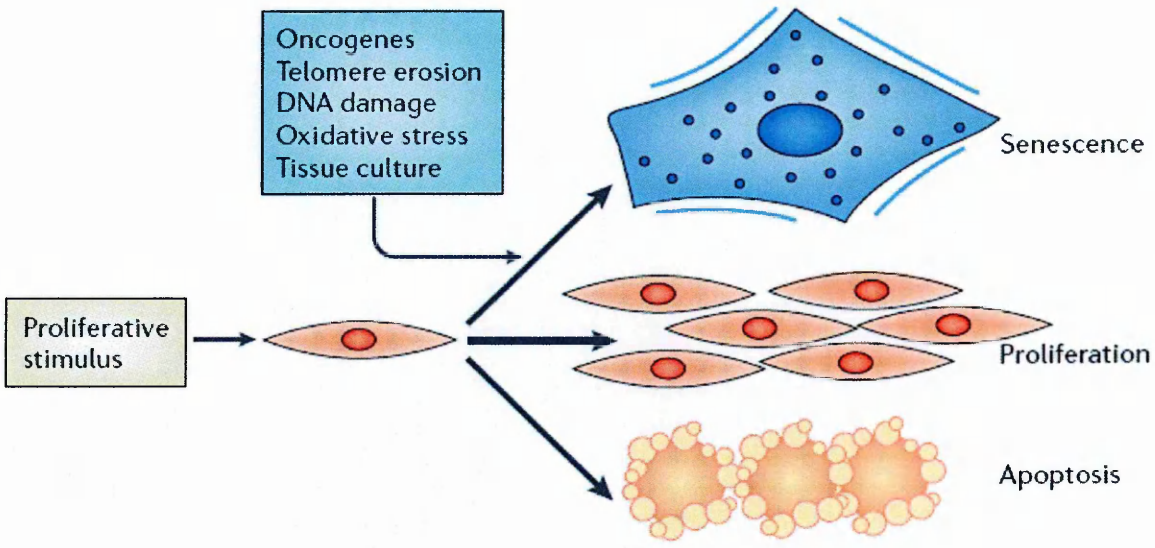

Figure 1.9 Senescence is a tumour suppressive mechanism. Two main mechanisms, senescence and apoptosis, act to prevent the proliferation of altered cells. Senescence can be triggered by several different stimuli, including telomere erosion, oxidative stress and others forms of DNA damage. Activation of oncogenes can also trigger senescence, highlighting the importance of senescence as a tumour suppressor mechanism. (Adapted from Gil and Peters, 2006)

1.2.3 Two pathways to senescence

During cell cycle progression, checkpoints ensure that cells are "ready" to progress to the next phase and that no defects during DNA replication or chromosome segregation are accumulated. Moreover, two DNA damage checkpoints, during G1/S and G2/M assure that cells that acquired DNA breaks or other forms of DNA damage, do not progress through the cell cycle. Arresting the cell cycle allows cells to repair these defects. If the damage is irreparable due to excessive or continuous DNA damage, cells may enter senescence or undergo apoptosis. Alternatively, accumulation of DNA alterations may result in genomic instability leading to cell transformation and oncogenesis (Malumbres and Barbacid, 2009).

Misregulation of cyclin-dependent kinases (CDKs) whose activity requires binding of regulatory subunits known as cyclins, is at the heart of the cell cycle defects that can lead to unscheduled proliferation. In unstressed cells at G1, the phase proceeding the

DNA replication phase, mitogenic signals are sensed by D-type cyclins that preferentially bind CDKs 4 and 6. Activation of the CDK4/6-Cyclin D complexes results in partial inactivation of the retinoblastoma protein (RB) and retinoblastoma-like proteins (RBL) 1 and 2 (p107 and p130). This allows expression of E-type cyclins that bind to and activate CDK2, which will further phosphorylate RB proteins thereby inactivating them. Inactivated RB releases E2F transcription factors that will induce transcription of genes necessary for DNA replication and cell cycle progression (Weinberg, 1995) (Figure 1.10).

If cells encounter various stresses, such as telomere uncapping or expression of oncogene, two main pathways are triggered that converge on modulation of CDK activity and are responsible for senescence onset. These pathways are controlled by the tumour suppressor proteins p53 and pRB, they interact but can independently halt cell-cycle progression and they also respond to different stimuli. In addition, depending on the cell type and species of origin, there are differences in the propensity with cells engage one or the other pathway, and in the ability of each pathway to induce senescence.

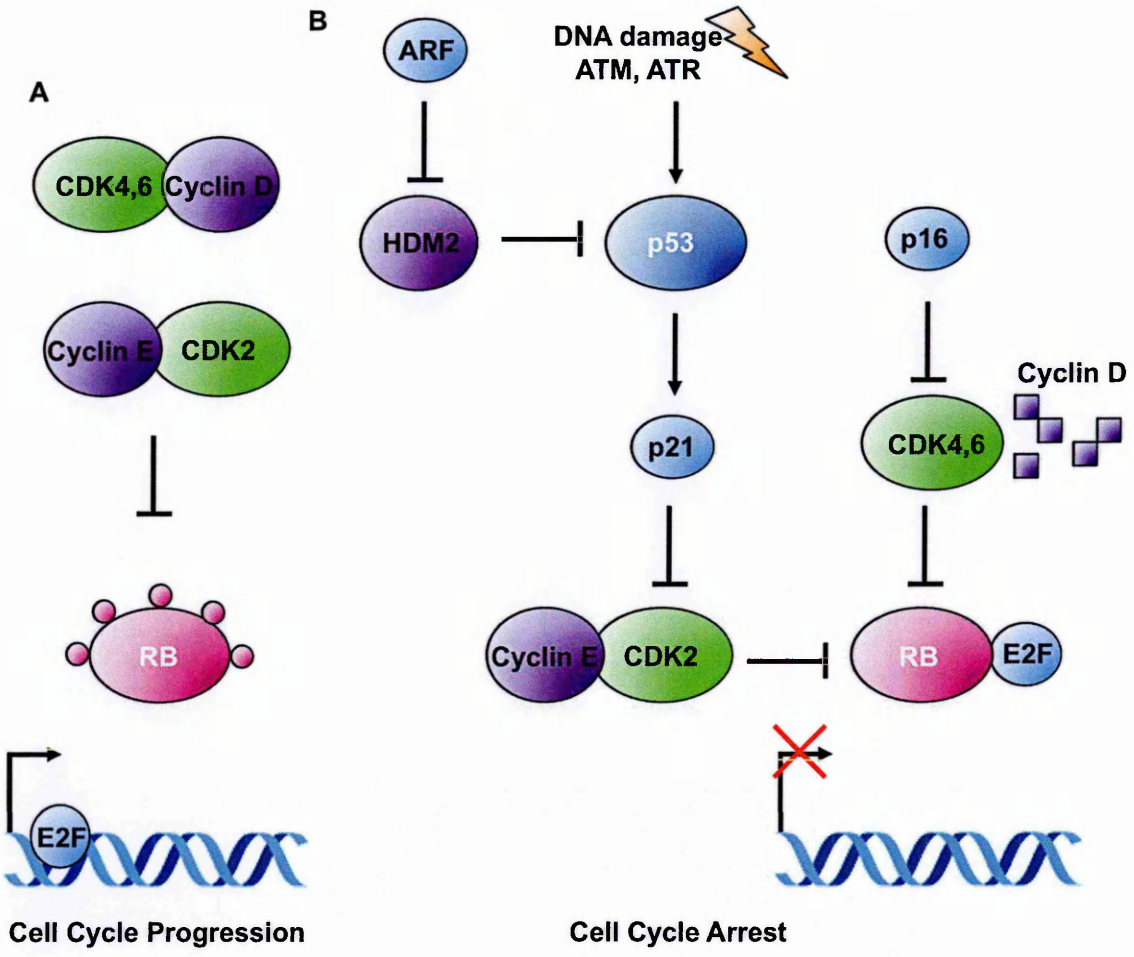

Figure 1.10 Two pathways to senescence. A) In unstressed cells and in the presence of mitogenic signals, activation of the CDK4/6-Cyclin D complexes results in partial inactivation of RB family proteins. This allows the expression of E-type cyclins that bind to and activate CDK2, which will further phosphorylate RB proteins, thus inactivating them. Inactive RB releases E2F transcription factors that activate transcription of genes necessary for entry into S-phase. **B)** Senescence-inducing signals usually engage either the p53 or the $p16^{INK4a}$-retinoblastoma protein (RB) tumour suppressor pathways. p53 is negatively regulated by HDM2, which facilitates its degradation. HDM2 is negatively regulated by ARF. Active p53 establishes senescence in part by inducing the expression of $p21^{CIP1}$, a cyclin-dependent kinase (CDK) inhibitor that suppresses the phosphorylation and hence, the inactivation of RB. Engagement of p16-Rb pathway also results in inhibition of RB phosphorylation and inactivation, by inhibition CDK4/6. RB halts cell proliferation by inhibiting the activity of E2F, and thereby suppressing expression of genes required for cell-cycle progression.

The p53 pathway is activated by DNA damage response mediated by ATM/ATR, and by the ARF protein. ATM/ATR are protein kinases that activate p53 mainly by phosphorylation whereas ARF activates p53 by inhibiting HMD2 an ubiquitin E3 ligase that targets p53 for degradation. Active p53 induces the expression of p21, a cyclin-dependent kinase (CDK) inhibitor that belongs to the Cip/Kip or CDKN1 family.

p21 inhibits cell cycle progression mainly through the inhibition of CDK2. However, it is known to interact with both CDK4/6-Cyclin D complexes and CDK2-Cyclin E complexes resulting in the suppression of phosphorylation and, hence, inactivation of pRB (Sherr and Roberts, 1999). Senescence signals that engage p16-pRB pathway generally do so by inducing the expression of p16, another CDK inhibitor that belongs to the INK4a or CDKN2 family. p16 binds to CDK4 and 6 and inhibits their ability to interact with D-type cyclins, which is the early and essential step in the phosphorylation of pRB. Thus, p16 maintains pRB in its active, growth-inhibitory state. In turn, pRB halts cell proliferation by suppressing the activity of E2F, a transcription factor that stimulates the expression of genes that are required for cells cycle progression (Sherr and McCormick, 2002).

1.2.3.1 The DNA damage response (DDR)

Several stresses that can lead to senescence converge on a DNA damage response (DDR). Telomeres consist of nucleoprotein complexes that cap the end of chromosomes and protect them from degradation or fusion. The progressive telomere shortening eventually causes chromosome ends to be recognized as DNA breaks, which consequently activates a DDR and enforces replicative senescence (Verdun and Karlseder, 2006).

Induction of p53 in response to DNA damage is coordinated by the serine/threonine protein kinase ataxia telangiectasia mutated (ATM) and the ataxia telangiectasia and Rad3-related (ATR). These modify a large number of substrates, including signal-amplifying checkpoint kinases CHK1 and CHK2, whose engagement is favoured by mediator proteins, such as 53BP1, MDC1 and BRCA1, and chromatin modifiers such as γ-H2AX. These signals converge on p53 and lead to p21 induction, halting cell-cycle progression (Figure 1.11).

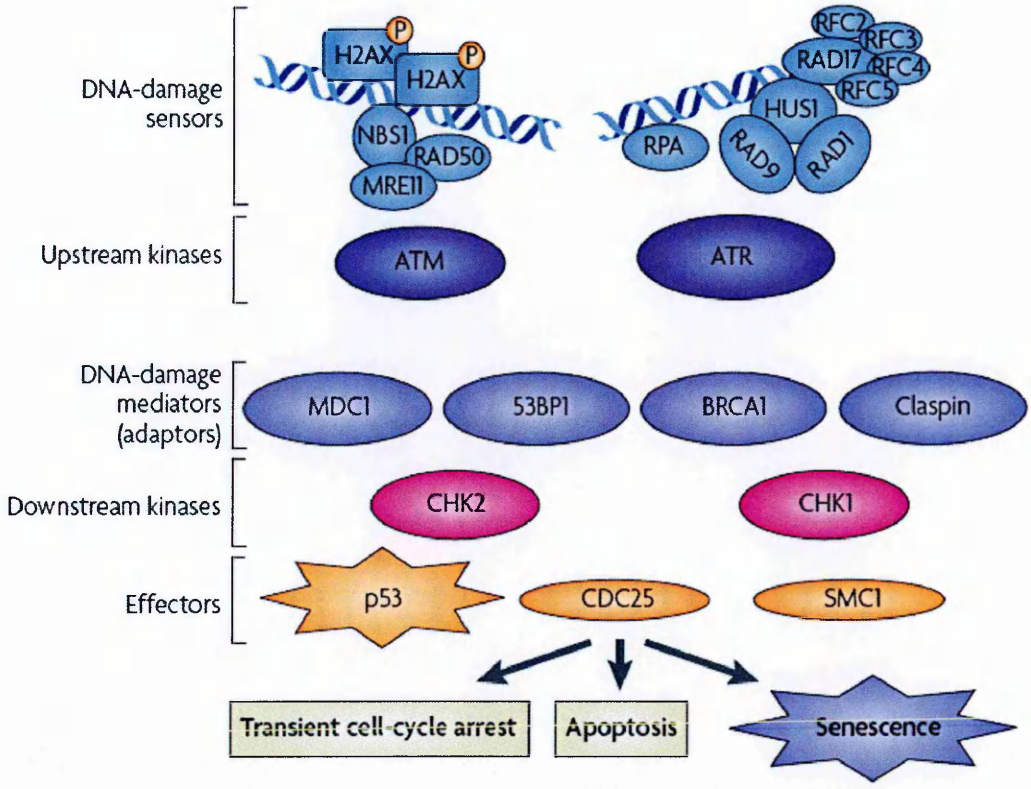

Figure 1.11 The DNA damage response. Double strand breaks are recognized by the MRN complex (composed by MRE11, RAD50 and NBS1) and lead to the activation of the kinase ataxia-telangiectasia mutated (ATM) and subsequent amplification of the response by recruitment of other DNA damage signalling proteins. ATM phosphorylates several proteins including MDM2, MDM4, p53 and checkpoint-2 (CHK2), which phosphorylates p53 and other proteins. Single strand breaks become coated with replication protein A (RPA) that attracts ATM and Rad3-related (ATR)-interacting protein (ATRIP) complex which phosphorylates the 9-1-1 complex (constituted by RAD9, RAD1 and HUS1) further activating ATR. Active ATR phosphorylates p53, MDM2, checkpoint-1 (CHK1) and other substrates. The DNA damage response ultimately results in activation of effector molecules such as p53, CDC25 or structural maintenance of chromosomes (SMC1). Activated p53 will induce expression of several genes involved either in cell cycle arrest or apoptosis. (Adapted from Campisi and d'Adda di Fagagna, 2007)

Like replicative senescence, OIS is often associated with activation of the DDR (Bartkova et al., 2006; Di Micco et al., 2006; Mallette et al., 2007). This is linked to DNA replication stress that might result from impaired or inappropriately activated origins of replication, although the exact mechanism has not yet been fully established (D'Adda di Fagagna et al., 2003). These findings raise the possibility that the DDR and OIS are causally linked. Indeed, RNA interference-mediated depletion of different DDR signal transduction components, including ATM and CHK2, allows for rescue of OIS (Bartkova et al., 2006; Di Micco et al., 2006; Mallette et al., 2007).

How then does the DDR contribute to OIS? For instance, in analogy to replicative senescence, the DDR could activate p53. Indeed, in all the settings where interference with the DDR allows a bypass from senescence, induction of the arrest is accompanied by p53 activation. This strongly suggests that the DDR and p53 function in a single signal transduction cascade. The close link between the DDR and p53 activation has other important implications with regard OIS. If all type of OIS would rely on DDR signalling for their onset and/or maintenance, one would expect that OIS is always accompanied by p53 activation. However, this is not the case in mice and in the context of several human senescent cells, suggesting that DDR activation is not a universal feature of OIS and that is involved in certain, but not all, OIS settings.

1.2.4 Occurrence of cellular senescence *in vivo*

During the paste decade cellular senescence has been shown to occur and to be important *in vivo*. Senescent cells, identified by senescence-associated markers, are found in many renewable tissues in humans and murine model (Michaloglou et al., 2005; Collado et al., 2005; Braig et al., 2005; Chen et al., 2005).

In line with theories that senescence *in vitro* is a correlate of ageing, several studies have provided direct evidence that senescent cells accumulate in ageing individuals (Campisi, 2005). It has been reported that in skin samples from human donors, there was an age-dependent increase in SA-β-GAL activity in dermal fibroblasts and epidermal keratinocytes (Dimri et al., 1995).

Moreover, it has been proposed that senescence can also contribute to age-related pathology. Atherosclerosis is accompanied by an induction of SA-β-GAL activity and telomere shortening (Minamano et al., 2002; Foreman and Tang, 2003).

In osteoarthritis senescent cells are also observed (Price et al., 2002).

Recently, also beneficial aspects of replicative senescence have been uncovered. In a mouse model of liver fibrosis, senescent cells are found, as evidenced by positivity for SA-β-GAL activity, $p16^{INK4a}$, p53, $p21^{CIP1}$ and HMGA1 (Krizhanovsky et al., 2008). These senescent cells derive from activated hepatocellular stem cells and limit the progression of fibrosis, supporting the speculation from Hayflick's experiments that replicative senescence limits tumorigenesis. The observation of senescent cells has been extended to many premalignant lesions or benign tissues induced by different activation or tumour suppressor inactivation in human and mouse.

Human melanocytic nevi, which frequently harbour activating BRAF or NRAS mutations, display several characteristics of senescence. Nevi are benign tumours that rarely progress towards melanoma, which is accompanied by the implementation of a long-term proliferation arrest in these lesions. In line with this, nevi contain very few cells that stain positively for the proliferation marker Ki-67. Instead, they display elevated expression of $p16^{INK4a}$ and SA-β-Gal senescence markers (Michaloglou et al., 2005). Similarly, human prostatic intraepithelial neoplasia (PIN) lesions as well as human colon adenoma express markers of senescence (Acosta et al., 2008; Kuilman et al., 2008).

Cellular senescence *in vivo* can also be triggered by the loss of a tumour suppressor gene. The tumour suppressor NF1 encodes a RAS GTPase activating protein that is a negative regulator of RAS activity. It has been shown that the absence of NF1 results in hyperactivated RAS signalling and the formation of neoplastic lesions, known as neurofibromas, which display markers of senescence (Courtois-Cox et al., 2006).

The observation of senescent cells has also been reported in mouse models. Serrano and colleagues described a "knock-in" mouse model in which oncogenic RAS was expressed at a physiologic level. Unexpectedly, most RAS-expressing cells in these

mice remained normal for a long period with no apparent defects in differentiation or signs of unchecked proliferation. Lung adenoma did emerge, but only after a long latency period. In these adenomas, a low proliferative index was accompanied with elevated levels of SA-β-Gal and increased expression of senescence markers (Collado et al., 2005). Similarly, RAS-driven mouse T-cell lymphomas entered senescence after drug therapy, when apoptosis was blocked. Senescence has also been observed in lung tumours and melanocytic nevi when using mice with endogenous $BRAF^{V600E}$ (Dankort et al., 2007; Dhomen et al., 2009). To study the role of $BRAF^{V600E}$ in non-small-cell lung cancers (NSCLCs) its expression was targeted to the lungs. At eight weeks $BRAF^{V600E}$–expressing mice displayed benign adenomas, which accumulated some senescence-associated markers. Interestingly, no adenocarcinomas were detected after six months in $BRAF^{V600E}$–expressing mice (Dankort et al., 2007). Similarly, transgenic expression of $BRAF^{V600E}$ in the melanocytic lineage drives the formation of nevi with several signs of senescence (Dhomen et al., 2009).

Pandolfi and co-workers found that cellular senescence can be triggered *in vivo* not only by oncogene activation, but also by inactivation of tumour suppressor. Loss of the tumour suppressor Pten, a phosphatase that opposes PI3K activity in murine prostate cells leads to the formation of PIN lesion with features of senescence (Chen et al., 2005).

1.2.4.1 Cellular senescence as a barrier to tumorigenesis

Tumorigenesis is a multistep process, in which a normal cell acquires mutations that allow it to avoid replicative and oncogene-induced senescence. These mutations typically occur in the p53 and p16-pRB pathways. By restricting cell proliferation and thereby impeding the accumulation of mutations, senescence acts as an important tumour suppressor mechanism. The first evidence derived from the analysis of

senescence in tumours is its close association with the pre-malignant stages of tumorigenesis. In fact, the identification of senescent cells was obtained from lung adenomas, pancreatic intraductal neoplasia, PIN lesions and melanocytic nevi, which are premalignant tumours (Collado et al., 2005; Chen et al., 2005; Michaloglou et al., 2005). By contrast, senescence was absent in their corresponding malignant stages.

Nonetheless, there are several evidences in which loss of senescence appears to be a crucial, albeit insufficient, step in the development of cancer. For example, genetically engineered mice that are deficient in a histone methyltransferase or p53 contain cells that fail to senescence in response to appropriate stimuli; these mice are cancer-prone (Braig et al., 2005; Chen et al., 2005; Donehower et al., 1992). Similarly, cells from patients with Li-Fraumeni syndrome, which carry mutations in p53 or CHK2, abrogate senescence and allow progression to malignant stages (Shay et al., 1993). These observations point to a causal link between loss of senescence and malignant transformation. All this evidence strongly suggests a role of senescence as a barrier to tumour progression, as a physiologic response that cells must overcome in order to divide indefinitely and develop into tumours (Figure 1.12).

However, it is not clear whether malignant tumours emerge from a senescent cell upon acquisition of an escape mutation or expand from a clone that *a priori* bypassed senescence. In addition, genetic defects that inactive senescence are necessary but insufficient for malignant tumorigenesis. In fact, the inactivation of $p16^{INK4a}$, $p21^{CIP1}$ or even p53 or pRB increases the replicative lifespan of human cells but does not transform them *per se* (Di Micco et al., 2006; Brown et al., 1997); thus, additional mutations might be required to establish cancer cells that eventually expand as a clinically relevant tumour mass (Figure 1.13).

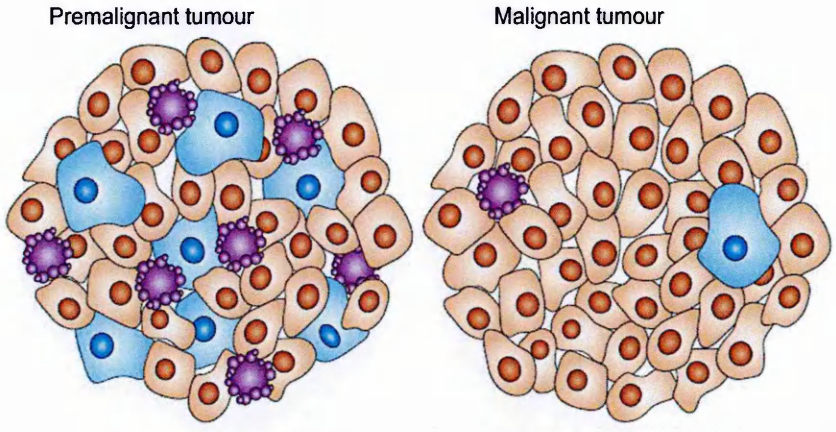

Figure 1.12 Senescence as a barrier to tumorigenesis. Premalignant lesions usually comprise of a heterogeneous population of tumour cells, some undergoing apoptosis (purple) others senescence (blue). These lesions may remain restricted in growth or if cells are able to override tumour suppressive mechanisms, tumour progression to a malignant state will be favoured. (Adapted from Collado and Serrano, 2006)

1.2.4.2 Cellular senescence as anticancer therapy

In light of the increasing evidence that senescence protects humans and other organisms against cancer, the idea to restore this process in tumour cells in which it has become deficient, represents an attractive therapeutic approach.

As mentioned above, senescence induced by oncogene activation or inactivation of tumour suppressor genes must be evaded for tumours to progress to malignancy, which is often associated with inhibition of senescence regulators. Considering the critical role of p53 in senescence onset and common occurrence of p53 mutations in cancer cells, p53 is an attractive target for reactivation of senescence in cancer cells. The feasibility of such an approach has been recently demonstrated. In a mouse model of hepatocellular carcinoma, reactivation of p53 in these tumours triggers senescence response and subsequent immune cell infiltration, which leads to clearance of tumour cells (Xue et al., 2007). Likewise, restoration of p53 in p53-deficient mouse models of lymphoma and osteosarcoma leads a rapid tumour regression (Ventura et al., 2007). In this context, the artificial expression of p53 induces senescence selectively in tumour

cells, leaving normal tissue completely unaffected. Thus, these models support the idea that drugs targeted at restoring p53 in tumours might be an effective manner to restrict tumour growth by inducing senescence and promoting tumour cell clearance. Such p53-restoring drugs are currently being developed and some of their preliminary results suggest that senescence could be an important outcome in cancer therapy (Efeyan et al., 2007; Kumamoto et al., 2008).

In addition to restoration of tumour suppressor genes, oncogene inactivation offers another possible intervention to induce senescence in cancer cells. Suppression of c-Mcy oncogene causes rapid regression accompanied by senescence in several tumours including hepatocellular carcinoma, lymphoma and osteosarcoma (Wu et al., 2007). These studies serve as proof of principle for the premise that reactivation of senescence is an efficient way to intervene with cancer.

Moreover, senescence-inducing drugs, attacking tumour cells, might prove effective alone or in combination with classic therapeutic approaches, and might reduce the toxicity of chemotherapy. It has been shown that primary murine lymphomas respond to chemotherapy by engaging a senescence program controlled by p53 and $p16^{INK4a}$ and this correlated with a better prognosis following chemotherapy (Schmitt et al., 2002). Senescence markers have been observed also in biopsies from patients with lung, breast or prostate cancer after chemotherapy (Roberson et al., 2005; te Poele et al., 2002; Coppé et al., 2008). This therapy-induced senescence is associated with treatment success.

However, it is conceivable that some cancer cells in a senescence-like state might remain as "dormant" tumour cells and therefore represent a dangerous potential for tumour relapse. The mechanisms that allow tumour cells to overcome this terminal arrest might contribute to anticancer drug resistance and tumour relapse.

In vivo observations suggest that escaping from drug-induced senescence is responsible, at least in part, for treatment failure.

As mentioned above, senescent cells secrete a complex mixture of secreted and extracellular factors usually referred to as the SASP or SMS. These components establish or reinforce the cell cycle arrest and contribute to tumour suppression by signalling to and recruiting the immune system (Acosta et al., 2008; Kuilman and Peeper, 2009). Secreted factors and their receptors are prototypic druggable molecules. Thus, it is feasible to manipulate components of the senescence secretome for prosenescence therapies. Despite increased knowledge on SASP composition and the existence of recombinant proteins, small molecules and antibodies to target these factors, there are not yet examples of prosenescence cancer therapies that use components of the senescence secretome, at either the experimental or the preclinical stage. A word of caution must be added as some factors of senescence secretome may also display protumorigenic activities stimulating malignant phenotype in nearby tumour cells (Coppé et al., 2008).

Overall, prosenescence therapies could be a new weapon for the fight against cancer.

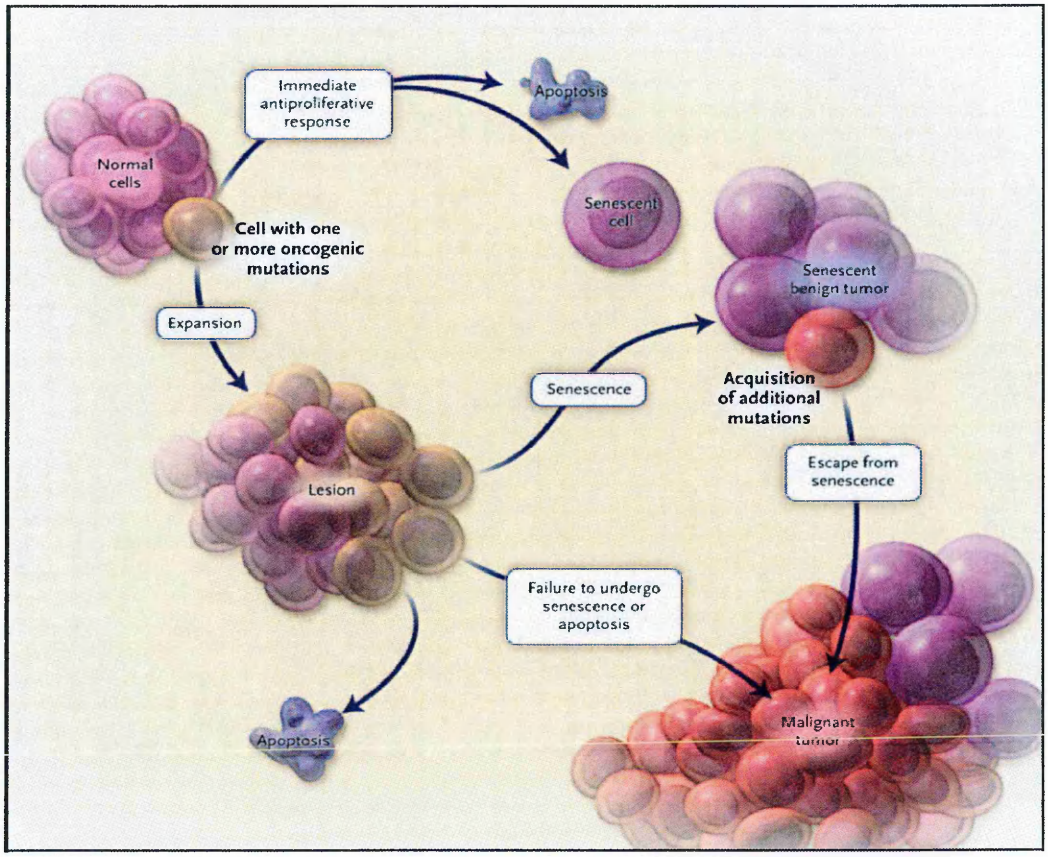

Figure 1.13 A model for tumour progression. Acquirement of an oncogenic mutation in normal cells can trigger three types of response. An antiproliferative response can be activated, leading to apoptosis or senescence. Alternatively, in the absence of an immediate response, the mutation-driven cell proliferation may produce a lesion. At this stage, both apoptosis and senescence might be activated. In the absence of appropriate defence mechanisms, continued growth with additional genetic events may lead to a malignant lesion.

Aim of the thesis

Oncogene induced senescence (OIS) acts as an important tumour suppressor mechanism. Overcoming senescence and acquiring a limitless replicative potential has been proposed to be one of the key events required for malignant transformation. In the last few years a flood of studies showed evidence of senescence in a plethora of benign lesions in mice and human. However, the underlying mechanisms that control senescence as well as the key players that are mechanistically involved remain poorly understood.

The aim of this work is to investigate the role of OIS in tumours originating from the thyroid epithelium. We provided evidence that the activation of thyroid tumour-associated oncogenes (BRAF, RAS, RET and TRK) triggers senescence in human primary thyrocytes as demonstrated by the presence of several hallmarks of senescence. With the aim to increase our understanding of the molecular principles of thyroid tumour progression we dissected the signalling transduction pathways and molecules regulating senescence in our cellular model. To achieve these goals, we combined classical biochemical and genetic approaches with more advanced techniques including loss-of-function RNA interference strategy and high content analysis. We next extended our findings obtained *in vitro* in humans examining a panel of thyroid lesions characterized by different aggressiveness.

In a nutshell, our data *in vitro* and *in vivo* demonstrated that OIS serves as a potent tumour suppressor mechanism limiting thyroid cancer progression.

CHAPTER 2

Chapter 2 - IGFBP7: an oncosuppressor gene in thyroid carcinogenesis

The insulin-like growth factor (IGF) axis plays a key role in the growth, differentiation, and proliferation of mammalian cells (Pollak et al., 2004). It consists of two growth factors (IGF-I and IGF-II), their receptors (IGF-IR and IGF-IIR), a group of IGF-binding proteins (IGFBP) and IGFBP proteases. IGF signalling, mediated by interaction with IGF-Rs, is modulated by IGFBPs, which influence IGF bioavailability (Burger et al., 2005). When bound to IGFs, IGFBPs function by regulating their transport between intra- and extra-vascular spaces and by interaction with their receptors (Zapf, 1995), resulting in prolonging IGF-I/II half life and precluding their mitogenic activity (Stewart and Rotwein, 1996).

Insulin-like growth factor-binding protein 7 (IGFBP7), also known as mac25 or IGFBP-related protein-1 (IGFBP-rP1) is a secreted protein belonging to the IGFBP family which includes six proteins (IGFBP-1 to IGFBP-6) that bind IGFs with high affinity and a group of ten IGFBP-related proteins (IGFBP-rPs) that bind IGFs with low affinity (Burger et al., 2005). IGFBP7 binds IGFs with low affinity, but recognizes insulin with high affinity, and thereby modifies its metabolism, distribution, and ability to bind to the insulin receptor (Yamanaka et al., 1997). IGFBP7 has also IGF/insulin independent actions (Kato, 2000). IGFBP7 is expressed in an ubiquitous fashion in normal tissues (Degeorges et al., 2000) and is inactivated by proteolytic processing (Ahmed et al., 2003). A large body of evidence suggests that IGFBP7 functions as an oncosuppressor gene in human prostate, breast, lung and colorectal cancer, as it regulates cell proliferation, cell adhesion, cellular senescence and angiogenesis (Akaogi et al., 1996; Sprenger et al., 1999; Wilson et al., 2002; Burger et al., 2005; Ruan et al., 2006; Chen et al., 2007; Sato et al., 2007).

IGFBP7 is silenced by promoter hypermethylation in several neoplastic tissues, including colorectal and gastric cancers (Ahmed et al. 2003; Kanemitsu et al. 2000; Lin et al. 2007).

More recently, IGFBP7 has been shown to mediate senescence in melanocytes, and to suppress melanoma growth *in vivo* by inducing apoptosis (Wajapeyee et al., 2008). Studies in mouse models have proposed IGFBP7 as a therapeutic agent for treatment of metastatic melanoma and colorectal tumours carrying RAS or BRAF mutations (Wajapeyee et al., 2009). However, the critical role of IGFBP7 in mediating $BRAF^{V600E}$-induced senescence in melanocytes has been challenged recently (Scurr et al., 2010).

In this work we investigate the role of IGFBP7 in PTC aiming to increase our understanding of molecular mechanisms underlying thyroid carcinogenesis. Analysis of expression levels in microarray datasets highlighted that IGFBP7 was dowregulated in a consistent fraction of PTC, with respect to normal thyroid. To address the functional consequences of IGFBP7 downregulation we used the PTC-derived NIM1 cell line, in which the expression of IGFBP7 is lacking. Exposure to soluble IGFBP7 protein or restoration of IGFBP7 expression by cDNA transfection reduced growth rate, migration, anchorage independent growth and tumorigenicity of NIM1 cells. We provide evidence that the effects of IGFBP7 are related to apoptosis. Overall, our data suggest that IGFBP7 gene exerts an oncosuppressor role in thyroid epithelial carcinogenesis.

2.1 Results

2.1.1 Expression of IGFBP7 in PTC

To examine the biological relevance of IGFBP7 in papillary thyroid carcinogenesis, its expression level in normal thyroid tissues or thyroid carcinomas was first analyzed on cDNA microarray data produced in our laboratory (Ferrario et al., 2008). As shown in Figure 2.1A, in comparison to IGFBP7 gene expression level in normal thyroid (9 samples), IGFBP7 transcripts were significantly downregulated in both FTC (11 samples) and PTC (31 samples) histotypes with a p-value <0.05. Downregulation of IGFBP7 affected a consistent fraction of PTC cases, with 16 out of 31, including 80% of tall cell (TC) variants, displaying expression levels lower than the lowest level of normal samples. To further analyze the role of IGFBP7 in PTC we used three independent, publicly available datasets of microarray gene expression data of thyroid PTC samples, all obtained using Affymetrix HG-U133 series platforms. In the Vasko dataset (Vasko et al., 2007), which included normal thyroid and microscopically dissected intratumoral samples of PTC from four patients, both central and invasive regions displayed reduced expression of IGFBP7 transcripts ($p<0.01$) with both 201162_at and 201163_at probe sets, in comparison to the normal region (Figure 2.1B). In the Giordano dataset (Giordano et al., 2005) significantly reduced expression of IGFBP7 ($p<0.05$) was observed in the TC variants (10 TC out of 26 total PTC) when compared to normal thyroid with one of the two probe sets (201162_at). Even for the second probe set, however, 40% of TC variants displayed hybridization values lower than the lowest level of normal samples (Figure 2.2A). In the He dataset (He et al., 2005), PTC displayed a reduced IGFBP7 expression when compared to unaffected thyroid tissues from the same patients in 5 out of 9 cases with both probe sets (201162_at and 201163_at) but did not reach statistical significance (Figure 2.2B).

Overall these results suggest that expression of IGFBP7 is downregulated in a consistent fraction of PTC with respect to normal thyroid.

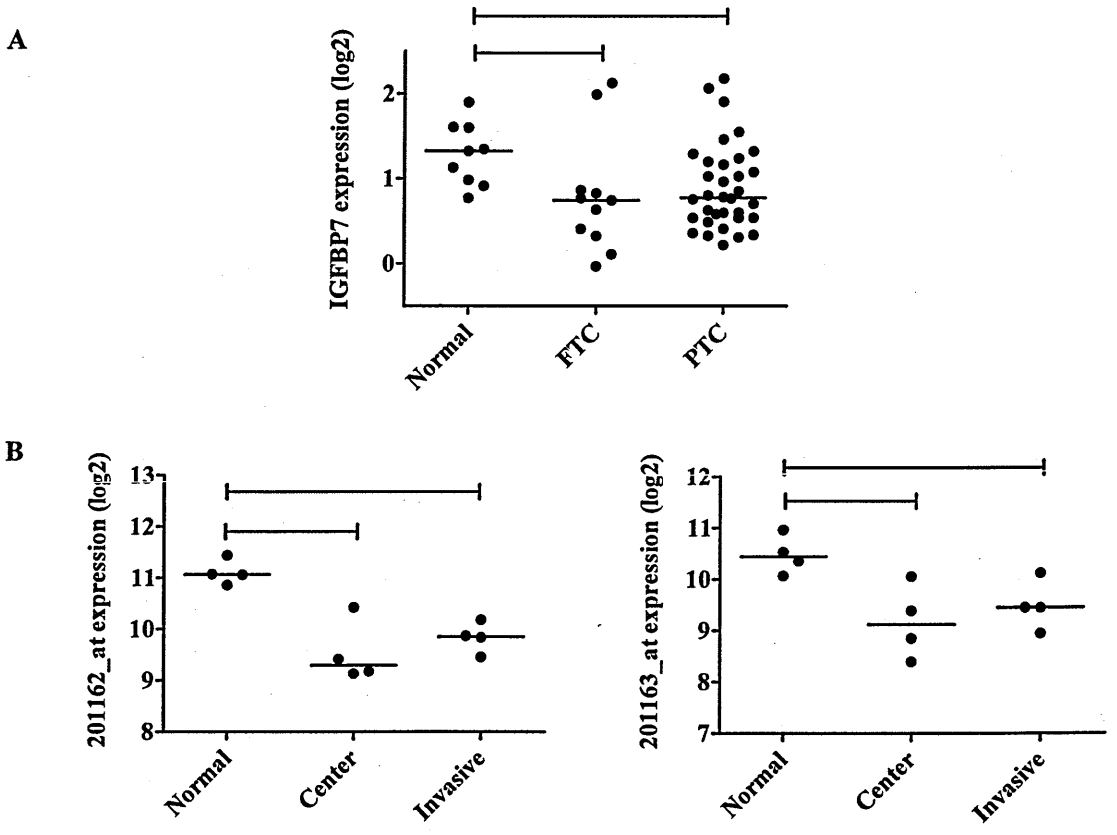

Figure 2.1 IGFBP7 gene expression levels in PTC in two different data sets. Data are reported as scatter plots of log2 values and median is recorded. **A)** Our data set: FTC and PTC thyroid carcinoma presented a significantly lower IGFBP7 expression as compared with normal thyroid samples. IGFBP7 relative expression values were measured as log2 ratio between expression level of the specimen and that of the reference. $*$ = $p<0.05$ by Kruskal-Wallis followed by multiple comparisons post-tests.
B) Vasko dataset: central and invasive area of PTC display reduced expression of IGFBP7 when compared to the normal thyroid in paired tissue samples. Expression values relative to the two different IGFBP7 probe sets (201162_at, left panel and 201163_at, right panel) are shown. $**$ = $p<0.01$ by one-way ANOVA followed by multiple comparisons post-tests.

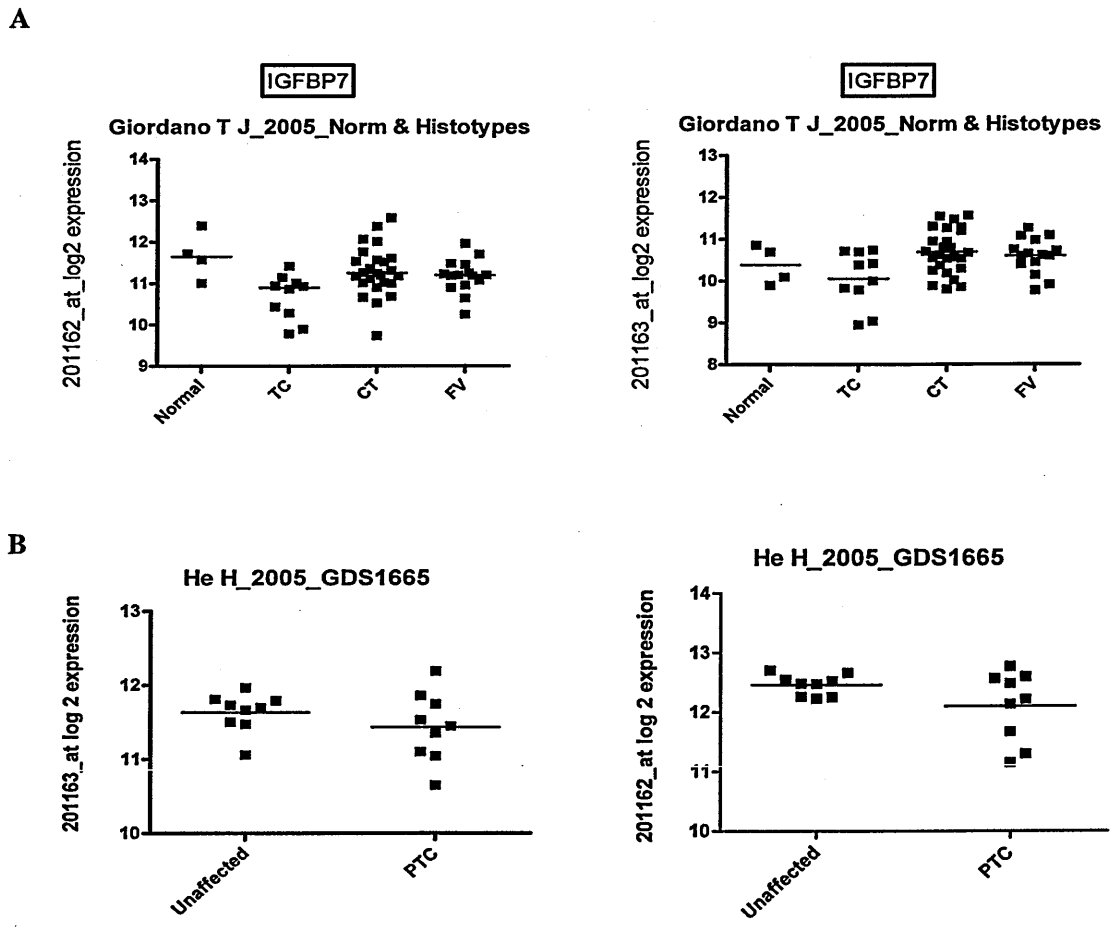

Figure 2.2 Two different data sets showing IGFBP7 gene expression levels in PTC. A) Giordano dataset: 51 PTC samples including 26 classic PTC types, 15 follicular variants (FV), 10 tall cell variants (TC) and 4 normal thyroid tissues were compared. **B)** He dataset: PTC samples from 9 patients showed reduced IGFBP7 expression when compared to unaffected thyroid tissue samples. Expression values relative to the two different IGFBP7 probe sets (201162_at, left panel and 201163_at, right panel) are shown.

2.1.2 Expression analysis of IGFBP7 in thyroid tumour cell lines

To further explore the role of IGFBP7 in thyroid carcinogenesis we investigated its expression in several thyroid tumour cell lines, including PTC-derived (TPC1, NIM1, BCPAP and K1) and ATC-derived (BHT and KAT4) cell lines. Except for TPC1, which carries the RET/PTC1 oncogene, all the other cell lines harbour the $BRAF^{V600E}$ mutation. As control the melanoma SKMEL-31 cell line, known to express IGFBP7, was used (Wajapeyee et al., 2008). As IGFBP7 is a secreted protein, its presence in the conditioned medium (CM) was investigated. For each cell line an aliquot of CM

corresponding to $4x10^5$ cells was analyzed by Western blot with anti-IGFBP7 antibodies. Expression of IGFBP7 protein was strong in BCPAP, K1 and BHT cell lines, reduced in TPC1 and KAT4, and undetectable in NIM1 cell line (Figure 2.3A). The lack of expression of IGFBP7 in NIM1 cells was due to the absence of the relative mRNA, as demonstrated by RT-PCR (Figure 2.3B). Treatment with the demethylating agent 5-Aza-2'Deoxycitidine (5-Aza-dC) restored the IGFBP7 mRNA expression, indicating that the lack of IGFBP7 protein in NIM1 cells is caused by promoter DNA hypermethylation.

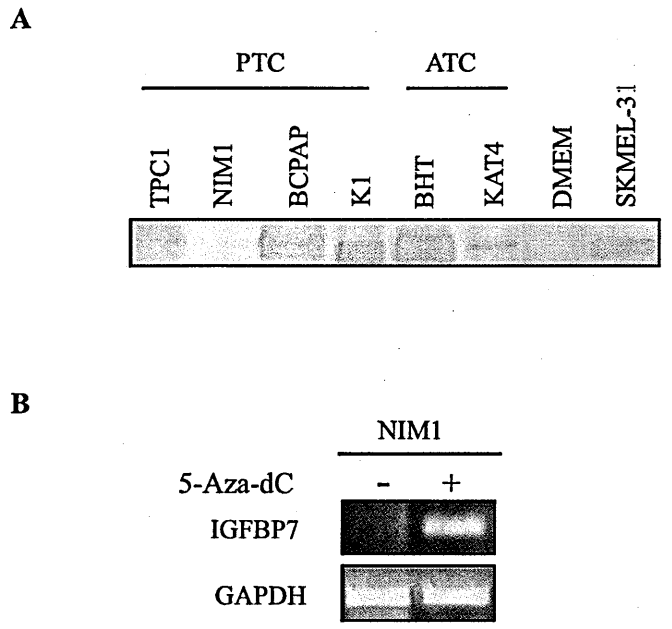

Figure 2.3 IGFBP7 expression in thyroid cell lines. A) Immunoblot analysis monitoring IGFBP7 protein levels in the conditioned medium (CM) from a panel of thyroid carcinoma cell lines. SKMEL-31 cell line was used as a positive control for IGFBP7 expression. **B)** Expression of IGFBP7 mRNA in NIM1 cells in the absence (-) or presence (+) of 5-Aza-dC treatment detected by RT-PCR. GAPDH gene expression served as loading control.

2.1.3 IGFBP7 reduces NIM1 cells growth rate

To investigate the potential pathogenic role of IGFBP7 in PTC, we produced an *in vitro* model of thyroid cancer based on the restoration of the IGFBP7 expression in NIM1 cells. The latter, derived from a PTC, harbour the $BRAF^{V600E}$ mutation and are tumorigenic in nude mice (Zeki et al., 1993). As first approach, we determined the growth rate of NIM1 cells exposed to CM from K1 cell line, expressing IGFBP7 (Figure 2.4A), or to their own CM. The experiment reported in Figure 2.4A shows that growth rate of NIM1 cells exposed to IGFBP7-containing medium is reduced with respect to control. The reduction was evident at day 2, and accounted for 47% at day 4. To verify whether the inhibitory effect of the K1 CM is due to the presence of IGFBP7 we performed an immunodepletion with anti-IGFBP7 antibodies. Although the immunodepletion did not remove completely IGFBP7 from K1 CM (Figure 2.4A, inset), we observed a partial restoration of the NIM1 cells growth.

We next investigated the effect of restoration of IGFBP7 expression in NIM1 cells by cDNA transfection. To this end, NIM1 cells were transfected with a plasmid expression vector containing the IGFBP7 cDNA in frame with myc epitope or the empty vector, and selected in G418. NIM1 cells transfected with IGFBP7 expression vector produced G418-resistant colonies smaller than those obtained with the empty vector (Figure 2.4B), supporting the notion that IGFBP7 protein negatively regulates NIM1 growth rate. Several NIM1-IGFBP7 clones were isolated and analyzed; in 6 out of 12 the expression of the IGFBP7 protein was detected at variable levels in the CM (Figure 2.4C). The growth rate of three clones expressing different level of IGFBP7, namely NIM1-I2, NIM1-I11, and NIM1-I13 was determined (Figure 2.4D). For all the clones a growth decrease with respect to parental NIM1 cells was observed, and such decrease correlated with the expression level of IGFBP7 protein. In fact at day 5, growth rate was reduced of 39% for NIM1-I11, of 59% for NIM1-I13, of 66% for NIM1-I2.

Overall these data demonstrate that IGFBP7 negatively regulates growth of thyroid tumour cells.

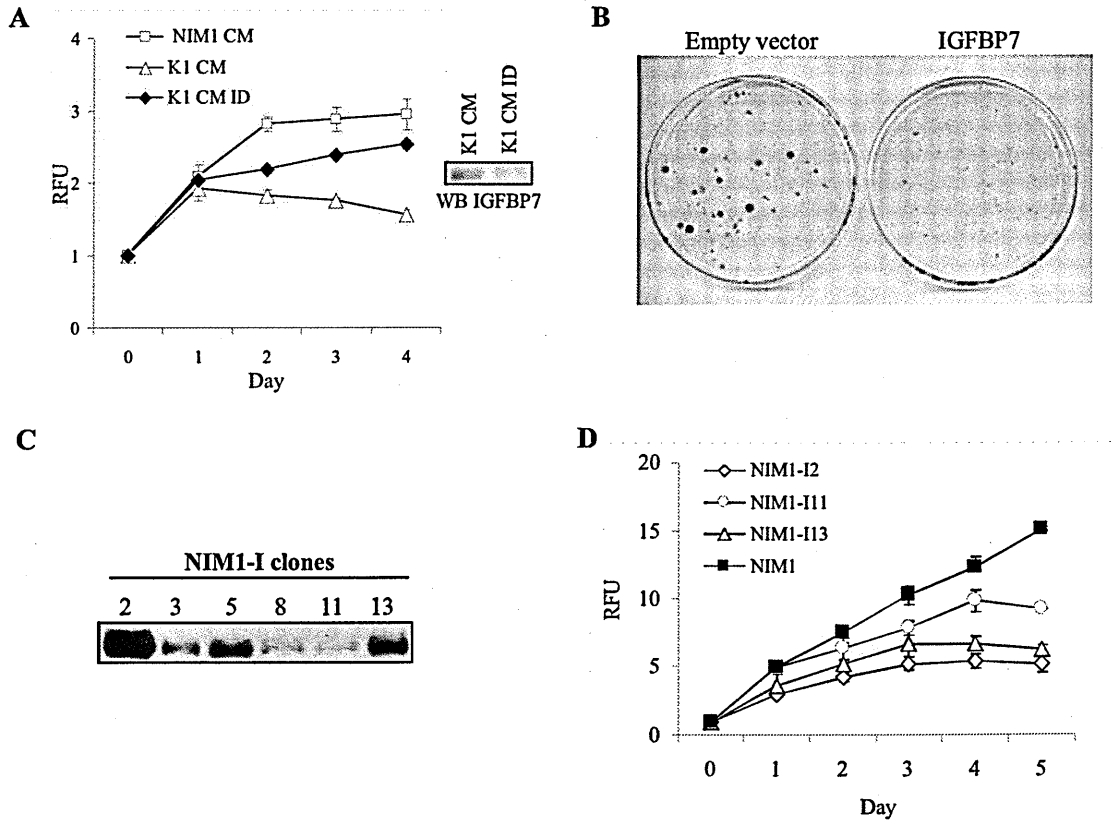

Figure 2.4 Effect of IGFBP7 re-expression on NIM1 cells growth. A) Growth curves of NIM1 cells in the presence of conditioned medium (CM) taken from K1 cell line expressing IGFBP7 (K1 CM) or immunodepleted (K1 CM ID) with an anti-IGFBP7 antibody. At the indicate time points the growth rate was determinated by alamarBlue®Assay. CM from parental NIM1 cells was used as control (NIM1 CM). RFU: relative fluorescence units. The inset shows the efficiency of immunodepletion determined by Western blot analysis of CM. **B)** Colonies formed by NIM1 cells transfected with the empty vector (NIM1-EV) or the IGFBP7 expression vector (NIM1-IGFBP7). Forty-eight hours after transfection 4000 cells were seeded on 10 cm Petri dishes and subjected to G418 (400 μg/ml) selection; colonies were fixed and stained after 2 weeks. **C)** Detection of IGFBP7 protein in the CM of NIM1 cells stably transfected with IGFBP7 construct by Western blot analysis with anti-IGFBP7 antibodies. **D)** Growth rate of three NIM1-IGFBP7 clones (NIM1-I2, NIM1-I11, NIM1-I13 expressing different levels of IGFBP7) evaluated by alamarBlue®Assay. Parental NIM1 cells were used as a control.

2.1.4 IGFBP7 reduces anchorage-independent growth and migration of NIM1 cells

Tumour cells display the capability to grow in the absence of adhesion. We wondered whether this feature in NIM1 cells is affected by IGFBP7 by performing soft agar assay. For these experiments we used clones NIM1-I2, NIM1-I5 and NIM1-I13, all producing high but variable levels of IGFBP7 protein (Figure 2.4C); as control, the NIM1-EV clone, transfected with empty vector, was used. As shown in Figure 2.5A, the colonies formed by NIM1-IGFBP7 clones were smaller than those formed by the control cells. In addition, NIM1-IGFBP7 clones formed colonies with efficiency reduced with respect to the control; reduction accounted to 82 % for NIM1-I2, 67% for NIM1-I5, and 75% for NIM1-I13 (Figure 2.5B).

We next analyzed the migration capability of NIM1-IGFBP7 clones by the wound healing assay; as control, the NIM1-EV clone was used. The wound healing was monitored between 4 and 24 hours, and the wound closure rate was calculated 4 and 8 hours after scratching (Figure 2.6). All the NIM1-IGFBP7 clones showed reduced wound healing capability with respect to empty vector transfected NIM1 cells. Such reduction ranged from 30% to 35% 4 hours after scratching, and from 31% to 51% 8 hours after scratching. The wound of control cells was completely healed after 8 hours (Figure 2.6), whereas for NIM1-IGFBP7 clones the scratch was not yet closed within 24 hours.

2.1.5 IGFBP7 reduces tumorigenicity of NIM1 cells

We next asked whether re-expression of IGFBP7 could affect the *in vivo* growth of NIM1 cells. To this end, NIM1-IGFBP7 clones and NIM1 cells were injected into nude mice at two different cell concentrations (Table 2.1). In mice injected with $2x10^6$ cells, tumour growth was observed in 3/3 mice injected with NIM1 cells, whereas no tumour growth occurred in those injected with NIM1-IGFBP7 clones. When $5x10^6$ cells were

injected, no take was observed in mice xenografted with NIM1-I2 cells. In mice injected with NIM-I5 and NIM1-I13 cells, 3/3 takes were observed, but regression occurred in 1/3 animal for each clone; in the remaining animals tumours grew slower than NIM1 tumours.

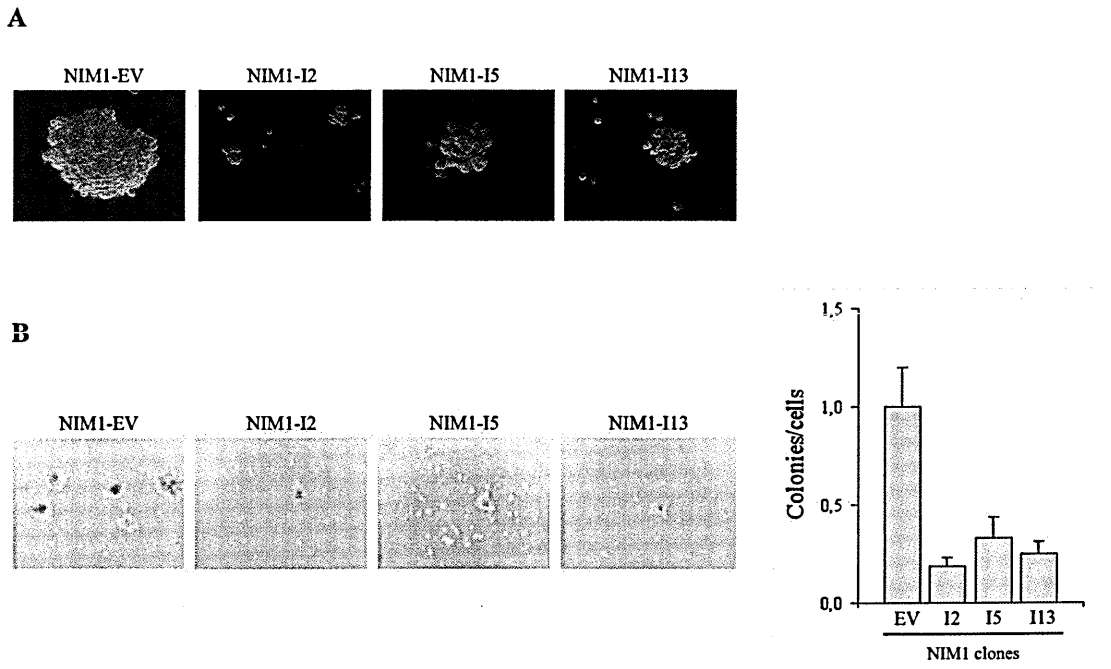

Figure 2.5 Anchorage-independent growth of NIM1-IGFBP7 transfected and control cells. A-B) Representative pictures of colonies formed by NIM1-IGFBP7 clones and control cells after 21 days of incubation in soft agar are shown (magnification 4X). **B)** Colony forming efficiency of NIM1-IGFBP7 clones was determined by the ratio between number of colonies and number of cells, and normalized to that of control NIM1-EV clone. Bars represent standard deviation.

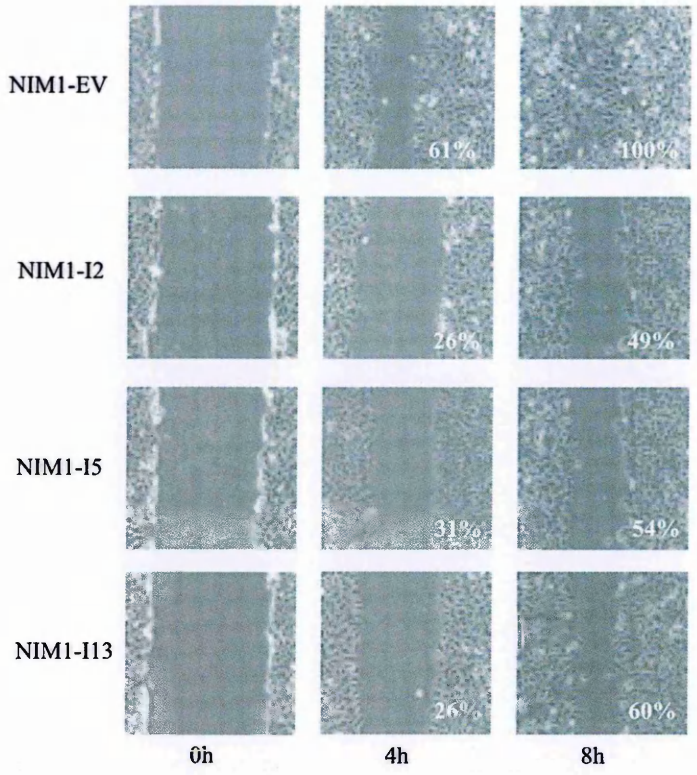

Figure 2.6 Effect of IGFBP7 re-expression on migration capability of NIM1 transfected and control cells. Migration of NIM1-IGFBP7 clones (NIM1-I2, NIM1-I5, NIM1-I13) and empty vector transfected clone (NIM1-EV) was analyzed by wound healing assay. Representative images of the wound captured at 0, 4, 8 hours are shown. In each panel the percentage of migration, determined by dividing the migrated distance by the scratched distance, is indicated.

Table 2.1 *In vivo* tumour growth[a]

Cell line	$2x10^6$ cells	$5x10^6$ cells			
	Tumor-bearing mice	*Tumor-bearing mice*	*Regression*	*Days at 0.1g*	*Days at 1g*
NIM1	3/3	6/6	0/6	<8	11(7-40)
NIM1-I2	0/3	0/3	-	-	-
NIM1-I5	0/3	3/3	1/3	<8	22,41
NIM1-I13	0/3	3/3	1/3	<8	14,59

[a]NIM1-IGFBP7 clones and parental NIM1 cells were inoculated subcutaneously into the left flank of athymic nude mice. Tumor growth was monitored twice a week from day 8 to day 60.

2.1.6 IGFBP7 impairs cell cycle progression and modulates ERK activation, p21 and p53 expression

To explore the mechanisms by which IGFBP7 negatively regulates the growth of NIM1 cells we performed cell cycle phase distribution of transiently transfected NIM1 cells through flow cytometric analysis. As shown in Figure 2.7A, re-expression of IGFBP7 in NIM1 cells increased the percentage of cells in G1 (84%) compared with the empty vector transfected NIM1 cells (65%) with a consequent decrease of the percentage of cells in S phase (8% in NIM1-IGFBP7 versus 24% in control) as evaluated by DNA content analysis (Figure 2.7A). The G1 arrest caused by IGFBP7 was associated with a strong decline of phospho-ERK (pERK) levels and an up-regulation of p53 and p21 tumour suppressors (Figure 2.7B). IGFBP7-transfected NIM1 cells compared to the control displayed 70% reduction of pERK levels, and an increase of p53 and p21 expression of 49% and of 54%, respectively, as assessed by densitometric analysis (Figure 2.7B).

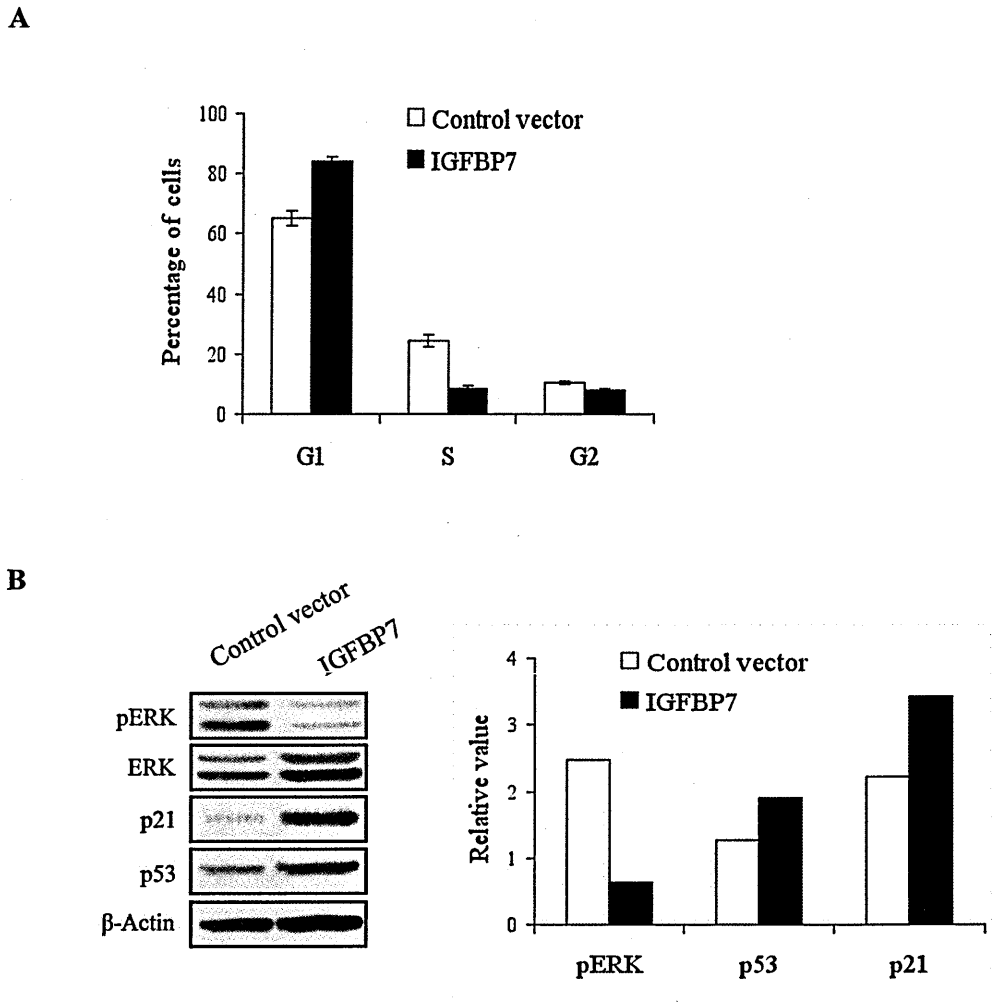

Figure 2.7 Analysis of cell cycle, ERK activation, p53 and p21 levels in NIM1-IGFBP7 transfected cells. Cells were transfected with either empty vector (vector) or IGFBP7 expression vector (IGFBP7), and analyzed 3 days after transfection. **A)** Quantification of the percentage of cells in different stages of the cell cycle as analyzed by flow cytometry assay. The data represent the average of three independent experiments. **B)** Western blot analysis with the antibodies against phosphorylated ERK or ERK, p53 and p21. β-Actin was used for normalization of gel loading. Band intensity was assessed by densitometry to evaluate the ratio between phosphorylated ERK and total ERK, p53 and β-Actin, p21 and β-Actin.

2.1.7 IGFBP7 mediates cell growth suppression through induction of apoptosis

We next wondered whether the effects induced by IGFBP7 in NIM1 cells could be related to apoptosis. To this end, we analyzed the capacity of IGFBP7 to induce apoptosis, alone or in combination with TRAIL, a proapoptotic agent effective in NIM1 cells, by determining the levels of cleaved PARP. We observed that IGFBP7 transiently

transfected NIM1 cells exhibited higher levels of cleaved PARP compared with empty vector transfected cells (Figure 2.8A). Exposure to TRAIL (50ng/ml for 5 hours) generated a higher induction of apoptosis in IGFBP7 transfected NIM1 cells with respect to the control (Figure 2.8A), suggesting that IGFBP7 may cooperate with other stimuli in inducing apoptosis. These observations were also confirmed by analyzing the levels of cleaved PARP in NIM1-IGFBP7 clones (Figure 2.8B). In clone NIM1-I2, expressing the highest amount of IGFBP7 protein (Figure 2.4C), cleaved PARP was observed in untreated cells, and it was strongly induced by TRAIL treatment. Clones NIM1-I5 and NIM1-I13, both expressing lower amount of IGFBP7 protein with respect to NIM1-I2, displayed low levels of cleaved PARP, which increased after TRAIL exposure. In the control cells, cleaved PARP was detectable after TRAIL treatment, but to a lesser extent with respect to NIM1-I5 and NIM1-I13 in the presence of TRAIL.

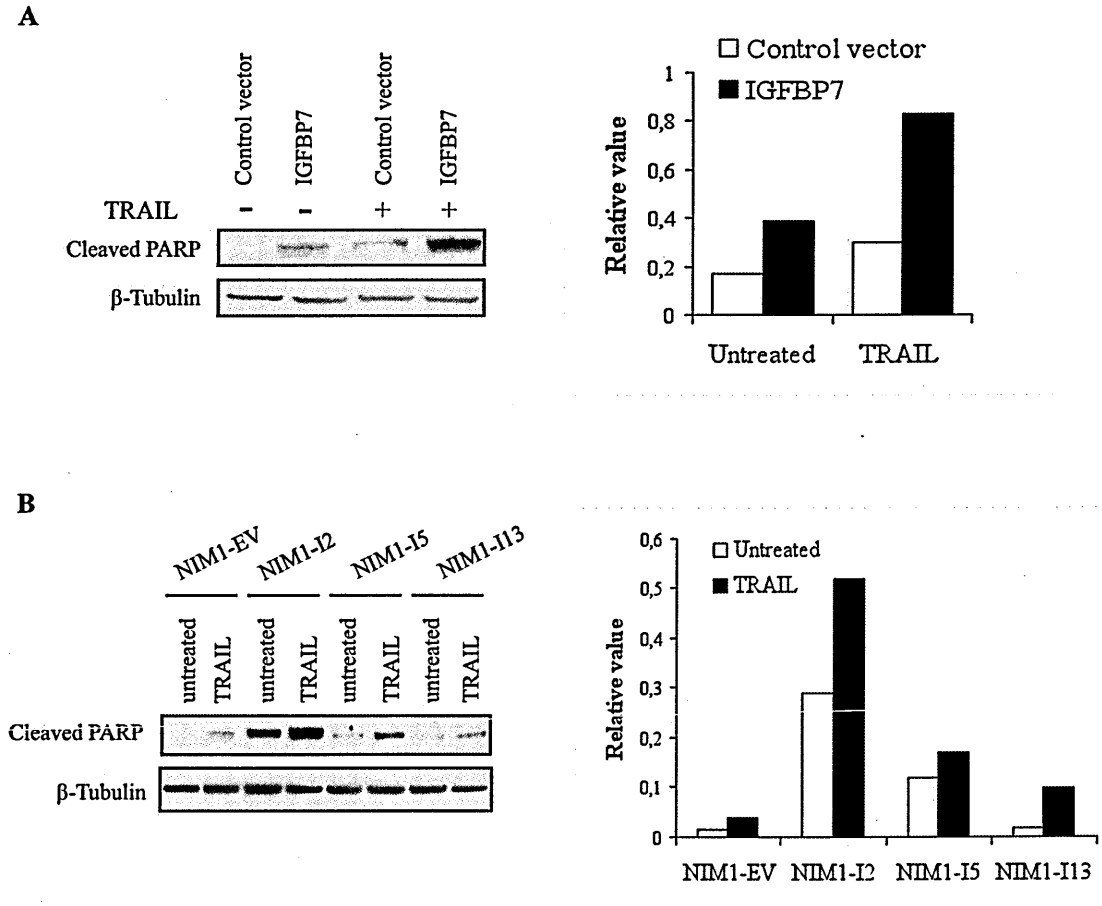

Figure 2.8 Detection of apoptosis in NIM1-IGFBP7 transfected and control cells. Untransfected or transiently transfected cells (**A**) or NIM1-IGFBP7 and NIM1-EV clones (**B**), treated or not with TRAIL (50 ng/ml for 5 hours) were analyzed for the expression of cleaved PARP by Western blot with cleaved PARP antibodies. β-Tubulin was used for normalization of gel loading. Band intensity was assessed by densitometry to evaluate the ratio between cleaved PARP and β-Tubulin.

2.2 Discussion

We have shown that IGFBP7 protein exerts a negative regulation on thyroid tumour cells. By analysis of gene expression data produced in our laboratory we have detected significant reduction of IGFBP7 gene expression in both FTC and PTC. Down regulation of IGFBP7 gene in PTC compared to normal thyroid was also observed in different, publicly available gene expression datasets. This *in silico* analysis even indicated that IGFBP7 downregulation is associated to the TC variant of PTC.

Silencing of IGFBP7 gene in melanoma was originally found associated with the $BRAF^{V600E}$ mutation (Wajapeyee et al., 2008). However, such correlation was not confirmed by subsequent studies showing loss of IGFBP7 expression regardless of BRAF status (Schrama et al., 2009; Wajapeyee et al., 2009). In colorectal cancer loss of IGFBP7 has been associated to $BRAF^{V600E}$ mutation by two different studies (Hinoue et al., 2009; Suzuki et al., 2010). Our gene expression analysis indicates the absence of correlation between loss of IGFBP7 and $BRAF^{V600E}$ mutation in thyroid carcinoma. In keeping with this, among 5 cell lines carrying the $BRAF^{V600E}$ mutation, only 2 showed downregulation of IGFBP7 expression.

To determine whether IGFBP7 contributes to thyroid carcinogenesis we used the NIM1 cell line, derived from a PTC carrying the $BRAF^{V600E}$ mutation, in which the expression of IGFBP7 gene is abrogated by promoter hypermethylation. Several lines of evidence suggest that restoration of IGFBP7 in NIM1 cells interferes with cell growth. Reduction of growth rate was in fact detected in NIM1 cells exposed to soluble IGFBP7 and in clones obtained by stable transfection with an IGFBP7 expression vector. We provided also evidence that IGFBP7 interferes with other tumour cell properties, such as anchorage-independent growth and migration capability: both of them were reduced in NIM1 clones stably expressing the IGFBP7 protein.

In vivo experiments showed that restoration of IGFBP7 expression reduces the NIM1 cells capability to induce tumour formation in mouse xenografts.

IGFBP7 negatively regulates NIM1 cell growth by triggering apoptosis. Concomitantly to growth inhibition and attenuation of ERKs signalling, we observed upregulation of p53 and p21, which led to G1 arrest and apoptosis in IGFBP7-expressing NIM1 cells. Altogether our data propose IGFBP7 as a tumour suppressor in thyroid carcinogenesis.

As mentioned in chapter 1, IGFBP7 has been identified as a mediator of oncogene-induced senescence in benign nevi. Loss of IGFBP7 expression accounts for uncontrolled proliferation of melanoma; addition of IGFBP7 to melanoma cells inhibits ERK signalling and activates apoptosis (Wajapeyee et al., 2008). The capacity of IGFBP7 to induce apoptosis has been also demonstrated in cell lines derived from different tumour types, such as colorectal, prostate, lung (Chen et al., 2007; Ruan et al., 2007; Sprenger et al., 1999). More recently, IGFBP7 has been proposed as an efficacious agent for treating malignancies that are dependent on BRAF-MEK-ERK signalling (Wajapeyee et al., 2009).

Our study provides evidence that apoptosis is also involved in the suppressor effects of IGFBP7 in thyroid tumour cells. In our experimental system IGFBP7 was capable to induce apoptosis and to potentiate the apoptotic effect of TRAIL. The mechanisms of apoptosis are highly complex, involving energy dependent cascade of molecular events. Two main apoptotic signalling pathways have been delineated: the intrinsic and extrinsic pathways. TRAIL has been shown to mediate the extrinsic pathway of apoptosis by binding to two transmembrane receptors, TRAILR1 and TRAILR2 (Wang and El-Deiry, 2003). However, the intrinsic pathway involves mitochondria and is triggered and controlled by members of the Bcl-2 protein family. Both pathways converge at caspase 3, leading to activation of others proteases, including PARP (Taylor et al., 2008).

In light of this crosstalk, further studies on the involvement of which signalling cascades leading PARP cleavage might be important for a better characterization and understanding of cellular apoptotic events induced by IGFBP7. Moreover, the capacity of IGFBP7 to induce senescence in primary cells and apoptosis in tumour cells supports the notion that cancer cells that have bypassed senescence are in general more susceptible to apoptosis (Lowe et al. 2004).

The molecular events underlying thyroid cancer initiation and progression have been in part elucidated. Nevertheless, a role for tumour suppressor genes in thyroid carcinogenesis has not been assessed yet. Several recent studies highlight the power of gene expression analysis as a tool for the identification, among others, of putative oncosuppressor genes. In the last few years, in fact, some genes identified as downregulated in the context of gene expression studies, were classified as tumour suppressors by functional studies, as their re-expression modulated transformed properties of thyroid carcinoma cell lines. Restoration of MT1G (Ferrario et al., 2008), CBX7 (Pallante et al., 2008), ABI3BP (Latini et al., 2008), TIMP3 genes (Anania et al., 2011), or IGFBP7 (present study) in thyroid tumor cell lines lacking their expression affected cell growth and transformed properties.

The downregulation of IGFBP7 gene expression in PTC raises the attractive hypothesis that oncogene-induced senescence might represent a relevant mechanism in thyroid carcinogenesis. The involvement of IGFBP7 in mediating senescence in our cellular system is reported in chapter 3.

2.3 Materials and methods

2.3.1 Microarray datasets and statistical analysis

The expression of IGFBP7 was examined on microarray datasets containing normal thyroid tissues and PTC. One dataset, generated in our laboratory from cDNA microarray hybridization, contains the expression profile data of 45 thyroid samples collected at the Department of Pathology of our Institute. Sample collection includes: 9 normal thyroid tissues, 11 FTC and 34 PTC. The PTC collection (24 classical types and 10 TC variants) consists of cases carrying $BRAF^{V600E}$ mutation (12 samples), RET/PTC rearrangements (7 samples), TRK rearrangements (2 samples), none of the above genetic lesions (13 samples). The details of gene expression analysis have been previously reported (Ferrario et al. 2008). The other datasets are publicly available and all derived from experiments using HG-U133 series microarrays (Affymetrix, Santa Clara, CA, USA). These datasets contained data obtained from: a) 51 PTC samples (including 26 classical types, 15 follicular variants, 10 TC variants) and 4 normal thyroid tissues (Giordano et al. 2005); among PTC samples, 25 carry the $BRAF^{V600E}$ mutation, 6 RAS mutations, 1 RET/PTC rearrangement; 19 samples none of the above genetic lesions; b) paired PTC and unaffected thyroid tissue samples from 9 patients (He et al. 2005); c) paired central and invasive region of PTC and normal tissue from 4 patients (Vasko et al. 2007). RMA normalized data were extracted from the NCBI Gene Expression Omnibus database (GSE3467 for the He dataset and GSE6004 for the Vasko dataset) or from the author's website (Giordano dataset). All IGFBP7 probe sets were considered for expression analysis. Statistical analysis and graphs were generated using GraphPad Prism version 5.0. Comparison between two groups was performed by the non parametric Mann-Whitney or, in case of matched samples by Wilcoxon tests.

Comparison between three or more groups was performed by ANOVA followed by multiple comparisons post-tests. A p-value <0.05 was considered significant.

2.3.2 RNA extraction and RT-PCR

Total RNA was extracted using TRIZOL reagent (Invitrogen, Carlsbad, CA), according to the manufacturer's instructions. One microgram of RNA was retro-transcribed using SuperscriptIII (Invitrogen, Carlsbad, CA) with random examers. Quality of RT reactions was monitored by PCR amplification of the housekeeping gene glyceraldehyde-3 phosphate dehydrogenase (GAPDH) using primers 5'-ACCATCTTCCCAGGAGCGAGAT-3' and 5'-GGCAGAGATGATGACCCTTT-3', producing a 142 nucleotides fragment. After a denaturation at 94°C for 2 min, 35 PCR cycles were performed (94°C for 1 min, 54°C for 1 min, 72°C for 1 min), followed by a final extension at 72°C for 2 min. For IGFBP7 amplification the following primers were used: 5'-TGGGTGCTGGTATCTCCTCT-3' and 5'-TATAGCTCGGCACCTTCACC-3', producing a 154 nucleotides fragment. After a denaturation at 95°C for 7 min, 35 PCR cycles were performed (95°C for 1 min, 56°C for 40 s, 72°C for 1 min) followed by a final extension at 75°C for 5 min. PCR reactions were performed in a total volume of 20 µl containing 15 ng of single strand cDNAs, 1xPCR buffer, 1.0 mM $MgCl_2$, 200 µM each dNTP, 0.5 µM each primer and 0.25U of AmpliTaq-Gold polymerase (Applied Biosystem, Foster City, CA, USA). PCR products were separated on 2% agarose gel.

2.3.3 IGFBP7 expression vector preparation

The IGFBP7 cDNA was obtained from HeLa cells by RT-PCR using the following primers: 5'-CCG**GAATTC**CTGCCACCGCACCCCGCCAT-3' and 5'-GCCC**AAGCT**TTAGCTCGGCACCTTCACCTT-3' encompassing the IGFBP7

coding region and containing, respectively, the EcoRI and HindIII restriction sites (bold). The 923 nucleotides PCR product was digested with EcoRI and HindIII endonuclease and inserted into the pcDNA3.1/mycHis(-)A vector carrying compatible ends. The resulting construct encodes the IGFBP7-myc fusion protein.

2.3.4 Cell culture, transfection and treatments

The following thyroid tumour cells were used: TPC1, NIM1, BCPAP and K1, derived from PTC; BHT and KAT4, derived from ATC; SK-MEL 31, derived from melanoma. All thyroid tumour cells were maintained at 37°C, 5% CO_2 humidified atmosphere; K1 cell line was cultured in DMEM:HAM'S F12:MCDB 105 (2:1:1) with 2mM glutamine and 10% fetal calf serum (FCS). All the other thyroid carcinoma cell lines were maintained in DMEM medium containing 10% FCS, 2 mM glutamine and 100U/ml penicillin/streptomycin. SK-MEL 31 cells were cultured in MEM Eagle's supplemented with 10% FCS at 37°C, 10% CO_2 humidified atmosphere.

Transient and stable transfection of NIM1 cells was performed using Lipofectamine LTX (Invitrogen, Carlsbad, CA). Cells ($4x10^5$) were seeded in 60mm dishes, cultured for 24 hours and transfected with 2 μg of plasmid DNA (pcDNA3.1/IGFBP7-myc or pCDNA3.1-myc, as control) and 5 μl of LTX, according to the manufacturer's instructions. After 48 hours transfected cells were either harvested and processed, or subjected to G418 (Lifetechnologies, Invitrogen, Carlsbad, CA) selection (400 μg/ml). After 2 weeks of selection G418-resistant colonies were either fixed and stained, or isolated and propagated in G418-containing medium.

For the 5-Aza-dC (Sigma Aldrich, St. Louis, MO, USA) treatment, $6x10^5$ NIM1 cells were seeded in 100 mm dishes and treated with 5 μmol/L of 5-Aza-dC 24 hours later. After 3 days of treatment, cells were harvested and processed for RNA isolation. For TRAIL (Genentech Inc, USA) treatment, $4x10^5$ cells were seeded in 60 mm dishes and

exposed to 50 ng/ml TRAIL 24 hours later. After 5 hours of treatment both attached and floating cells were collected and processed for protein extraction.

2.3.5 Immunodepletion of IGFBP7

Conditioned medium (CM) from K1 cell line was collected and incubated with 2 µg/ml of IGFBP7 antibodies for 2 hours at 4°C with rotation. Afterwards, 1 ml aliquot was incubated with 50 µl of protein A agarose beads (previously washed once with PBS and once with serum-free medium) for 24 hours at 4°C with rotation. After centrifugation the supernatant was filtered through a 0.22 µM Millipore filter and added to the cells.

2.3.6 Growth curves

Growth curves were determined by alamarBlue®Assay (Biosource, Nivelles, Belgium). Cells were plated in sextuple in 96-well multiwell (400 cells/well). After adhesion of cells the alamarBlue reagent was added to the medium at 10% v/v. The fluorescence at λ = 590 and 535 nm was detected every 24 hours from day 1 to day 5, using a microplate reader (TecanUltra Tecan Trading AG, Switzerland). Data were normalized for values detected at day 1.

2.3.7 Wound healing assay

Cells ($1.5x10^6$) were seeded into 60mm dishes and incubated until they reached 80% confluency. A scratch was made through the center of the plate using a micropipette tip. Plates were washed with PBS, reefed with complete medium, and returned to the incubator. Images of the wound were collected at 0, 4, 8 and 24 hours using a microscope magnification of x10 (LEICA, DMIRB). The migration rate was quantified

by measuring the distance between the wound edges, and the percentage of migration was determined as ratio between migrated distance and scratched distance.

2.3.8 Soft agar assay

Cells ($5x10^4$) were suspended in 1.5 ml of DMEM containing 0.33% agar and 10% FCS, added into a layer of medium containing 0.5% agar and 10% FCS in 60mm dishes, and incubated for 3 weeks. After staining with p-iodonitrotetrazolium chloride (Sigma Aldrich, St. Louis, MO, USA) the plates were analyzed for colony number and size.

2.3.9 Flow cytometry assay

Cells were collected 3 days after transient transfection for DNA content analysis. Cells were washed twice with PBS and fixed for 24 hours in cold ethanol (70%). After two washes with PBS, cells were incubated in PBS containing 1μg/ml RNase and 50 μg/ml propidium iodide at room temperature for 30 min in the dark. Analysis was carried out using FACSCalibur (Becton Dickinson, San Jose, CA, USA) and data analysis was carried out using Cell Quest software.

2.3.10 Western blot analysis

Proteins were extracted in RIPA modified buffer (20mM Tris-HCl, pH 7.4, 150mM NaCl, 5mM EDTA, 1% NonidetP-40) supplemented with Complete Mini EDTA-free protease Inhibitor Cocktail (Roche, Manheim, Germany), 1mM Na_3VO_4 and 1mM PMSF. Protein samples were quantified by Bradford's assay with BIO-RAD Protein Assay (Bio-Rad, Munchen, Germany). Conditioned media, obtained by incubating cells in serum-free medium for 24 hours, were concentrated by centrifugation at 4000 rmp using AgilentSpin Concentrators (Agilent Technologies Inc, Wilmington, DE, USA)

and normalized to cell number. Protein and conditioned medium samples were boiled in NuPAGE LDS sample buffer (Invitrogen, Carlsbad, CA) and separated on 4-12% or 10% NuPAGE Novex Gel (Invitrogen, Carlsbad, CA) with MOPS or MES running buffer, respectively. Proteins were transferred onto nitrocellulose filters and immunoblotted with the appropriated antibodies: α-phospho-ERK (pERK), α-ERK and α-Cleaved PARP (Cell Signaling Technology, Beverly MA, USA); α-p21 and α-IGFBP7 (Santa Cruz, Biotechnology, Inc Santa Cruz, CA, USA); α-p53 (YLEM); α-β-Actin and α-β-Tubulin (Sigma, Aldrich St Louis, Mo, USA). The immunoreactive bands were visualized using horseradish peroxidase-conjugated secondary antibodies followed by enhanced chemiluminescence (GE, Bio-Rad Hercules, CA, USA). The membranes were scanned using the Chemidoc XRS and densitometric analysis was performed by using Quantitative One software (Bio-Rad Hercules, CA, USA).

2.3.11 *In vivo* studies

Animal studies were reviewed and approved by the Ethics Committee for Animal Experimentation of the Fondazione IRCCS 'Istituto Nazionale dei Tumori' and are in accordance with the guidelines of the UK Coordinating Committee for Cancer Research (U.K.Coordinating Committee on Cancer Research 1988). Female CD-1 nu/nu mice (8- to 9-week old) (Charles River, Calco, Italy) were injected subcutaneously into the left flank with $2x10^6$ or $5x10^6$cells in 0.2 ml PBS volume. Tumor growth was assessed by evaluating tumour latency, ie days to reach 0.1 g, and by monitoring tumour weight (TW) twice a week. TW was estimated by the formula TW(g)=d2xD/2 where d and D are the shortest and the longest diameters of the tumour, respectively, measured in cm.

CHAPTER 3

Chapter 3 – Evidence of oncogene-induced senescence in thyroid carcinogenesis

The acquirement of oncogenic lesions can result in abnormal proliferation and generate early neoplastic cells. However, this is generally not sufficient for full oncogenic transformation, as expansion of such cells is limited by several tumour suppressive mechanisms. These include telomere-induced cellular senescence, apoptosis, but also oncogene-induced senescence (OIS).

The role of OIS *in vivo* has been a matter of debate for a long time, but recent advances in our understanding of this process strongly point to OIS as tumour suppressive mechanism in several model systems (see chapter 1). OIS operates during early tumorigenesis and involves the activation of several tumour suppressor networks, including the $p16^{INK4A}$/pRb and p53/$p21^{CIP1}$ pathways. They keep incipient tumour cells in check and thereby prevent them from progressing toward malignancy. In addition to classical senescence players, like $p16^{INK4A}$ and p53, several secreted factors have recently been found to play an essential role in senescence including growth factors, cytokines, and chemokines.

In this study, we investigate the occurrence of OIS in thyroid carcinogenesis with *in vitro* and *in vivo* studies. We found that PTC-associated oncogenes trigger OIS in primary human thyrocytes, as demonstrated by lack of proliferation, changes in cell morphology, induction of various biomarkers including elevated senescence-associated (SA) β-galactosidase activity, presence of SA heterochromatic foci (SAHF) as well as increased expression of $p16^{INK4A}$, $p21^{CIP1}$ and p53.

To assess whether OIS represents a barrier to thyroid cancer *in vivo*, we performed immunohistochemical staining to monitor the expression of the classical OIS hallmarks in panel of thyroid tumours characterized by different aggressiveness.

A strong immunopositivity for $p16^{INK4a}$, $p21^{CIP1}$ and IGFBP7 was observed in PTMCs, which represent the early stage of thyroid tumorigenesis, whereas such positivity was progressively lost in PTCs and ATCs.

Our observations made *in vitro* and *in vivo* support the notion that OIS may counteract oncogenic activity in thyroid tumours, and its escape paves the way for oncogenic transformation and thyroid tumour progression.

3.1 Results

3.1.1 $BRAF^{V600E}$ induces cellular senescence in primary human thyrocytes

To evaluate the response of primary human thyrocytes to $BRAF^{V600E}$, the most frequent oncogene in PTC, we transduced cells with a lentiviral vector carrying an activated BRAF allele ($BRAF^{V600E}$); as control, thyrocytes infected with lentivirus encoding only the blasticidin resistance gene were used. After selection with blasticidin, cells were monitored for morphology, proliferation, and presence of senescence specific markers. As early as 4 days after infection, $BRAF^{V600E}$-transduced thyrocytes displayed a spindle-shaped morphology compared to cells transduced with the empty vector (Figure 3.1A). Concomitantly, a marked growth arrest was observed, whereas control cells continued proliferating. Thus, as measured 7 days after infection, thyrocytes transduced with $BRAF^{V600E}$ exhibited dramatic reduction of S phase (0.47% of cells incorporated BrdU, vs. 18.7% for control cells), and they accumulated preferentially in G1 phase (65% in cells expressing $BRAF^{V600E}$ vs. 51% for control cells) (Figure 3.1B).

$BRAF^{V600E}$ transduced thyrocytes were next analyzed for the presence of two well-known OIS markers: senescence-associated β-galactosidase (SA-β-Gal) activity and senescence-associated heterochromatic foci (SAHFs). A high portion of thyrocytes expressing $BRAF^{V600E}$ exhibited SA-β-gal activity (85%) and SAHFs (80%), whereas

in thyrocytes transfected with the empty vector SA-β-Gal activity and SAHFs were detected in 8% and 3% of cells, respectively (Figure 3.1C).

The expression of $BRAF^{V600E}$, of its downstream effectors ERKs, and of proteins involved in OIS such as $p16^{INK4a}$, $p21^{CIP1}$, p53 and HMGA2, a structural component of SAHFs (Narita et al., 2006), was investigated at day 7 and 14 post infection in oncogene and empty vector transduced thyrocytes (Figure 3.1D). $BRAF^{V600E}$ was expressed to similar levels at both time points, in large excess with respect to endogenous BRAF. Concomitantly, an increase of ERKs phosphorylation, with respect to control, was detected at day 7, and persisted at day 14. Importantly, $BRAF^{V600E}$ induced expression of $p16^{INK4a}$, further increased at day 14, whereas p53 and $p21^{CIP1}$ levels increased slightly only at the later time point. Moreover, elevated expression of HMGA2 protein was maintained up to 14 day after transduction in the $BRAF^{V600E}$ expressing cells, thus corroborating the heterochromatin changes detected by DAPI staining.

To rule out the possibility that OIS observed in thyrocytes could be related to the abnormal $BRAF^{V600E}$ expression levels obtained by lentiviral transduction we performed nucleofection of thyrocytes, thus achieving low level of expression of the oncoprotein (two-three times more abundant than endogenous BRAF, data not shown). A significant number of SA-β-Gal -positive (50%) and SAHFs-bearing (30%) cells with respect to control (20% and 4%, respectively) were detected (data not shown).

Taken together these results indicate that oncogenic $BRAF^{V600E}$ induces senescence in human thyrocytes, and this is associated with the activation of the MAPK pathway, $p16^{INK4a}$, $p21^{CIP1}$ and p53 signal transduction cascades.

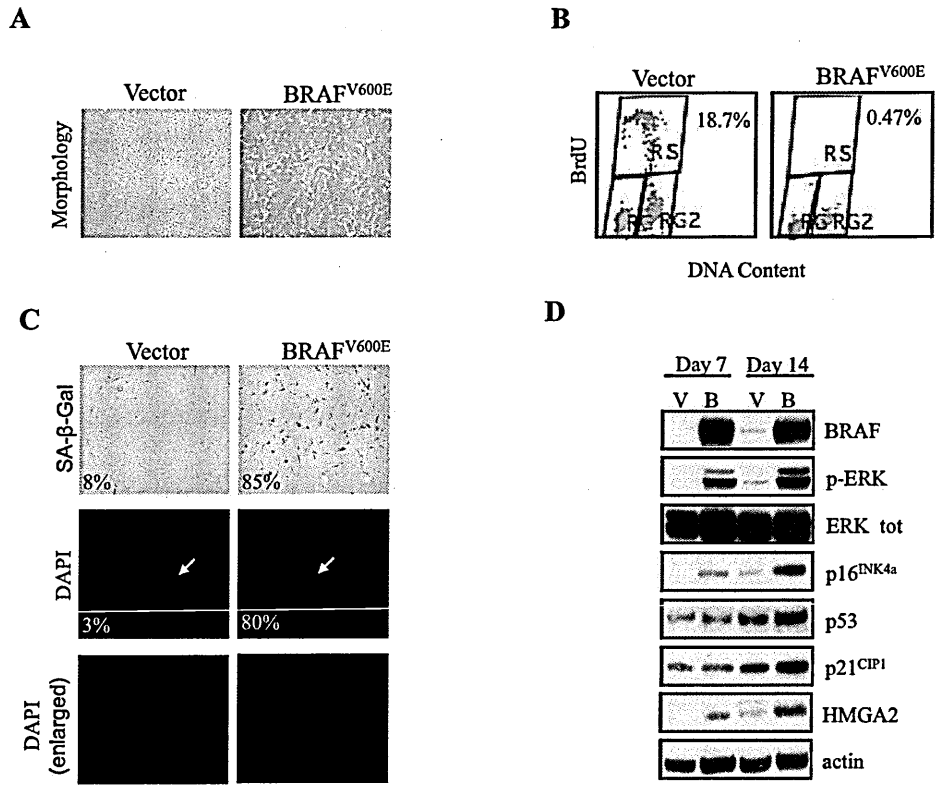

Figure 3.1 BRAF^{V600E} induces senescence in primary human thyrocytes. Primary human thyrocytes were infected with a lentivirus encoding BRAF^{V600E} oncogene or control vector. **A)** Representative photographs showing cell morphology at 4 day after infection (magnification 10X). **B)** Cell proliferation was monitored by BrdU labelling followed by FACS analysis 7 days after infection. The upper box identifies BrdU positive cells (S phase), the lower left box displays G0/G1 cells and the lower right box shows G2/M cells. The percentage of cells incorporating BrdU is indicated in the upper right of each graph. **C)** Cells were analyzed for SA-β-Gal activity (upper panel; magnification 10X) and for SAHFs formation (middle panel; magnification 20X) 14 days after infection. The percentage of cells positive for SA-β-Gal activity or carrying SAHFs is shown. Cells enlarged to show DAPI-stained chromatin foci are indicated with arrows and shown in lower panel. **D)** Expression of the indicated proteins was determined by Western Blot analysis at 7 and 14 day after infection. β-actin was used as a loading control. V: empty vector; B: BRAF^{V600E}

3.1.2 p16^{INK4a} is not strictly required for BRAF^{V600E} induced thyrocytes senescence

To investigate whether p16^{INK4a} is required for BRAF^{V600E}-mediated senescence in thyrocytes, we suppressed the expression of p16^{INK4a} using two independent lentiviral shRNA vectors (#5 and #13). Six days after infection, cells were re-transduced with a lentiviral vector encoding BRAF^{V600E}, selected for expression of the oncogene, and

analyzed 7 days later. Both shRNAs could silence $p16^{INK4a}$ expression. However, $p16^{INK4a}$ depletion did affect neither the level of ERK phosphorylation induced by $BRAF^{V600E}$, nor the basal $p21^{CIP1}$ levels (Figure 3.2A). Similarly, inhibition of $p16^{INK4a}$ expression did not rescue the growth arrest caused by $BRAF^{V600E}$ (Figure 3.2B). The percentage of $p16^{INK4a}$-null $BRAF^{V600E}$ thyrocytes positive for SA-β-Gal activity was similar to $BRAF^{V600E}$ cells, whereas the percentage of $p16^{INK4a}$-null $BRAF^{V600E}$ thyrocytes with SAHFs was reduced by approximately 40% compared with $BRAF^{V600E}$ cells (Table in Figure 3.2C). These data indicated $p16^{INK4a}$ is not sufficient to fully execute $BRAF^{V600E}$-induced senescence in thyrocytes.

3.1.3 $BRAF^{V600E}$ -induced senescence does not correlate with IGFBP7 expression

As mentioned in the chapter 2, IGFBP7 is a secreted protein recently proposed as a mediator of $BRAF^{V600E}$-induced senescence in melanocytes (Wajapeyee et al., 2008); this role, however, has been questioned by other authors (Scurr et al., 2010).

In light of these evidence we wondered whether IGFBP7 is involved in $BRAF^{V600E}$-induced thyrocytes senescence. To this end, we analyzed the expression of soluble IGFBP7 in thyrocytes 7 days after $BRAF^{V600E}$ transduction. Surprisingly, $BRAF^{V600E}$-infected cells showed reduced levels of secreted IGFBP7 protein compared to the control infected cells (Figure 3.3A). To further characterize such reduction we performed quantitative RT-PCR (qRT-PCR) (Figure 3.3B). Also in this case, we observed a decrease of IGFBP7 mRNA expression in senescent cells (day 7). Of note, such reduction was detectable as early as one day after infection.

A

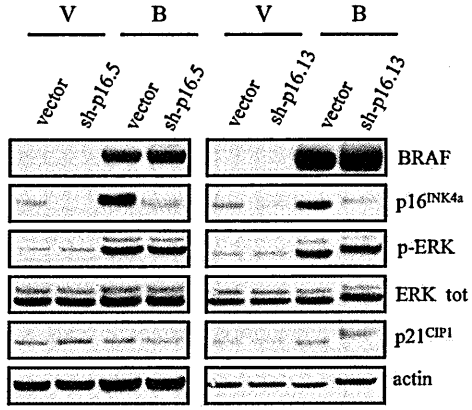

B

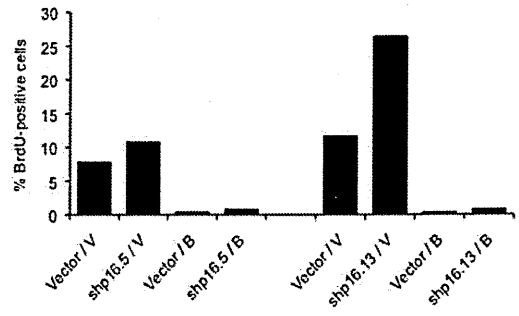

C

	β-Gal	SAHF
Vector / V	8%	1%
shp16.5 / V	10%	1%
shp16.13 / V	5%	1%
Vector / B	85%	75%
shp16.5 / B	80%	50%
shp16.13 / B	80%	40%

Figure 3.2 Effect of $p16^{INK4a}$ silencing on $BRAF^{V600E}$ –induced senescence in primary human thyrocytes. Cells were transduced with two nonoverlapping shRNA against $p16^{INK4a}$ (#5 and #13) upon infection with $BRAF^{V600E}$ encoding lentivirus. The analysis of OIS markers was performed at 14 days after infection with the two $shp16^{INK4a}$ constructs. **A)** Expression of the indicated proteins was determined by Western Blot analysis. β-actin was used as a loading control. **B)** The percentage of cells for BrdU incorporation is shown. **C)** The percentage of cells positive for each indicated markers is shown in the table. V: empty vector; B: $BRAF^{V600E}$

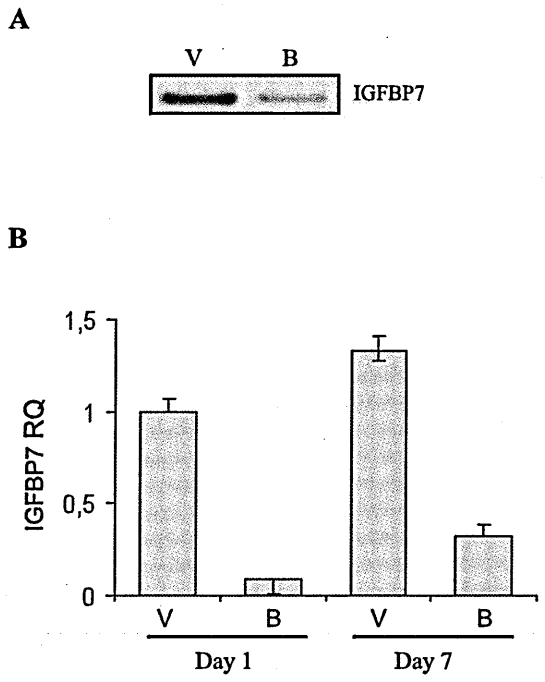

Figure 3.3 Detection of IGFBP7 expression in BRAF^{V600E}-transduced primary human thyrocytes. The expression of IGFBP7 in primary thyrocytes infected with control lentivirus or lentivirus expressing BRAF^{V600E} was monitored by Western Blot analysis 7 days after infection (**A**), and by real-time RT-PCR analysis 1 and 7 days after infection (**B**). V: control vector; B: BRAF^{V600E}. RQ: relative quantity of IGFBP7 mRNA normalized for HPRT housekeeping gene expression

3.1.4 Expression of oncogenic RET/PTC, TRK and H-RAS^{G12V} triggers cellular senescence

The evidence that BRAF^{V600E} establishes senescence arrest in primary thyrocytes raised the question whether the other PTC-associated oncogenes (RET/PTC, TRK and H-RAS^{G12V}) have also the capability to induce senescence program. Thus, to investigate the effect of RET/PTC oncogenes in primary thyrocytes we used cells transduced with a retrovirus encoding RET/PTC1 oncogene produced in the course of a previous study, and shown to display an increased growth rate compared to control uninfected thyrocytes, as determined in analyses performed between passages 3 and 7 after transduction (Borrello et al., 2005). Later on, however, by extending the number of passages in culture with respect to the previous study we noted that RET/PTC1-infected thyrocytes, at variance with control cells, ceased proliferating and showed several

morphological abnormalities, which were not further investigated at that time. In the course of the present work, we re-evaluated the previous observation, taking advantage of frozen stocks of RET/PTC1-transduced thyrocytes and relative controls. Here again, 10-12 passages after infection, RET/PTC1-expressing cells ceased proliferating and displayed morphological features of senescence, such as extensive vacuolization. Moreover, SA-β-Gal and SAHFs were found in 80% and 70%, respectively of cells infected with RET/PTC1, but only in 10% and 2% of control cells, respectively (Figure 3.4A). Biochemical analysis showed slight increase of ERKs phosphorylation compared to control cells. In addition, a marked upregulation of $p16^{INK4a}$, p53 and HMGA2, and a slight increase of $p21^{CIP1}$ was observed in RET/PTC1 infected cells (Figure 3.4B).

To introduce into thyrocytes TRK and RAS oncogenes we employed the nucleofection technology, based on the evidence that $BRAF^{V600E}$-induced senescence in thyrocytes is detectable with this transfection method, as described above. Plasmid expression vectors carrying TRK-T3 or $H\text{-}RAS^{G12V}$ oncogenes, and the empty vector as control, were transfected by nucleofection in primary human thyrocytes. Thyrocytes transfected with the TRK-T3 or $H\text{-}RAS^{G12V}$ oncogenes underwent growth arrest and displayed flat, enlarged morphology and massive vacuolization. Moreover, an increase of SA-β-Gal positive cells was detected in TRK-T3 and $H\text{-}RAS^{G12V}$ transfected cells (60% and 70%), respectively, whereas in thyrocytes transfected with empty vector SA-β-Gal activity was observed in 10% of cells. SAHFs were detected in 40% and 50% of TRK-T3 and $H\text{-}RAS^{G12V}$ transfected thyrocytes, respectively, but only in a small fraction (4%) of control-transfected cells (Figure 3.5A).

Biochemical analysis was performed at day 5 and 10 post nucleofection (Figure 3.5B). The expression of TRK-T3 and $H\text{-}RAS^{G12V}$ was constant. An increase in ERK phosphorylation level, with respect to control cells, was induced by both oncoproteins at the two times points analyzed.

Similarly, an increase of $p16^{INK4a}$ expression was observed. None of the oncogenes affected the levels of $p21^{CIP1}$. A slight increase of p53 was observed in $H\text{-}RAS^{G12V}$ transfected cells at day 10.

On the whole our *in vitro* data suggest that all the PTC-associated oncogenes are capable to triggering senescence in primary human thyrocytes, and this is not related to the oncoprotein expression level.

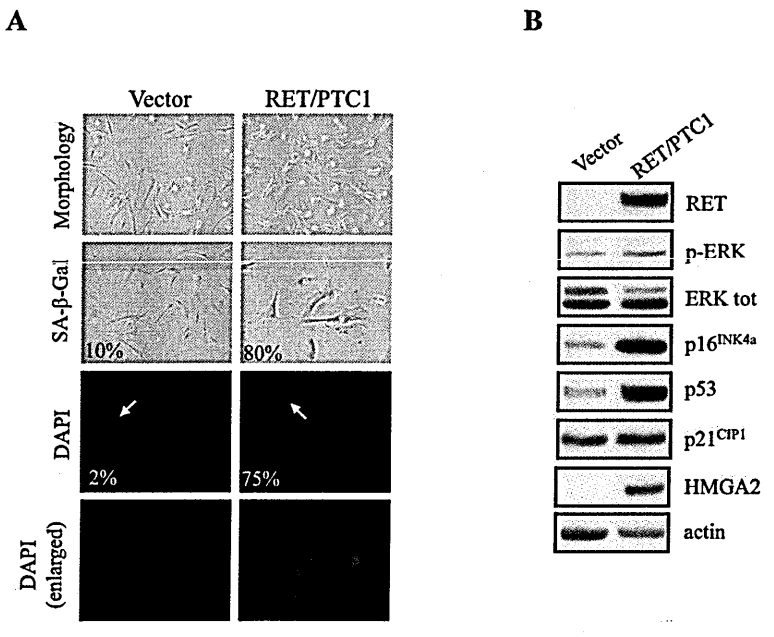

Figure 3.4 Senescence program is induced by oncogenic RET/PTC1 in primary human thyrocytes. Primary human thyrocytes transduced with retroviral vector carrying RET/PTC1 oncogene (Borrello et al., 2005) were analyzed for the presence of OIS markers at passage 10-12; uninfected cells were used as control. **A)** Analysis of cell morphology (upper panel; magnification 10X), SA-β-Gal activity (middle panel; magnification 10X for vector and 20X for RET/PTC1) and SAHFs formation (bottom panel; magnification 40X). Percentage of cells positive for SA-β-Gal activity and SAHFs are shown in each photograph. Cells enlarged to show DAPI-stained chromatin foci are indicated with arrows and shown in lower panel. **B)** Western Blot analysis of the indicated proteins in uninfected or infected cells. β-actin was monitored as a loading control.

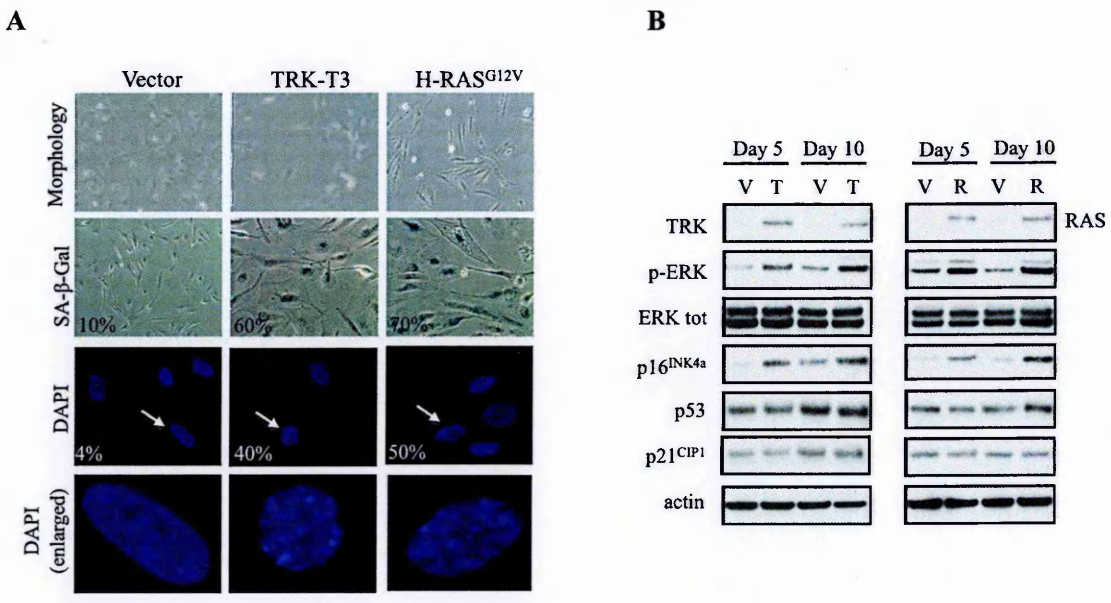

Figure 3.5 Expression of TRK-T3 and H-Ras^{G12V} oncogenes triggers senescence in primary human thyrocytes. Primary human thyrocytes were transfected with plasmid expression vectors encoding TRK-T3 and H-Ras^{G12V} or empty vector by nucleofection technology. **A)** Cell morphology (upper panel; magnification 10X) 4 days after transfection, the appearance of SA-β-Gal (middle panel, magnification 10X for vector, 20X for TRK-T3 and H-Ras^{G12V}) and SAHFs (lower panel; magnification 40X) at 10 day after transfection are shown. Cells enlarged to show DAPI-stained chromatin foci are indicated with arrows and shown in lower panel. **B)** Immunoblot analysis monitoring the expression of the indicated proteins at 5 and 10 day after transfection. β-actin was used as a loading control. V: empty vector; T: TRK-T3; R: H-Ras^{G12V}.

3.1.5 Analysis of OIS markers in thyroid tumour samples

To study the relevance of OIS in thyroid tumour pathogenesis we performed IHC analysis for the detection of OIS markers in a series of thyroid tumour samples characterized by increasing aggressiveness, thus recapitulating epithelial thyroid tumour progression. The case collection included two PTMCs, seven PTCs (six NOS, and one SV (Nikiforov et al., 2001)), two PDTC, and one ATC. Clinical-pathological features and follow-up information for these cases are reported in Table 3.1.

Table 3.1 Clinical-pathological information of thyroid tumour case collection.

Case	*Age*	*Gender*	*Tumor type*	*Genetic lesion*	*ITS/LMN*	*Lenght of follow-up (months)*	*Clinical outcome*
1	55	F	PTMC	$BRAF^{V600E}$	ITS, LNM	102	NED
2	36	F	PTMC	$BRAF^{V600E}$	ITS, LNM	99	NED
3	31	F	PTC NOS	UN	ITS	60	NED
4	69	M	PTC NOS	UN	ITS	67	NED
5	49	F	PTC NOS	$BRAF^{V600E}$	---	lost	---
6	48	F	PTC NOS	UN	ITS	64	NED
7	55	F	PTC NOS	UN	ITS	lost	---
8	57	F	PTC NOS	UN	ITS, LNM	lost	---
9	46	F	PTC SV	$BRAF^{V600E}$	ITS	87	NED
10	67	F	PTDC	$BRAF^{V600E}$	LNM	12	Progression
11	75	M	PTCD	ND	ITS	12	Progression
12	54	F	ATC	ND	LNM	6	Died of disease
13	40	F	PTMC	UN	ITS	72	NED
14	53	M	PTMC	TRK	ITS, LNM	80	NED
15	48	F	PTMC	UN	ITS	81	NED
16	30	M	PTMC	UN	ITS	84	NED

PTC: papillary thyroid carcinoma; PTMC: papillary thyroid microcarcinoma; NOS: not otherwise specified; SV: solid variant; PDTC: poorly differentiated thyroid carcinoma; ATC: anaplastic thyroid carcinoma; UN: unknown (indicate case negative for $BRAF^{V600E}$ mutations, and *RET* or *TRK* rearrangement); ND: not determined; ITS: intrathyroidal spreading; LNM: lymph node metastasis; NED: no evidence of disease.

Notably, for PTMC # 2 three intrathyroidal spreads and a lymph node metastasis were available. Sample #9 (SV) and sample #10 (PDTC) presented areas with papillary and solid pattern of growth, thus providing a model of "in situ" tumour progression. The case collection was analyzed by IHC for the expression of $p16^{INK4a}$ and $p21^{CIP1}$, well-known effectors of *in vitro* OIS, of IGFBP7, recently proposed as a factor required for OIS in melanocytes, and of the proliferation marker Ki-67. The results of IHC analysis are reported in Table 3.2; representative pictures are shown in Figure 3.6 and 3.7.

PTMC samples showed the highest expression of $p16^{INK4a}$, which resulted upregulated in tumour areas with respect to the adjacent non tumoral thyroid tissue; $p16^{INK4a}$ positive cells accounted for 50-60%.

Immunolabeling for $p16^{INK4a}$ was both cytoplasmic and nuclear. In PTMC #2 $p16^{INK4a}$ was expressed at similar level in all the different tumour areas analyzed, including lymph node metastasis. The PTCs NOS samples showed a variable extent of $p16^{INK4a}$ expression: one case was scored negative (< 10% of positive cells); four cases showed 11-40% of positive cells, whereas only one case displayed more than 40% positive cells. In general, the distribution of $p16^{INK4a}$ was scattered; we observed groups of positive cells within the tumour mass. The PTC SV sample was scored positive in the areas with papillary growth, but negative in the solid ones. With respect to PDTC samples the papillary areas of case #10 were positive, whereas the solid areas as well as case #11 were negative. No expression of $p16^{INK4a}$ was detected in the ATC sample.

With respect to $p21^{CIP1}$ no staining was observed in the non tumoral tissue surrounding the tumour area. The highest expression was detected in PTMCs, showing 30% to 70% of positive cells, which persisted in the different lesions of PTMC #2. PTCs NOS were classified as negative, except for two cases that showed 11-40% of positive cells. The Solid Variant sample was scored positive in papillary areas and negative in solid ones. In the PDTC expression of $p21^{CIP1}$ was detected only in the papillary areas of sample #10. No expression of $p21^{CIP1}$ was observed in the ATC sample.

Table 3.2 Immunohistochemical analysis for $p16^{INK4a}$, $p21^{CIP1}$, IGFBP7 and Ki-67 in thyroid carcinomas

	$p16^{INK4a}$	$p21^{CIP1}$	IGFBP7	Ki-67
PTCM				
1	++	+	++	L
2 PT,RL	++	+++	++	vL
2 ITS,RL	++	+++	++	vL
2 ITS,IS	++	+++	++	vL
2 ITS,LL	++	+++	++	vL
2 LNM	++	+++	++	vL
PTC				
NOS				
3	+	+	-	L
4	-	-	+	L
5	+	-	++	L/M
6	+	+	++	M
7	+	-	-	L
8	++	-	++	L
SV				
9 papillary	+	+	+/++	L
9 solid	-	-	-	ND
PDTC				
10 papillary	+	++	++	L
10 solid	-	-	-	H
11	-	+	+	M/H
ATC				
12	-		-	H

PTMC, papillary thyroid microcarcinoma; PTC, papillary thyroid carcinoma; ATC, anaplastic thyroid carcinoma; ATC, anaplastic thyroid carcinoma; NOS, not otherwise specified; SV, solid variant; PT, primary tumour; ITS, intrathyroidal spread; LNM, lymph node metastasis; RL, right lobe; LL, left lobe; Is, isthmus. The percentage of cells with staining for $p16^{INK4a}$ and $p21^{CIP1}$ was scored from 0 to 3: (-) <10% of positive cells; (1+) 11-40%; (2+) 41-70%; (3+) 71-100%. The intensity of staining for IGFBP7 was from: (-) to (3+): (-) negative; (+) weakly positive; (++) moderately positive; (+++) strongly positive. Ki-67 staining was scored as very low (vL, 1-5% positive cells), low (L, 6-10% positive cells), medium (M, 11-30% positive cells) and high (H, ≥ 31% positive cells). ND, not done (no material available).

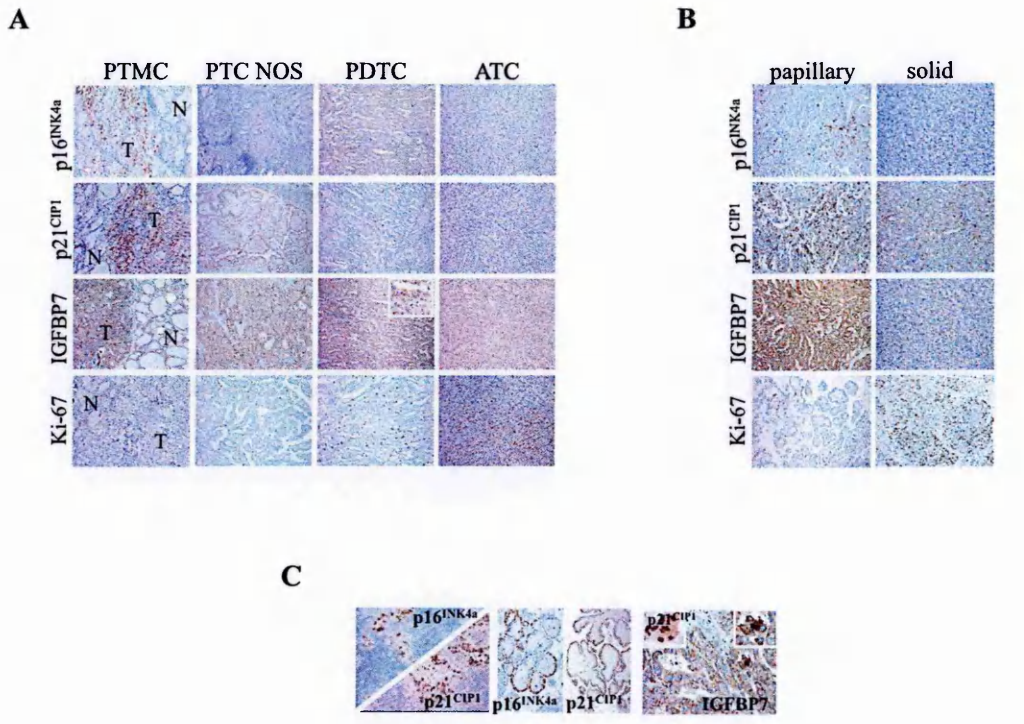

Figure 3.6 Immunohistochemical analysis of OIS markers ($p16^{INK4a}$, $p21^{CIP1}$, IGFBP7) and Ki-67 in thyroid tumour samples. A) Representative pictures of a papillary thyroid microcarcinoma (PTMC), a PTC not otherwise specified (NOS) variant, a poorly differentiated thyroid carcinoma (PDTC) and an anaplastic thyroid carcinoma (ATC) are shown. N: normal; T: tumour. B) Papillary and solid areas of PDTC # 10. C) PTC sample distinguished by the presence of lymphocyte infiltration (first panel); edematous papillae cores (second panel); multinucleated giant cells (third panel).

IGFBP7 showed the same trend of expression as $p16^{INK4a}$ and $p21^{CIP1}$. In both PTMC primary tumour samples, and in the intrathyroidal and lymph node spreads of PTCM #2, IGFBP7 was upregulated with respect to the adjacent non tumoral tissue. PTCs NOS showed variable expression levels: three cases were scored as moderately positive, one case as weakly, and two as negative. IGFBP7 expression was detected in the papillary, but not in the solid areas of SV sample; a similar trend was observed for PDTC #10, whereas PDTC #11 showed weak expression, and no expression was detected in the ATC sample. The expression of $p16^{INK4a}$, $p21^{CIP1}$ and IGFBP7 proteins was inversely correlated with the proliferative index.

The expression of the Ki-67 proliferation marker was very low or low in PTMCs; it ranged from low to medium in PTC NOS and in the papillary areas of samples #9 and #10; it increased to medium/high and high in PDTC and ATC, respectively. In Figure 3.6A representative pictures of PTMC, PTC NOS, PDTC, and ATC are shown; Figure 3.6B reports the analysis of papillary and solid areas of PDTC sample #10. Interestingly, in PTC samples the expression of OIS markers was often associated to several structures suggestive of tumour regression (Figure 3.6C) such as: i) areas with lymphocyte infiltration (left panel), which has been reported to play a protective role in thyroid cancer (Ugolini et al., 2007); ii) swelling oedematous papillae cores (middle panel); and iii) syncytial clusters of tumoral cells (right panel), a frequent finding in PTC (Fulciniti et al., 2001), resulting from papillae apex detachment.

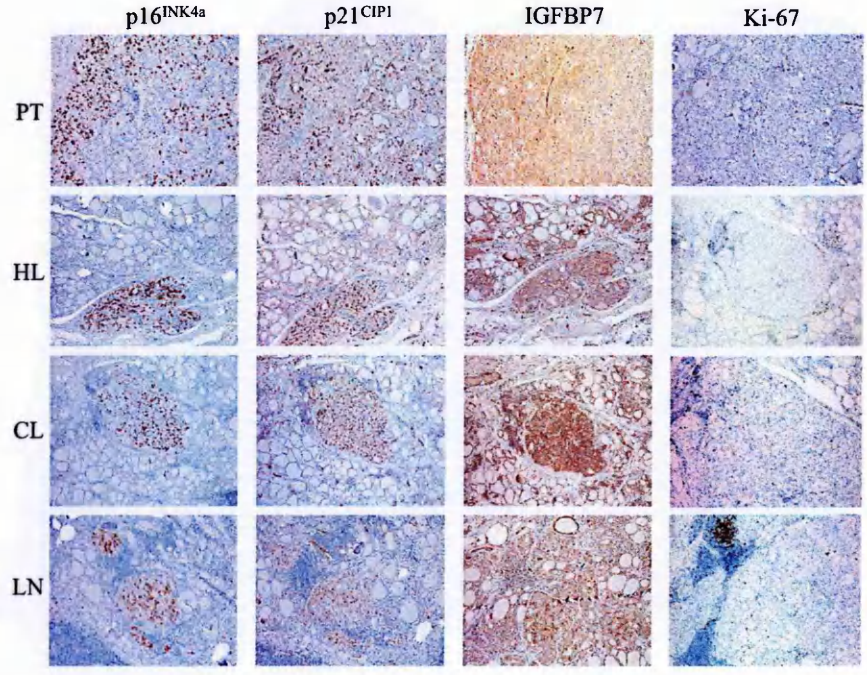

Figure 3.7 Immunohistochemical analysis for the expression of $p16^{INK4a}$, $p21^{CIP1}$, IGFBP7 and Ki-67 in primary tumour (PT), homolateral (HL), controlateral (CL) and lymph-node (LN) spreads of papillary thyroid microcarcinoma (PTMC) # 2. The Ki-67 panel of primary tumour is the same of Figure 3.6A.

The first conclusion that can be drawn from the IHC analysis is that the expression of OIS markers is upregulated at early stages and then lost during thyroid tumour progression. This issue is strengthened by the evidence that in samples #9 and #10, which recapitulate "*in situ*" tumour progression, the expression of the three protein analyzed was detected in areas featuring papillary growth but not in the solid ones.

The highest expression of all OIS markers analyzed observed in PTMCs would suggest that OIS may play a role in the general indolent clinical course of this PTC variant by keeping proliferation under check even in the presence of intrathyroidal and lymph node spread, as suggested by the analysis of PTMC #2 (Table 3.1 and Figure 3.7). To further explore this issue we analyzed four additional PTMCs presenting intraglandular and/or lymph node spread (Table 3.3); due to material shortage the analysis was limited to Ki-67 and $p16^{INK4a}$. As shown in Table 3.2 the primary tumours showed relative intense $p16^{INK4a}$ expression and very low Ki-67 immunolabeling. The same pattern of expression was observed in the intraglandular and/or lymph node tumour foci. Interestingly, in none of the PTMC patients recurrence was documented in the follow-up period, which ranged from 72 to 102 months (Table 3.3).

Table 3.3 Immunohistochemical analysis for $p16^{INK4a}$ and Ki-67 in a small series of PTMCs

	Sample	*$p16^{INK4a}$*	*Ki-67*
13	PT, Is	++	vL/L
	ITS, RL	++	vL
	ITS, LL	+	vL
14	PT, LL	++	vL
	ITS, Is	Na	Na
	LNM	++	vL
15	PT, RL	++	vL
	ITS, RL	Na	vL
16	PT, RL	++	vL
	ITS, Is	Na	Na
	ITS, LL	+	vL

PT: primary tumour; ITS: intrathyroidal spread; LNM: lymph node metastasis; RL: right lobe; LL: left lobe; Is: isthmus. The percentage of cells with staining for $p16^{INK4a}$ was scored from 0 to3: (-) < 10% of positive cells; (1+) 11- 40%; (2+) 41-70%; (3+) 71-100%. Ki-67 staining was scored as very low (vL, 1-5% positive cells), low (L, 6-10% positive cells), medium (M, 11-30 % positive cells), high (H, ≥ 31% positive cells). ND: not done (no material available).

Overall our data demonstrate the presence of OIS in PTMC, and suggests that this mechanism maintains the indolent behaviour of this tumour type, despite multifocality within thyroid gland and loco-regional spread.

3.2 Discussion

We provided evidence that OIS may represent a barrier to the progression of thyroid tumour. *In vitro* studies, using different gene transfer methods, demonstrated that all the oncogenes activated in thyroid tumours, namely $BRAF^{V600E}$, RET/PTC1, TRK-T3, and $H\text{-}Ras^{G12V}$, are capable to induce cellular senescence in primary human thyrocytes, as judged by the presence of growth arrest, changes in cell morphology, accumulation of SA-β-Gal and chromatin modifications. Our conclusion is corroborated by the evidence that OIS is detectable with different oncogenes transfected with different methods and, thus, expressed at different levels. Differences in efficiency and onset of OIS observed by using the different oncogenes can be ascribed to experimental conditions and oncoprotein expression level, rather than to intrinsic oncogenic features.

Shading light on the molecular mechanisms responsible for the OIS onset, the predominant view is that aberrant levels of MAP kinase activate senescence program through the critical involvement of $p16^{INK4a}$/pRB and p53/$p21^{CIP1}$ networks (Lin et al., 1998). In our cellular setting, PTC-associated oncogenes trigger a marked activation of ERKs, accompanied by a persistent induction of $p16^{INK4a}$, whereas we failed to observe any significant upregulation of p53 and $p21^{CIP1}$, with exception of RET/PTC1 expressing thyrocytes in which an increase of p53 was detected. Of note, we did not observe involvement of IGFBP7 in $BRAF^{V600E}$-transduced thyrocytes.

The relative contribution of the $p16^{INK4a}$/pRB and the p53/$p21^{CIP1}$ pathways in mediating senescence program remains poorly understood. It has been shown that $p16^{INK4a}$ plays a major role than $p21^{CIP1}$ in the induction of senescence in many contexts *in vitro*. In some cells $p16^{INK4a}$ is solely responsible for OIS onset (Ben-Porath and Weinberg, 2005), whereas in other cell types it has been shown that $p16^{INK4a}$ alone is not sufficient to execute the OIS program (Haferkamp et al., 2009; Michaloglou et al., 2005). In our experimental setting inactivation of $p16^{INK4a}$ with shRNA did not affect

$BRAF^{V600E}$-induced senescence in thyrocytes, except for a reduction of SAHFs-bearing cells. This raises the possibility that $p16^{INK4a}$ may cooperate with other factors in triggering senescence.

The upregulation of $p16^{INK4a}$ observed in our analysis is in agreement with previous studies, showing that the proliferation arrest induced in thyrocytes by $H\text{-}Ras^{G12V}$ was associated with upregulation of $p16^{INK4a}$ (Jones et al., 2000). In that setting, however, silencing of $p16^{INK4a}$ rescued $H\text{-}Ras^{G12V}$ expressing thyrocytes from senescence (Bond et al., 2004). Thus, it is worth noting that OIS program does not seem to be universal across cell type and genetic context.

Although initially considered as an *in vitro* phenomenon, OIS is now view as an authentic cancer barrier. As mentioned above, several groups have reported its occurrence in different *in vivo* lesions including human melanocytic nevi, human dermal neurofibromas, human and murine prostatic and thyroid adenomas, and murine lymphomas and melanoma (Braig et al., 2005; Chen et al., 2005; Collado et al., 2005; Courtois-Cox et al., 2006; Dankort et al., 2007; Ha et al., 2007; Kortlever et al., 2006). To extend our observations to an *in vivo* context we analyzed a panel of thyroid tumour samples with increasing aggressiveness: PTMC, characterized by very indolent course; PTC NOS, differentiated carcinoma generally associated with good prognosis; PDTC associated with poor prognosis; ATC, undifferentiated, very aggressive carcinoma with fatal outcome, mostly arising from a time-dependent dedifferentiation of differentiated carcinoma, in particular PTC. We analyzed the expression of $p16^{INK4a}$ and $p21^{CIP1}$, two universally recognized OIS markers, and IGFBP7, a protein exerting an oncosuppressor role in thyroid tumours (Vizioli et al., 2010), and found involved in melanocyte OIS (Wajapeyee et al., 2008), although its role in this process is controversial (Scurr et al., 2010). Collectively, the three proteins resulted upregulated in PTMCs; the PTCs showed a variable pattern, including loss of expression; finally, the ATC sample was

scored negative for the all proteins. The upregulation in PTMCs and the progressive loss in PTCs and ATC support the notion that OIS may counteract oncogenic action in thyroid tumours, and its escape allows thyroid tumour progression.

Regarding IGFBP7 we have previously shown that its mRNA expression is frequently downregulated in PTC, and this is associated with the TC variant (Vizioli et al., 2010). Our IHC results are in agreement with the gene expression data, as we observed a progressive loss of IGFBP7 protein during thyroid tumour progression. In normal tissue IGFBP7 is distributed widely although with a lower expression compared with PTMC which showed the highest IGFBP7 levels. However, in PTC IGFBP7 expression, characterized by variable staining, is downregulated with respect to normal tissue. This is in harmony with the gene expression data (Vizioli et al., 2010), suggesting that IGFBP7 may also participate in counteracting the aberrant proliferative signals of oncogenes. However, we did not detect induction of IGFBP7 protein in senescent $BRAF^{V600E}$ thyrocytes. This discrepancy may be explained taking into account that induction of IGFBP7 *in vivo* might result from the complex crosstalk between tumour and stromal cells (Kuilman et al., 2009).

Further support to the issue that OIS counteract oncogenic activation is provided by the evidence that in PTC samples expression of OIS markers may be associated with several characteristics of tumour regression, such as lymphocytic infiltration, oedematous papillae cores, and syncytial clusters. The presence of these features is in keeping with the notion that OIS triggers activation of inflammatory network and evokes innate immunoresponse that ultimately counteract tumour progression (Ren et al., 2009).

Analysis of a small series of PTMC showed consistent upregulation of $p16^{INK4a}$ in association with very low proliferative index. Of note, $p16^{INK4a}$ expression and Ki-67 immunolabeling remained unchanged in synchronous intrathyroidal and nodal spreads.

In one PTMC samples the analysis of $p21^{CIP1}$ and IGFBP7 was possible, showing the same expression level in primary tumour and intrathyroidal and lymph node foci. Notably, none of the PTMC patients of our series experienced recurrence during the follow-up period (72-102 months).

Expression of $p16^{INK4a}$ in thyroid malignancies has been previously investigated by several groups. Overexpression of $p16^{INK4a}$ in adenomas, papillary and follicular tumours, and loss of expression in ATC was observed in previous works (Ball et al., 2007; Ferru et al., 2006), suggesting that $p16^{INK4a}$ expression is induced in early stage tumours and then progressively lost during tumour progression. Similarly, overexpression of $p21^{CIP1}$ in PTMC and progressive loss of expression with advancing tumour grade in PTC has been reported (Brzezinski et al., 2005). These previous reports together with our data suggest that the indolent course of PTMC as well as the characteristically slow growth of classical PTC may be explained by the persisting of severe limit to oncogene induced proliferation exerted by the OIS mechanism. In this light PTMC represents, among the variants examined, the most representative model for the tumour suppressor mechanism exerted by OIS. Indeed, all the foci examined across the thyroid and lymph nodes share the same "frozen phenotype" in terms of $p16^{INK4a}$, $p21^{CIP1}$ and IGFBP7.

The persistence of OIS signal in intrathyroidal and nodal spreads might explain the favourable prognosis of PTMC even in the presence of multifocality and lymph node metastasis, two features associated with lateral node recurrence, but not with increased risk of mortality (Hay et al., 2008).

Moreover, the constant expression of all the OIS markers analyzed and Ki-67 labelling across the different lesions of the same patient suggests that cells have acquired the capability to invade without changes in their proliferation capability.

This is in keeping with reports claiming invasion and proliferation as two distinct mechanisms (Gao et al., 2005), governed by different genes and pathways.

We have identified OIS as a mechanism involved in the pathogenesis of thyroid carcinoma by restraining the evolution of PTMC to PTC, as well as the transition of well differentiated and less aggressive PTC to undifferentiated and more aggressive variants. This raises the idea that restoration of this process in tumour cells may represent a therapeutic approach especially for those tumours non-responding to standard therapy. Moreover, a possible therapeutic strategy based on OIS restoration is independent from the oncogenic alteration carried by the tumour, as we have shown that all PTC-associated oncogenes are capable to trigger senescence program. The feasibility of enforced cellular senescence as therapeutic approach for thyroid as well as other tumour types remains to be investigated, and it will require a deeper understanding of the mechanisms involved in the process, as well as suitable *in vitro* and *in vivo* models.

3.3 Materials and methods

3.3.1 Cell culture

Normal thyroid samples were obtained from patients undergoing surgery at IRCCS Foundation Istituto Nazionale dei Tumori (Milan, Italy). All patients gave their written informed consent, and the study was approved by the Independent Ethical Committee of IRCCS Foundation Istituto Nazionale dei Tumori. Primary thyrocyte cultures were obtained from normal human thyroid gland after mechanical and enzymatical disaggregation. For instance, the enzymatic digestion was with a solution consisting of collagenase at 20 units/ml, trypsin at 0.75mg/ml, and 2% heat-inactivated dialyzed chicken serum in Ca^{2+} and Mg^{2+}-free HBSS (CTC solution). Two hours digestion at 37°C was followed by centrifugation for 10 min at 1 x g: the supernatant was eliminated and cells and small fragments of tissue were seeded and maintained in nutrient mixture Ham's F12 medium (custom made by Invitrogen, Paisley, UK) containing 5% calf serum and bovine hypothalamus and pituitary extracts (Curcio et al., 1994). Twenty four hours later conditioned medium was collected and assayed for thyroglobulin (Tg) secreted in the supernatant by an immunoradiometric assay according to manufacturer's instructions. Thyrocytes expressing RET/PTC1 oncogene, obtained from infection of primary thyrocytes with RET/PTC1 retroviral vector, have been previously described (Borrello et al., 2005).

HEK293T cells were maintained in Dulbecco's Modified Eagle Medium (DMEM Gibco) supplemented with 10% (v/v) FBS and 1% (v/v) antibiotic-antimycotic (Gibco).

3.3.2 Lentivirus production and transduction

HEK293T cells ($4x10^6$) were transfected with 8 μg of $BRAF^{V600E}$ lentiviral construct (HIV-CS-CG-Blast-$BRAF^{V600E}$) and 3 μg of each of the helper plasmids

pMDLglpRRE, pHCMV-G, and pRSVrev by calcium phosphate in complete medium containing 25 μM chloroquine. After 6-12 hours of incubation cells were washed and refed with complete medium. Supernatant containing lentiviral particles was collected and frozen 24 hours after transfection, and subsequently added to thyrocytes for 6 hours in the presence of 0.8 μg/μl of Polybrene (Sigma Aldrich, St Louis, Mo, USA), followed by blasticidin selection (5mg/ml) after 24 hours. Three days later cells were harvested and plated at different densities for further analyses. The efficiency of transduction was monitored in parallel infections using virus expressing enhanced green fluorescent protein (eGFP).

3.3.3 $p16^{INK4a}$ shRNA silencing

$p16^{INK4a}$ knockdown constructs were created into KH1 lentiviral vector, carrying the *GFP* reporter gene, with the following sense shRNA sequences: shp16.5 (TGCCCCCGGGGGAGACCCAAC), and shp16.13 (GCCGACCCCGCCACTCTCA) and used for thyrocytes transduction. Transduction efficient was monitored by GFP expression. Six days later cells were re-transduced with lentiviruses encoding BRAFV600E (HIV-CSCG-$BRAF^{V600E}$) and maintained under blasticidin selection for an additional six days.

3.3.4 Nucleofection

Human primary thyrocytes ($1x10^6$) were resuspended in 110 μl of Human Keratinocyte Nucleofector solution (Amaxa, Lonza AG Basel, Switzerland) together with 1 μg of plasmid DNA, transferred to the cuvette and nucleofected using Amaxa Nucleofector II Device (T003 program). Immediately after nucleofection, cells were resuspended in pre-heated complete culture medium and then seeded at different densities for further analyses. Cells were reefed 24 hours later and subjected to G418 (400 μg/ml) selection.

Plasmid vectors carrying TRK-T3 and H-RAS^{G12V} oncogenes have been previously described (Greco et al., 1995; Pulciani et al., 1982).

3.3.5 BrdU incorporation

Cells were labeled with 10 μM BrdU for 3 hours, harvested and fixed in 75% ethanol for 30 min. After washing with PBS, cells were treated with RNAse A (500 μg/ml) for 30 min, permeabilized with 5 M HCl/ 0.5% Triton for 20 min at room temperature, neutralized with 1M TRIS, and washed in 0.5% Tween/PBS. Incubation with primary anti-BrdU antibody (30 min RT) and secondary FITC conjugated antibodies (30 min RT) (DAKO, Seattle, WA) was followed by staining with propidium iodine (20 μg/ml) at 37°C for 30 min. Samples were analyzed by flow cytometry (Becton Dickinson, San Jose, CA, USA).

3.3.6 Senescence-associated β-galactosidase (SA-β-Gal) assay

Adherent cells were analyzed for SA-β-Gal production using Senescence-beta-Galactosidase Staining Kit (Cell Signaling, Danvers, MA, USA) following manufacturer's instructions. For each sample at least 200 cells were scored.

3.3.7 SAHFs formation

For the analysis of SAHFs, transfected/transduced cells growing on glass cover slips were fixed in 4% paraformaldehyde-2% sucrose, permeabilized with 0.1% Triton, and stained with Prolong Gold antifade reagent with DAPI (Molecular Probes, Invitrogen, Carlsbad, CA, USA). Stained nuclei were observed under a fluorescent microscope (Nikon Eclipse E1000). For each sample at least 100 cells were scored.

3.3.8 Western Blotting analysis

Proteins were extracted in RIPA modified buffer (20mM Tris-HCl, pH 7.4, 150mM NaCl, 5mM EDTA, 1% NonidetP-40) supplemented with Complete Mini EDTA-free protease Inhibitor Cocktail (Roche, Manheim, Germany), 1mM Na_3VO_4 and 1mM PMSF. Protein samples were quantified by Bradford's assay with BIO-RAD Protein Assay (Bio-Rad, Munchen, Germany). Supernatant obtained by incubating cells in serum-free medium for 24 hours were concentrated by centrifugation at 4000 rmp using AgilentSpin Concentrators (Agilent Technologies Inc, Wilmington, DE, USA) and normalized to cell number. Protein and supernatant samples were boiled in NuPAGE LDS sample buffer (Invitrogen, Carlsbad, CA, USA) and separated on 4-12% or 10% NuPAGE Novex Gel (Invitrogen, Carlsbad, CA, USA) with MOPS or MES running buffer, respectively. Proteins were transferred onto nitrocellulose filters and immunoblotted with the following primary antibodies to: $p16^{INK4a}$ (BD Becton Dickinson, NJ, USA); $p21^{CIP1}$, BRAF (F7), RET (C-19), TRK (C-14), IGFBP7 (Santa Cruz, Biotechnology, Inc, Santa Cruz, CA, USA); p53 (YLEM); phospho-ERK1/2 (p-ERK), ERK1/2 , β -Actin (Sigma Aldrich, St Louis, Mo, USA); RAS (Ab3) (Calbiochem, San Diego, CA, USA); HMGA2 (kindly provided from G. Manfioletti, University of Trieste). The immunoreactive bands were visualized using horseradish peroxidase-conjugated secondary antibodies followed by enhanced chemiluminescence (GE Healthcare, Buckinghamshire, UK).

3.3.9 Real time RT-PCR

RNA was isolated with TRIzol reagent (Invitrogen Paisley, UK) from cells collected at day 1 and 7 post infection and purified with RNeasy purification kit (Qiagen, Valencia, CA, USA). Reverse transcription was performed with Superscript Reverse TranscriptaseIII following the manufacturer's instructions (Invitrogen). For each

sample, 20 ng of retro-transcribed RNA were amplified in PCR reactions carried out in triplicate on an ABI PRISM 7900 using TaqMan gene expression assays (Applied Biosystem, Foster City, CA). Hs00266026_A1 was used for IGFBP7 expression; human HPRT (HPRT-Hs99999909_A1) was used as housekeeping gene for the normalization among samples. Data analysis was performed using the SDS (Sequence Detection System) 2.2.2 software.

3.3.10 Tumour samples and immunohistochemistry

The thyroid tumour samples analyzed were selected by reviewing a larger tumour series available at the Department of Pathology from patients operated at IRCCS Foundation Istituto Nazionale dei Tumori (Milan, Italy) from 2002 to 2009. Tumours were classified according to the histopathological typing of the World Health Organization (Delellis et al. 2004). Tumour collection included: PTMC (6 cases); PTC NOS (6 cases); PTC SV (1 case) (Nikiforov et al. 2001); PDTC (2 cases); ATC (1 case). Clinical pathological features are reported in Table 1. All patients gave their written informed consent, and the study was approved by the Independent Ethical Committee of IRCCS Foundation Istituto Nazionale dei Tumori.

The immunohistochemical analyses were performed on formalin-fixed, paraffin-embedded tissue sections of 2-μm thickness. Antigen retrieval was performed using 1 mM citrate buffer (pH 6) or 0.25 mM EDTA (pH 8) in an autoclave at 95°C for 6-15 minutes. Incubation with primary antibodies was performed overnight at 4°C for anti-$p21^{CIP1}$ and anti-IGFBP7 (Santa Cruz, Biotechnology, Inc, Santa Cruz, CA, USA); for 1 hour at room temperature for anti-human Ki-67 Antigen (Mib1) (DakoCytomation). Sections were then incubated for 30 minutes with biotinylated anti-goat, developed using 3,3'-diaminobenzidine (DakoCytomation) as chromogen, and finally counterstained with hematoxylin.

$p16^{INK4a}$ staining was performed using CINtec Histologic Kit (mtm laboratories AG, Heidelberg, Germany) following manufacturer's instructions.

The intensity of staining for IGFBP7 was scored from (-) negative to (3+) strong. The percentage of cells immunostained for $p16^{INK4a}$ and $p21^{CIP1}$ ranged from (-) <10% to (3+) 71-100%. Ki-67 staining was scored as very low (vL, 1-5% positive cells), low (L, 6-10% positive cells), medium (M, 11-30 % positive cells), high (H, ≥ 31% positive cells).

CHAPTER 4

Chapter 4 – H-RAS^{G12V} induces senescence in primary thyrocytes through p16^{INK4a}/pRb pathway and activation of inflammatory network

The study presented in this chapter was performed in the laboratory of Dr Jesus Gil (MRC, Imperial College, London) who is one of the Europe's most talented young researcher working in the field of oncogene-induced senescence.

An OIS inducible system, generated and well-characterized in the host laboratory, was used to study senescence in primary thyrocytes. A model based on thyrocytes retrovirally infected whit H-RAS^{G12V} and undergoing senescence upon 4-hydroxytamoxifen (4OHT) treatment was established. To identify OIS escape mechanisms we used shRNA vectors, designed in the host laboratory. The analysis of OIS markers was monitored using IN Cell Analyzer 1000, an automated cellular imaging system for high content analysis (as deeply described below).

The results presented in chapter 3 reveal that all the oncogenes activated in thyroid cancer, namely BRAF^{V600E}, RET/PTC1, TRK-T3 and H-RAS^{G12V} are capable of inducing cellular senescence in primary human thyrocytes. Here, we focus our attention on H-RAS^{G12V} that is the common mutation found in PTC with follicular variant histology.

Oncogenic mutant H-RAS^{G12V} is known to transform most immortal rodent cell lines to tumorigenic state (Newbold and Overell, 1983). However, transformation of primary cells by H-RAS^{G12V} requires either a cooperating oncogene or the inactivation of tumour suppressors such as p16^{INK4a} or p53 (Land et al., 1983).

Delineating the signalling networks that orchestrate the OIS response in our cellular model, we wondered whether the removal of these critical nodes can cause the senescence program

to collapse facilitating oncogenic transformation. For this purpose, we took advantage of H-RAS^{G12V}-inducible system.

4.1 Results

4.1.1 Establishment and characterization of H-RAS^{G12V}-inducible system.

As first step, in order to establish and characterize this new system, we transduced primary thyrocytes with a retroviral vector carrying an activated form of RAS oncogene (H-RAS^{G12V}) fused with the ligand binding domain of the estrogen receptor (ER). Cells infected with empty vector only were kept in parallel throughout the experiments as a negative control. Two days after transduction, cells were selected by adding G418 for approximately 15 days. Upon addition of 4-hydroxytamoxifen (4OHT), a time course experiment over 10 days was performed to monitor the effects of the activated H-RAS^{G12V} on primary thyrocytes.

By day 4, H-RAS^{G12V} transduced cells displayed changes in morphology, becoming flat and enlarged. No morphology changes were detected in cells transduced with empty vector and non 4OHT-treated counterparts (Figure 4.1A).

Expression of H-RAS^{G12V} caused a decrease in cellular density as shown by proliferation assay (Figure 4.1B), as well as a decrease in the percentage of cells incorporating BrdU (Figure 4.1C). The BrdU incorporation revealed that the H-RAS^{G12V} transduced population retained a lower percentage of BrdU positive cells when compared with the controls.

To further prove that the growth arrest had characteristics of senescence, cells were stained for senescence associated β-galactosidase (SA-β-Gal) activity, a widely used marker for identification of senescent cells. When H-RAS^{G12V} is activated, a higher percentage of cells

(89%) displayed SA-β-Gal activity compared with the percentage of positive cells in empty vector and H-RAS^{G12V} non 4OHT-treated (5% and 2%) respectively (Figure 4.1D).

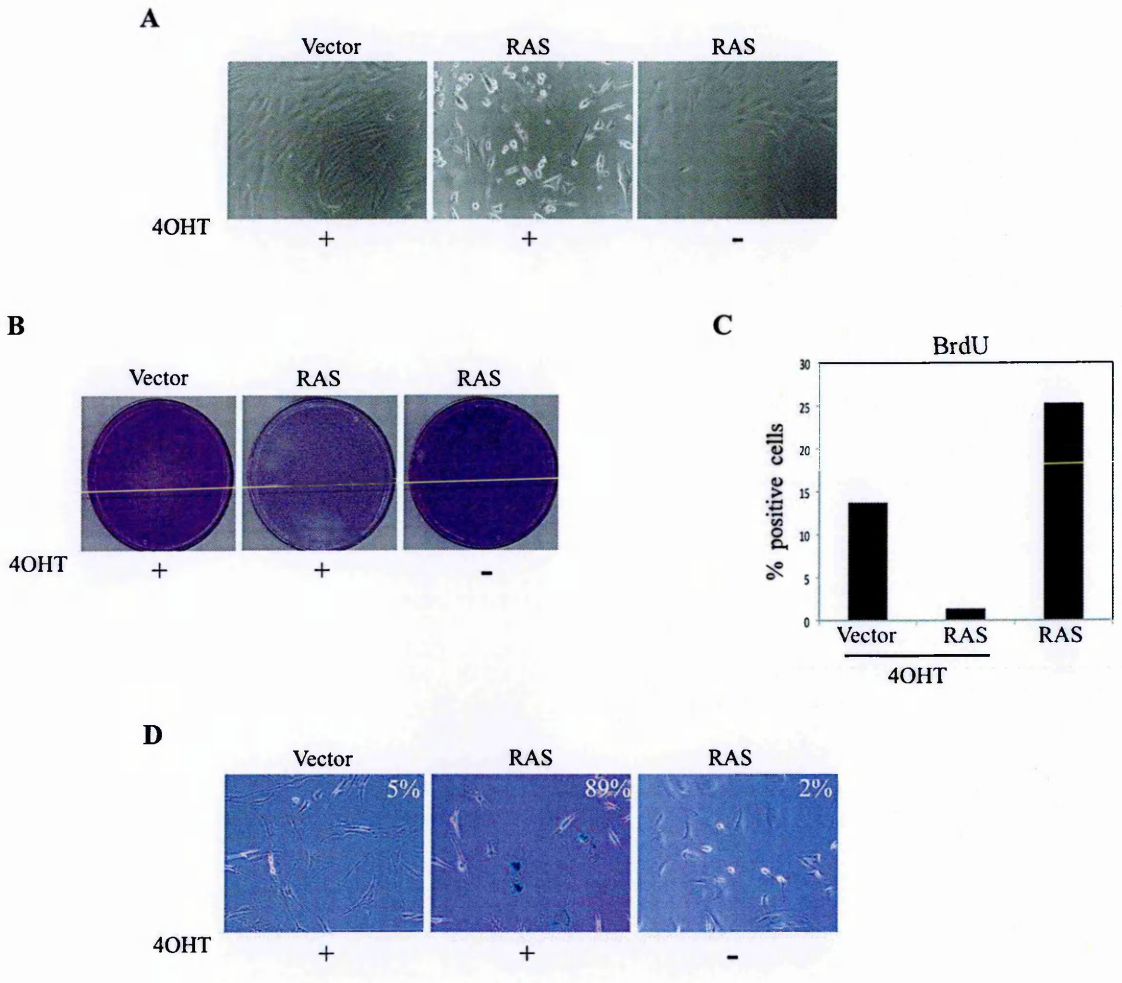

Figure 4.1 Expression of inducible H-RAS^{G12V} triggers senescence in primary thyrocytes.
A) Bright-field pictures acquired with a 10x objective 4 days after seeding, showed morphology of thyrocytes transduced with empty vector or H-RAS^{G12V} with (+) or without (-) 4-hydroxi-tamoxifen (4OHT) treatment. **B**) Samples were seeded at equal densities, fixed and stained 14 days post treatment with (+) or without (-) 4OHT. **C**) Samples were subjected to BrdU immunofluorescence. The percentage of positive cells was determined by high content analysis. Values generated at day 7 of a time-course experiment are reported. **D**) Representative images of SA-β-Gal staining (magnification 20x) are shown. Percentage of positive cells is indicated.

To address the mechanisms by which the inducible H-RAS^{G12V} triggered senescence in primary thyrocytes, we analyzed the expression of different senescence effectors by immunofluorescence. Activated H-RAS^{G12V} resulted in elevated expression of p16^{INK4a},

p53 and $p21^{CIP1}$ at 7 days after 4OHT treatment (Figure 4.2A-C). The levels of these negative regulators of cell cycle remained high during the time course.

Taking these results together we conclude that inducible H-RAS^{G12V} oncogene leads to senescence response in our cellular model and this is in harmony with our previous findings (see chapter 3).

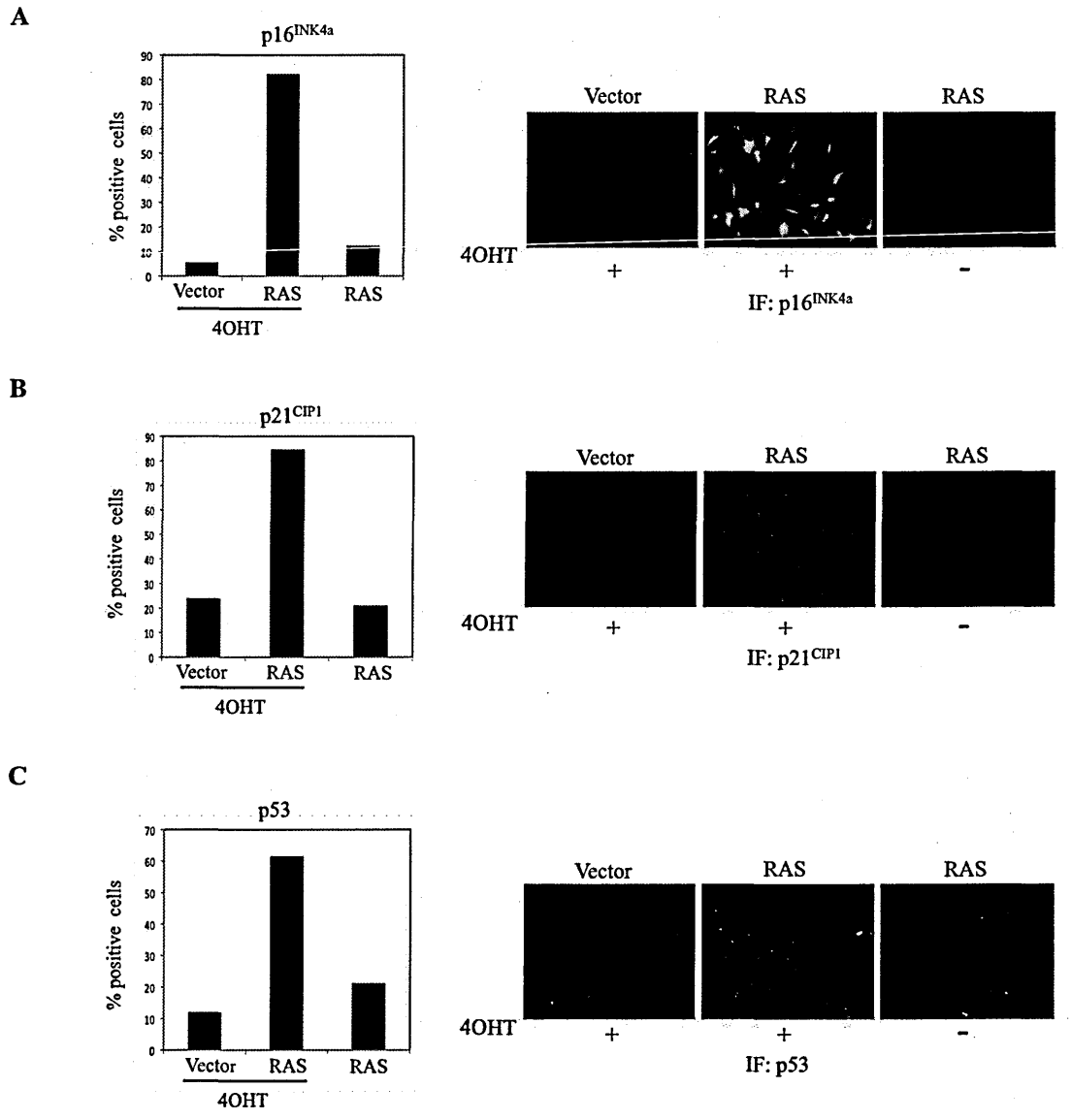

Figure 4.2 Molecular analysis of senescence induced by expression of H-RAS^{G12V}. A-C) The levels of $p16^{INK4a}$, $p21^{CIP1}$ and p53 expressed in thyrocytes transduced with empty vector or H-RAS^{G12V} and treated with (+) or without (-) 4OHT were analyzed by immunofluorescence and quantified by high content analysis. Values generated at day 7 of a time-course experiment are reported.

4.1.2 The relative contribution of $p16^{INK4a}$ and p53 pathways in $H\text{-}RAS^{G12V}$ induced senescence in thyrocytes

It is conceivable that the tumour suppressors $p16^{INK4a}$ and p53 owe, at least in part, their important role in cancer suppression by acting as critical mediators of oncogene-induced senescence. In light of this, we wondered what is the contribution of these two main tumour suppressors in the onset of senescence in $H\text{-}RAS^{G12V}$ transduced thyrocytes.

To examine the requirement of $p16^{INK4a}$ to $H\text{-}RAS^{G12V}$ mediated senescence we applied retroviral shRNA vector that specifically and efficiently suppresses the expression of $p16^{INK4a}$ (Figure 4.3A). Empty vector or $H\text{-}RAS^{G12V}$ cells expressing $p16^{INK4a}$ shRNA, selected for puromycin, were plated at equal densities. The cell proliferation assay showed that $p16^{INK4a}$ depletion caused cells to bypass OIS (Figure 4.3B). To quantify the rescue from senescence, we performed a BrdU incorporation assay (Figure 4.3C). As measured 7 days after adding 4OHT, the percentage of $H\text{-}RAS^{G12V}$ cells incorporating BrdU increased upon knockdown of $p16^{INK4a}$ and reached 13% compared with 1% of $p16^{INK4a}$-intact cells incorporated BrdU. Similar results were also observed following transfection of controls (All Stars) and $p16^{INK4a}$ siRNA into thyrocytes infected with empty vector and $H\text{-}RAS^{G12V}$. The silencing of $p16^{INK4a}$ expression was highly effective after sip16 transfection as shown in Figure 4.3D and this resulted in an increased of BrdU incorporation in $p16^{INK4a}$–null $H\text{-}RAS^{G12V}$ respect to $p16^{INK4a}$-positive senescent cells (10% versus 1%) (Figure 4.3E).

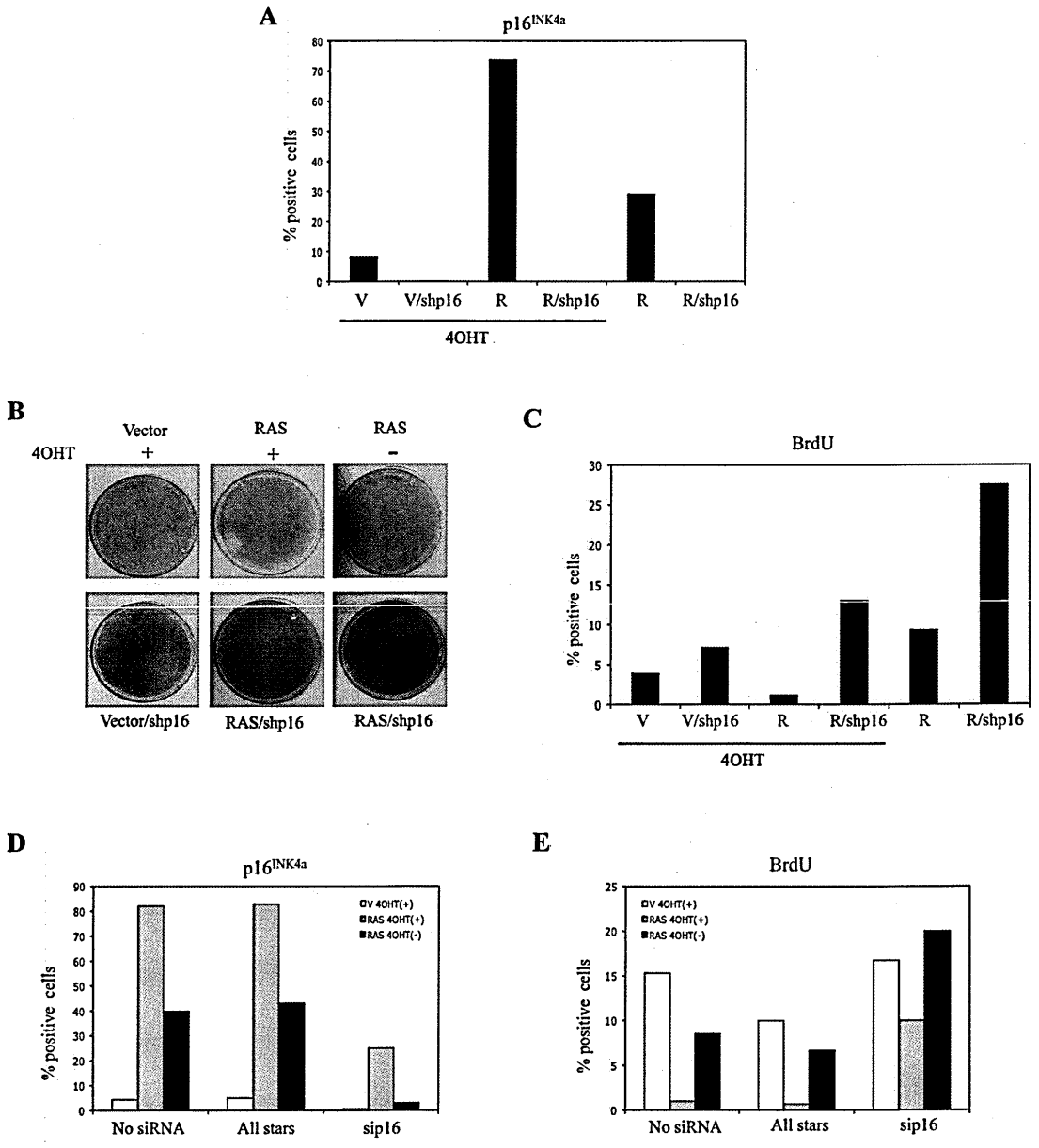

Figure 4.3 Silencing of $p16^{INK4a}$ with shRNA or siRNA extends cellular life span in H-RAS^{G12V}-transduced thyrocytes. A) Empty vector or H-RAS^{G12V} cells were retrovirally transduced with shRNA targeting $p16^{INK4a}$ which efficiently silenced $p16^{INK4a}$ expression. **B)** Samples were seeded at equal densities, fixed and stained 14 days after treatment with (+) or without (-) 4OHT. **C)** Seven days after exposure with or without 4OHT, samples were analyzed for BrdU incorporation via immunofluorescence. The percentage of positive cells was measured by high content analysis. **D-E)** Empty vector or H-RAS^{G12V} cells were transfected with 100 nM of siRNAs targeting $p16^{INK4a}$. Four days later, the expression of $p16^{INK4a}$ and BrdU incorporation was assessed by immunofluorescence and quantified by high content analysis. Non-siRNA and scrambled siRNA (All stars) transfected cells were used as negative controls.

Of other OIS markers analysed after shp16 transduction, we found that the percentage of H-RAS^{G12V} cells positive for SA-β-Gal activity was clearly reduced in absence of p16^{INK4a}: in fact only 5% of cells stained positively for SA-β-Gal versus 89% of H-RAS^{G12V} cells with intact p16^{INK4a} (Figure 4.4A).

Moreover, elevated levels of p21^{CIP1} were maintained in the p16^{INK4a}-null H-RAS^{G12V} thyrocytes (Figure 4.4B), whereas a slight decrease of p53 was observed (Figure 4.4C). Hence, we conclude that disruption of p16^{INK4a} allows primary thyrocytes to escape from H-RAS^{G12V} induced senescence.

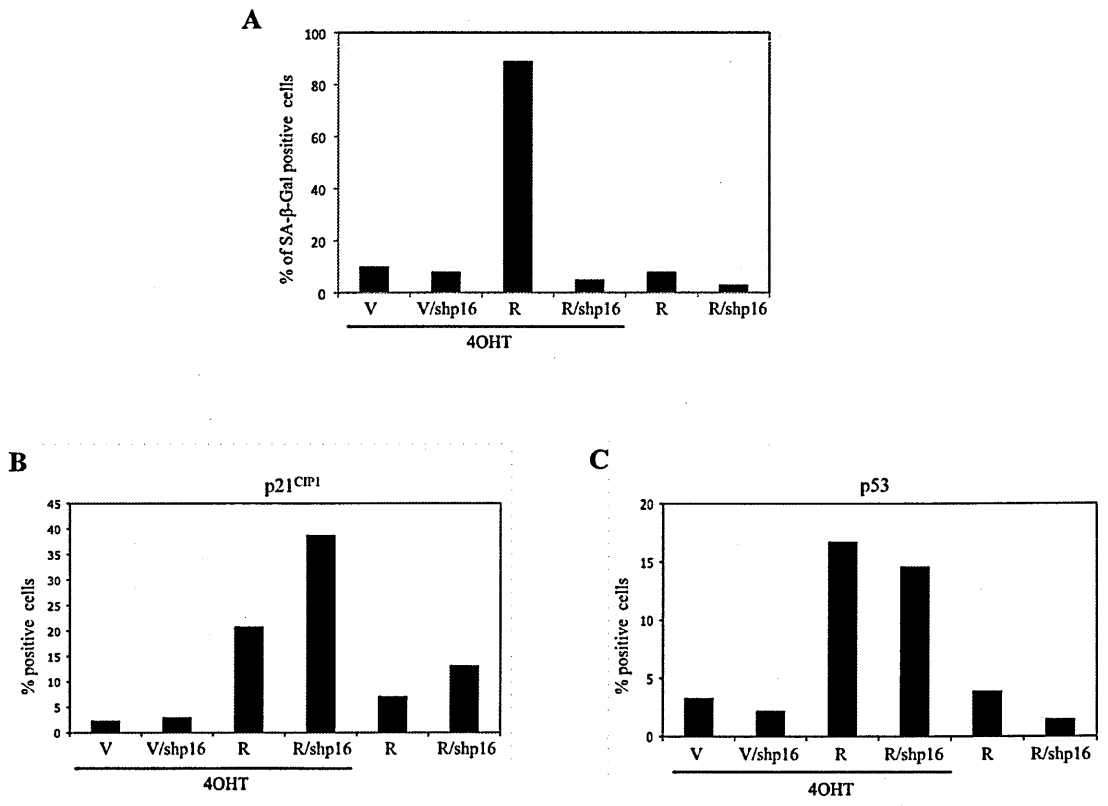

Figure 4.4 Primary thyrocytes transduced with shRNA against p16^{INK4a} fail to undergo H-RAS^{G12V} - induced senescence. **A)** Percentage of the indicated cells positive for SA-β-Gal activity was shown. **B-C)** Expression of p21^{CIP1} and p53 of cells infected with shp16 and either retrovirus expressing H-RAS^{G12V} or the empty vector was determined by high content analysis at 7 days after 4OHT treatment. V: Vector; R: RAS.

These results are in contrast with our previous findings described in chapter 3 in which suppression of $p16^{INK4a}$ with two independent lentiviral shRNA in $BRAF^{V600E}$ transduced thyrocytes did not alter the growth arrest induced by $BRAF^{V600E}$. To determine whether this different cellular response after $p16^{INK4a}$ inhibition is oncogene-specific ($BRAF^{V600E}$ versus $H\text{-}RAS^{G12V}$) or it is due to the different method of oncogene delivery (lentiviral versus retroviral) resulting in a different oncogene expression, we also evaluated the role of $p16^{INK4a}$ in thyrocytes infected with retroviral vector encoding $BRAF^{V600E}$ oncogene.

To this end, cells expressing $p16^{INK4a}$ shRNA produced by retroviral transduction, were selected using puromycin prior to retroviral reinfection with oncogenic $BRAF^{V600E}$.

We observed a strong suppression of $p16^{INK4a}$ expression as shown in Figure 4.5A. Interestingly, knockdown of $p16^{INK4a}$ enabled the cells to abrogate $BRAF^{V600E}$-induced senescence and to continue active proliferation, as demonstrated by BrdU incorporation (Figure 4.5B) and proliferation assays (Figure 4.5C). Moreover, in $p16^{INK4a}$-null $BRAF^{V600E}$ thyrocytes the induction of $p21^{CIP1}$ and p53 was maintained elevated (Figure 4.5D-E).

Such an escape from $BRAF^{V600E}$-induced senescence was also confirmed by sip16 transfection which efficiently silenced $p16^{INK4a}$ expression (Figure 4.6A). In BrdU incorporation assay the number of cells actively replicating DNA in the presence of oncogenic stress increased by ~4-fold upon $p16^{INK4a}$ depletion with siRNA (Figure 4.6B).

Together, these results suggest that in the absence of $p16^{INK4a}$ cells retrovirally transduced with $BRAF^{V600E}$ fail to undergo senescence.

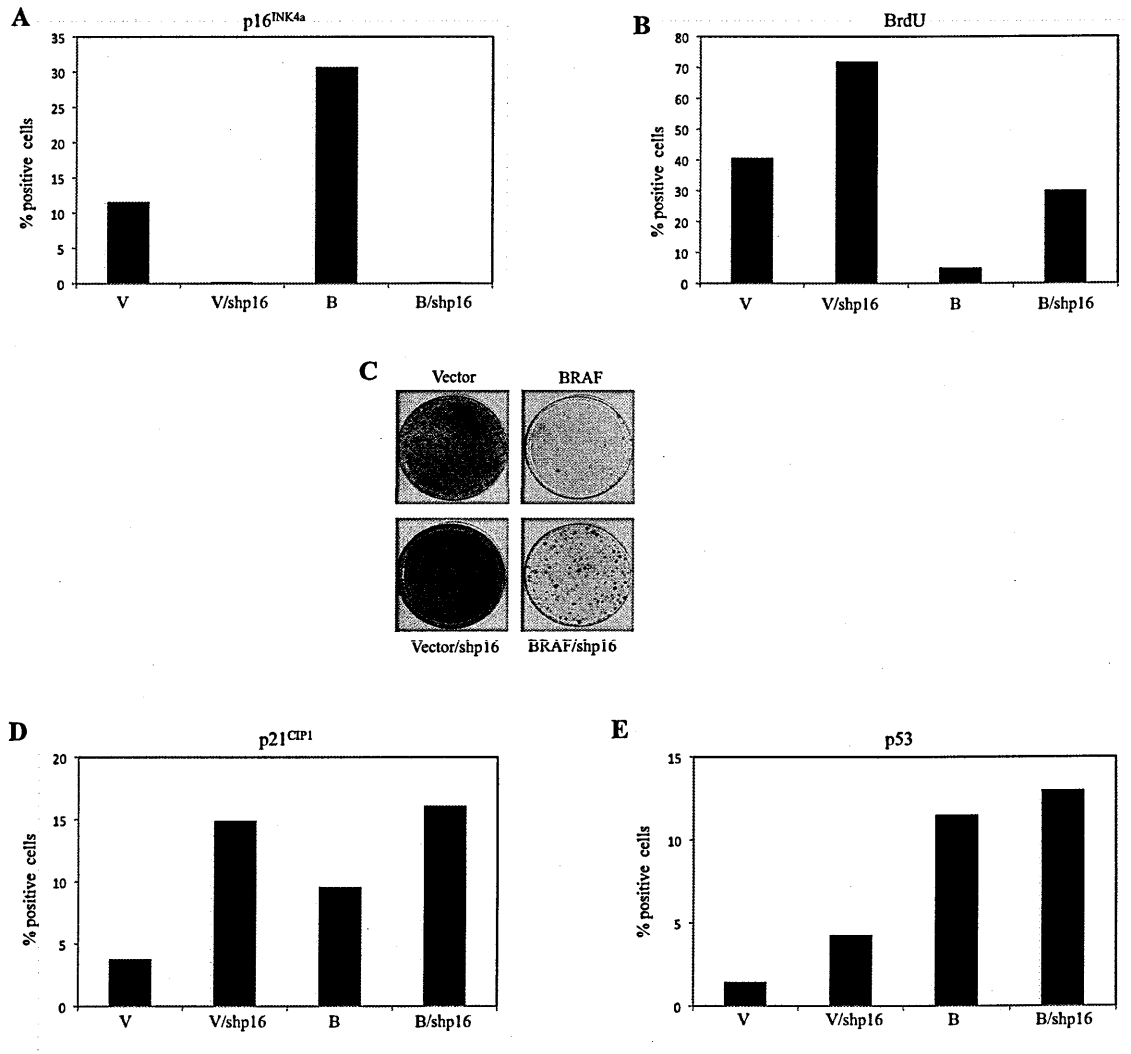

Figure 4.5 Primary thyrocytes retrovirally transduced with $BRAF^{V600E}$ override senescence after silencing of $p16^{INK4a}$. **A)** Cells infected with shRNA against $p16^{INK4a}$ were exposed to $BRAF^{V600E}$ (B) or empty vector (V) for 7 days. The amount of $p16^{INK4a}$ was analyzed by immunofluorescence and quantified by high content analysis. **B)** Samples were analyzed for BrdU incorporation by immunofluorescence. The percentage of positive cells was determined by high content analysis. **C)** Samples were seeded at equal densities and fixed and stained 14 days after exposure to $BRAF^{V600E}$. **D-E)** The expression of $p21^{CIP1}$ was assessed by immnunofluorescence and high content analysis was used for the quantification.

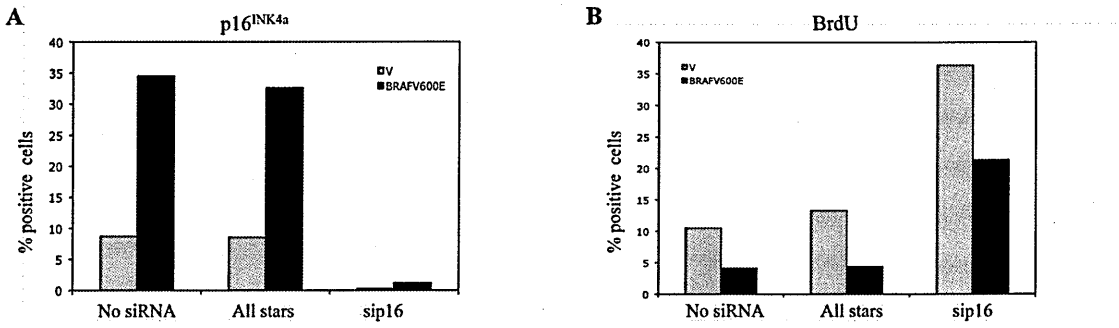

Figure 4.6 sip16 transfection in BRAF^{V600E} expressing thyrocytes allows for OIS abrogation. A-B) BRAF^{V600E} or empty vector (V) cells were transfected with 100 nM of siRNAs targeting p16^{INK4a}. Four days later the expression of p16^{INK4a} and BrdU incorporation were analyzed by immunofluorescence and quantified by high content analysis. Non-siRNA and scrambled siRNA (All stars) transfected cells were used as negative controls.

To investigate the possible role of the p53 pathway activation in evasion of H-RAS^{G12V}-induced senescence, we applied a shRNA vector to knockdown p53 expression using a retroviral delivery system. Cells were first infected with H-RAS^{G12V} oncogene or empty vector and then re-transduced with shRNA targeting p53 and selected for the integration of the construct. Seven days after adding 4OHT, immunofluorescence analysis revealed a drop in p53 levels upon shRNA transduction, only 1% of H-RAS^{G12V} cells expressing shp53 and treated with 4OHT displayed p53 expression compared with 26% of senescent H-RAS^{G12V} cells (Figure 4.7A).

However, in response to 4OHT treatment, no change in cell proliferation was observed between p53-intact and p53-null H-RAS^{G12V} thyrocytes as evident in cell proliferation assay (Figure 4.7B). Moreover, in BrdU incorporation assay p53 depletion did not alter the growth arrest induced by H-RAS^{G12V}, only 2.5% of p53 silenced H-RAS^{G12V} cells with 4OHT had incorporated BrdU, compared with the controls (Figure 4.7C). Likewise, cellular senescence was initiated and maintained in the presence or absence of p53

expression; we did not observe a significant difference in SA-β-Gal activity which appeared in 65% of p53-null compared to 80% in the p53 positive senescent cells, 7 days post 4OHT treatment (Figure 4.8A). Furthermore, in p53-deficient H-RAS^{G12V} cells the expression of p16^{INK4a} was maintained compared to p53-intact cells (Figure 4.8B). Similarly, upon depletion of p53, H-RAS^{G12V} cells treated with 4OHT showed p21^{CIP1} expression, albeit at level less that the one detected in H-RAS^{G12V} senescent cells (Figure 4.8C).

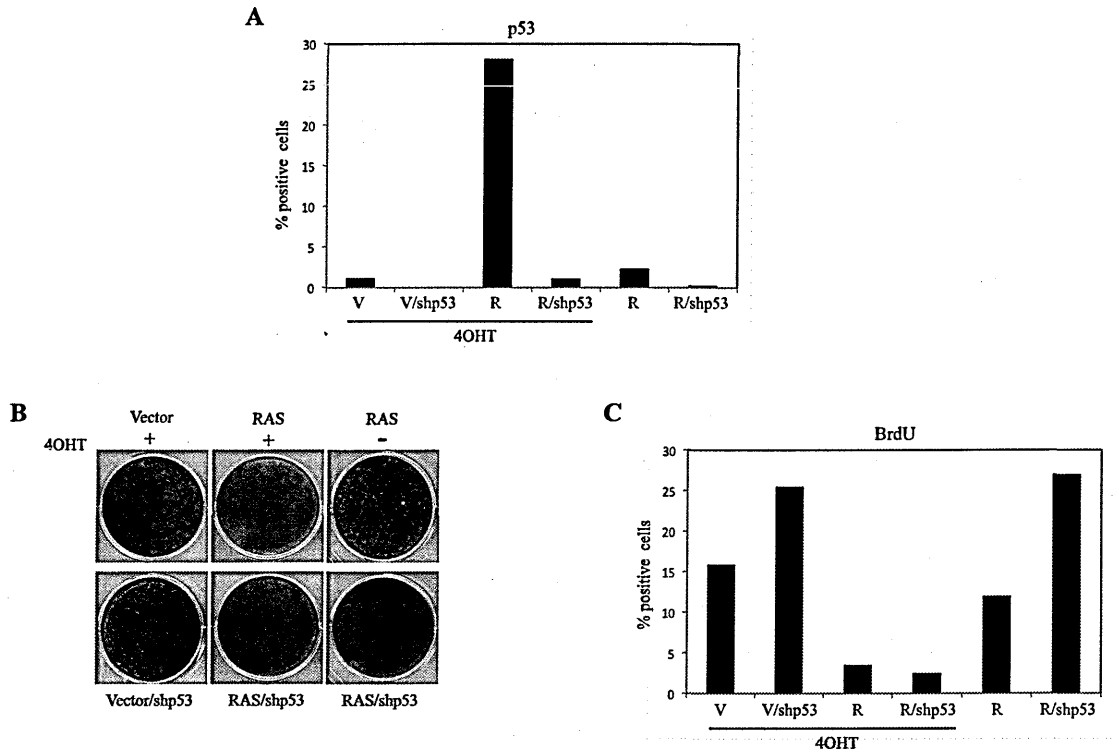

Figure 4.7 p53 tumour suppressor is not required for H-RAS^{G12V}-induced thyrocytes senescence. Cells infected with H-RAS^{G12V} (R) or empty vector (V) were re-transduced with p53 shRNA and pharmacologically selected for successful integration of the construct. Non-4OHT treated counterparts (R) and empty vector (V) were used as a negative controls. The analysis was performed 7 days after 4OHT treatment. **A)** The expression of p53 was detected via immunofluorescence and quantified by high content analysis. **B)** Samples were seeded at equal densities and fixed and stained with crystal violet. **C)** Samples were analyzed for BrdU incorporation by immunofluorescence.

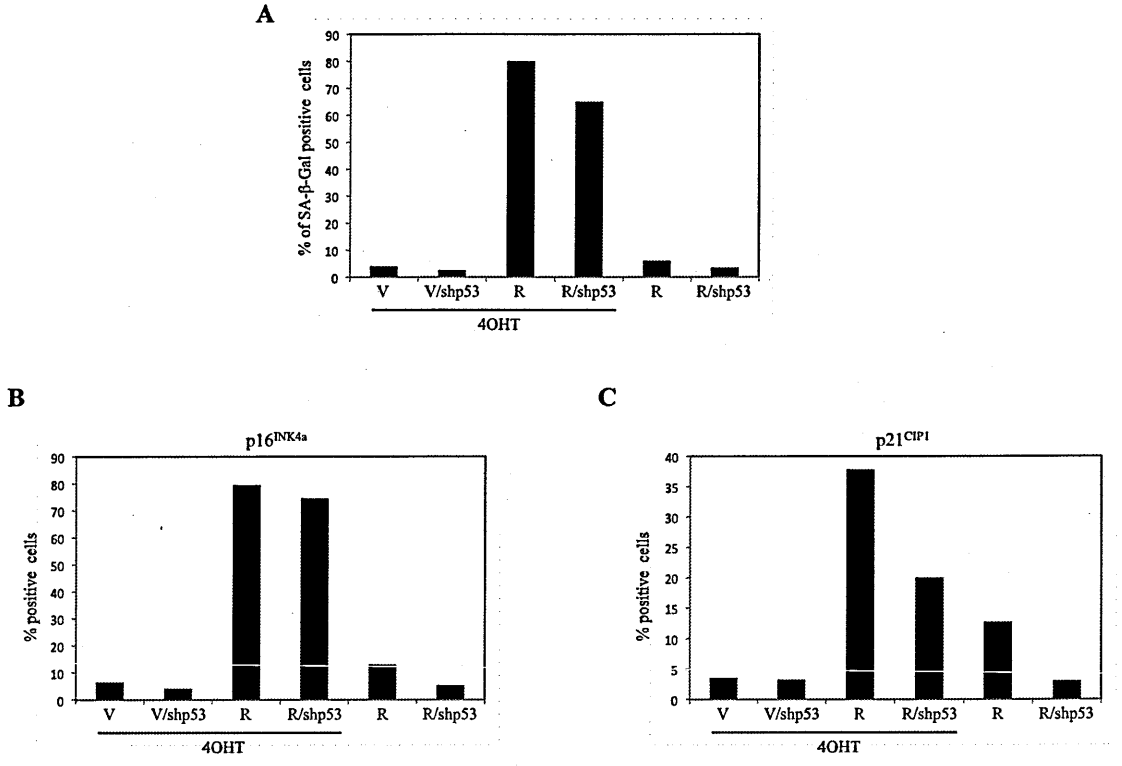

Figure 4.8 Depletion of p53 has no effect on OIS markers. A) Samples were fixed and analyzed for SA-β-Gal activity. The percentage of positive cells is shown. **B)** The percentage of positive cells for $p16^{INK4a}$ and $p21^{CIP1}$ expression, analyzed by immunofluorescence and quantified by high content analysis, is reported.

Similar results were also obtained after p53 siRNA transfection which resulted in a significant reduction of p53 levels, quantified around 80% (Figure 4.9A). We again observed that depletion of p53 had not effect on cell growth inhibition induced by activated $H\text{-}RAS^{G12V}$: the percentage of BrdU incorporation was not changed upon p53 silencing in $H\text{-}RAS^{G12V}$ cells with 4OHT (Figure 4.9B).

Together, these results indicate that p53 activation is not an essential effector of $H\text{-}RAS^{G12V}$-induced senescence in primary thyrocytes.

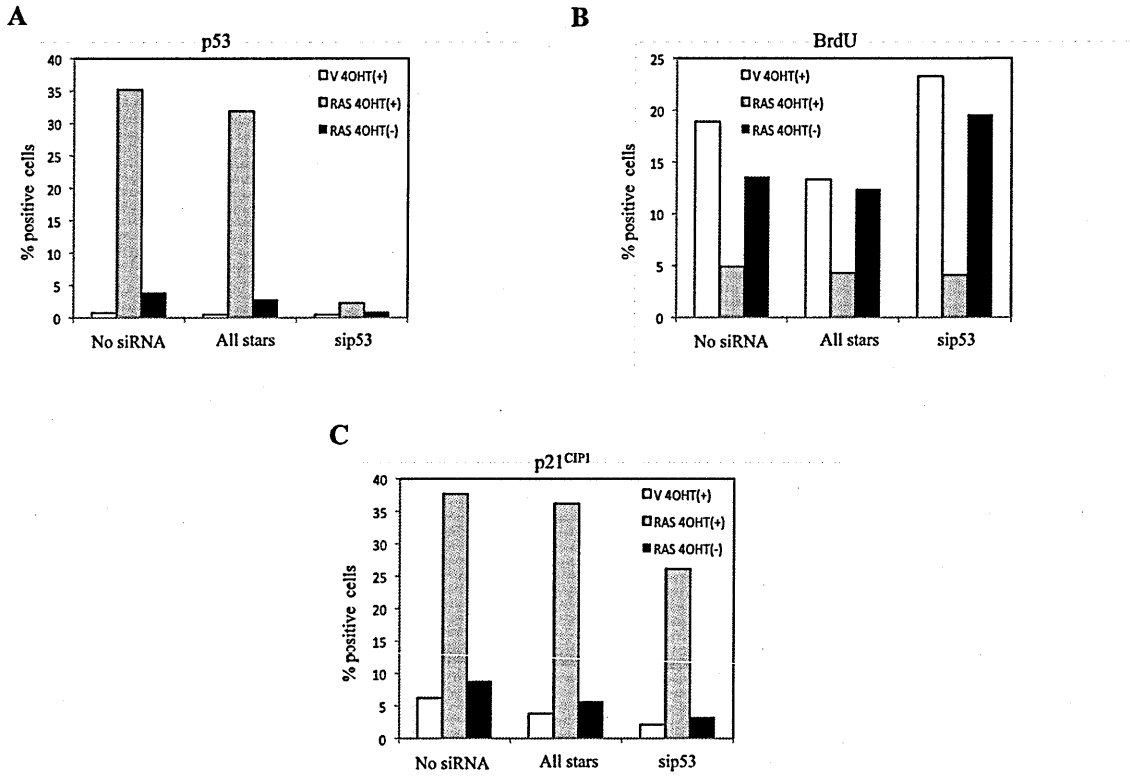

Figure 4.9 Knockdown of p53 with siRNA has no impact on OIS induced by H-RAS^{G12V} in primary thyrocytes. A-C) H-RAS^{G12V} or empty vector cells (V) were transfected with 100 nM of siRNA targeting p53. Four days later the expression of p53, BrdU incorporation and p21^{CIP1} were analyzed by immunofluorescence and quantified by high content analysis.

Moreover, it is important to note that, as already observed in shRNA p53 transduction, the induction of p21^{CIP1} expression was maintained in p53 knockdown H-RAS^{G12V} cells treated with 4OHT (Figure 4.9C), suggesting a p53-independent expression of p21^{CIP1}. In light of this regulation we asked whether depletion of p21^{CIP1} could also influence OIS. To this end, the efficiency of knockdown, estimated around 60%, was assessed 5 days after sip21 transfection via immunofluorescence. Such a depletion did not influence H-RAS^{G12V} induced growth arrest as evident by BrdU incorporation assay. The p21^{CIP1}-null cells responded to activated H-RAS^{G12V} by accumulating p53 (Figure 4.10A-C).

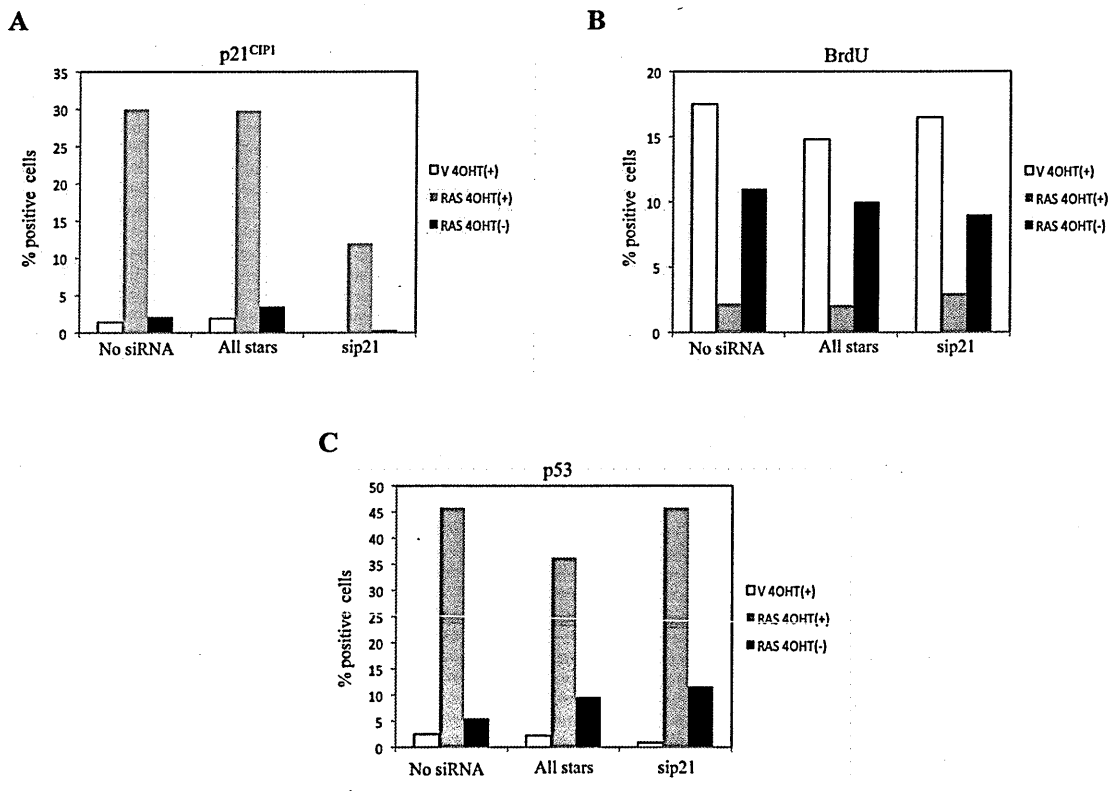

Figure 4.10 Depletion of $p21^{CIP1}$ expression does not allow for bypass OIS in primary thyrocytes. A-C) $H\text{-}RAS^{G12V}$ or empty vector (V) cells were transfected with 100 nM of siRNA targeting $p21^{CIP1}$. Four days later the expression of $p21^{CIP1}$, BrdU incorporation and p53 was analyzed by immunofluorescence and quantified by high content analysis.

4.1.3 Specific upregulation of IL8 and IL6 during OIS in thyrocytes

In addition to classical senescence players like $p16^{INK4a}$ and p53, as described above, several secreted factors such as PAI 1, IGFBP7, IL6 and CXCR2 and its ligands have been identified as a key components of the OIS response (Kortlever et al., 2006; Wajapeyee et al., 2008; Kuilman et al., 2008; Acosta et al., 2008). As preliminary analysis of senescent secretome we performed immunofluorescence for IL6 and IL8 to determine whether the expression of these factors is changed during OIS in our cellular model. Interestingly, we observed a strong induction of IL6 and IL8 in $H\text{-}RAS^{G12V}$-induced senescent cells as

compared with H-RAS^{G12V} untreated and to cells transfected with the empty vector, respectively (Figure 4.11A-B).

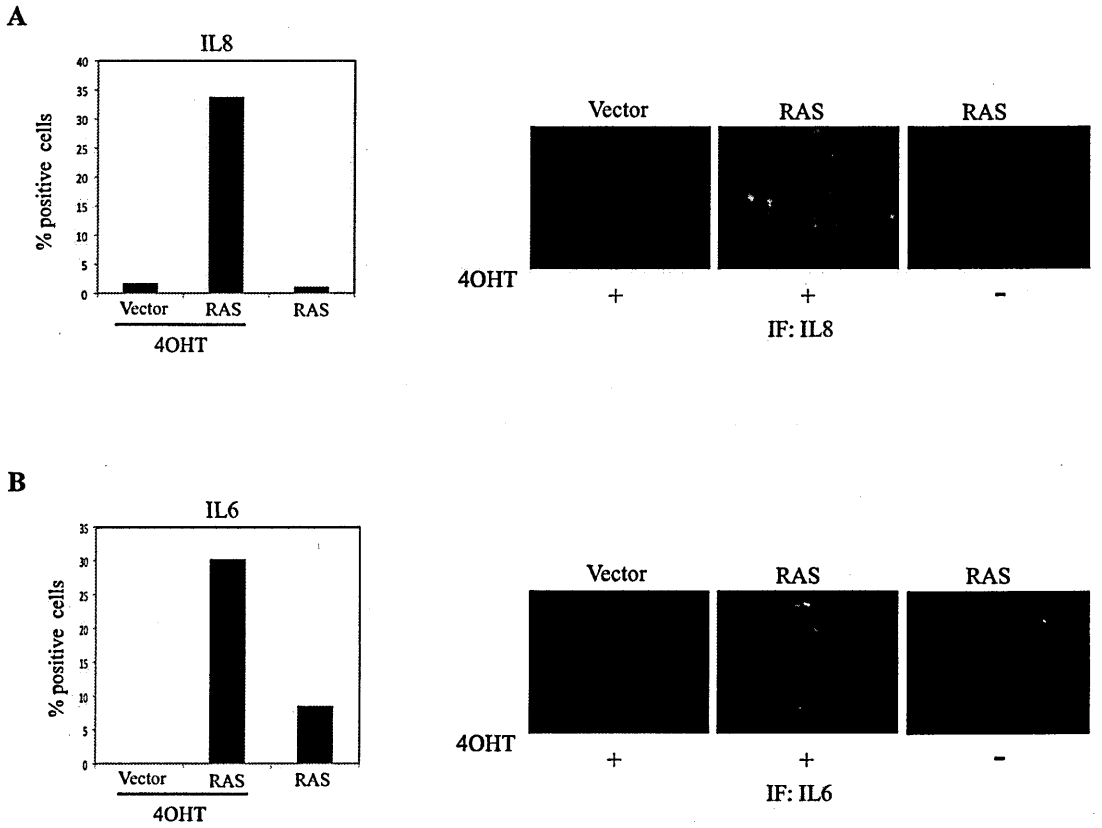

Figure 4.11 OIS is associated with activation of inflammatory transcriptome in primary thyrocytes.
A-B) The levels of IL8 and IL6 expressed in thyrocytes transduced with empty vector or H-RAS^{G12V} and treated with (+) or without (-) 4OHT were analyzed by immunofluorescence and quantified by high content analysis. Values generated at day 7 of a time-course experiment are reported.

4.1.4 A critical role for IL8R (CXCR2) in mediating OIS

In light of this specific regulation, we wondered whether these cytokines are required for OIS in primary thyrocytes. To this end, we focused on IL8, a multifunctional chemokine implicated in a variety of cellular functions, including immune response, proliferation and tumorigenesis (Xie K, 2001). IL8 binds to two cells surface G-protein coupled receptors (GPCR), CXCR1 and CXCR2, respectively (Holmes We et al., 1991).

In keeping with the well-known connection between IL8 and CXCR2 for the induction and maintenance of OIS (Acosta et al., 2008), we found that also in our cellular model CXCR2 expression increased during OIS compared with the non-senescent cells in which CXCR2 levels were low. To determine whether this receptor is required for the mediation of OIS we used shRNA vector targeting CXCR2 which prevented H-RAS^{G12V} cells from undergoing senescence, although its expression was not completely depleted by shRNA vector (Figure 4.12A). For instance, when H-RAS^{G12V} cells treated with 4OHT were plated at low density, depletion of CXCR2 conferred a growth advantage respect to the controls (Figure 4.12B). This was further illustrated by cell counting and BrdU incorporation assays. The cell number, quantified by high content analysis after DAPI staining, was duplicated upon CXCR2 depletion in H-RAS^{G12V} senescent cells (Figure 4.12C). Similarly the percentage of cells positive for BrdU incorporation in the presence of activated oncogene increased by ~4-fold upon CXCR2 knockdown (Figure 4.12D).

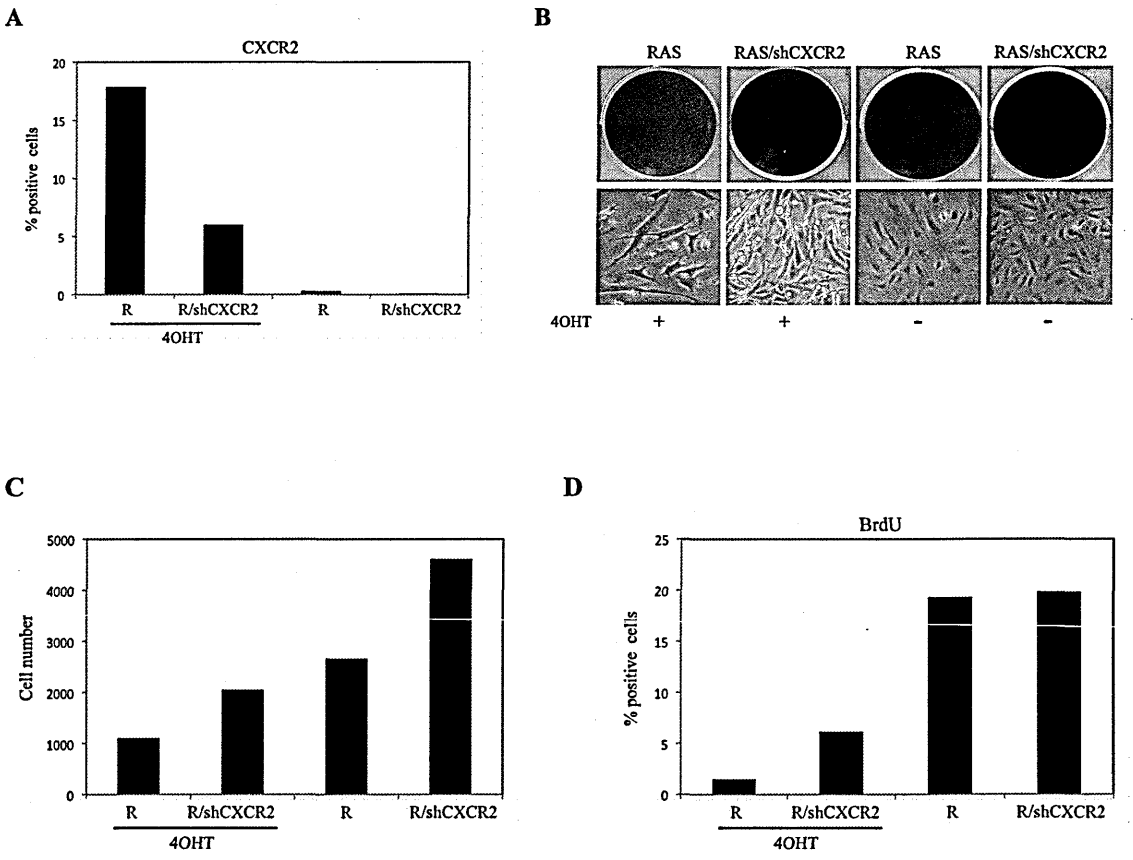

Figure 4.12 Depletion of CXCR2 extends the lifespan in primary thyrocytes. Cells infected with H-RAS^{G12V} (R) were re-transduced with sh-CXCR2, selected for integration of the construct and treated with (+) or without (-) 4OHT. The analysis was performed 7 days after adding 4OHT. **A)** The levels of CXCR2 were detected via immunofluorescence and quantified by high content analysis. **B)** Cells were seeded at equal number and fixed and stained with crystal violet. **C)** Cell counting after DAPI staining was quantified by high content analysis. **D)** Samples were analyzed for BrdU incorporation by immunofluorescence.

We next determined whether depletion of CXCR2 leads to changes in the expression of IL8 as well as in the well-known tumour suppressor genes controlling OIS. We found a decrease in IL8 availability (9% of activated H-RAS^{G12V} cells expressing CXCR2 shRNA were positive for IL8 staining compared with 25% of H-RAS^{G12V} senescent cells), as well as a drop in p53 levels (6% versus 15%) whereas the induction of p16^{INK4a} and p21^{CIP1} were maintained when CXCR2 is depleted (Figure 4.13A-D).

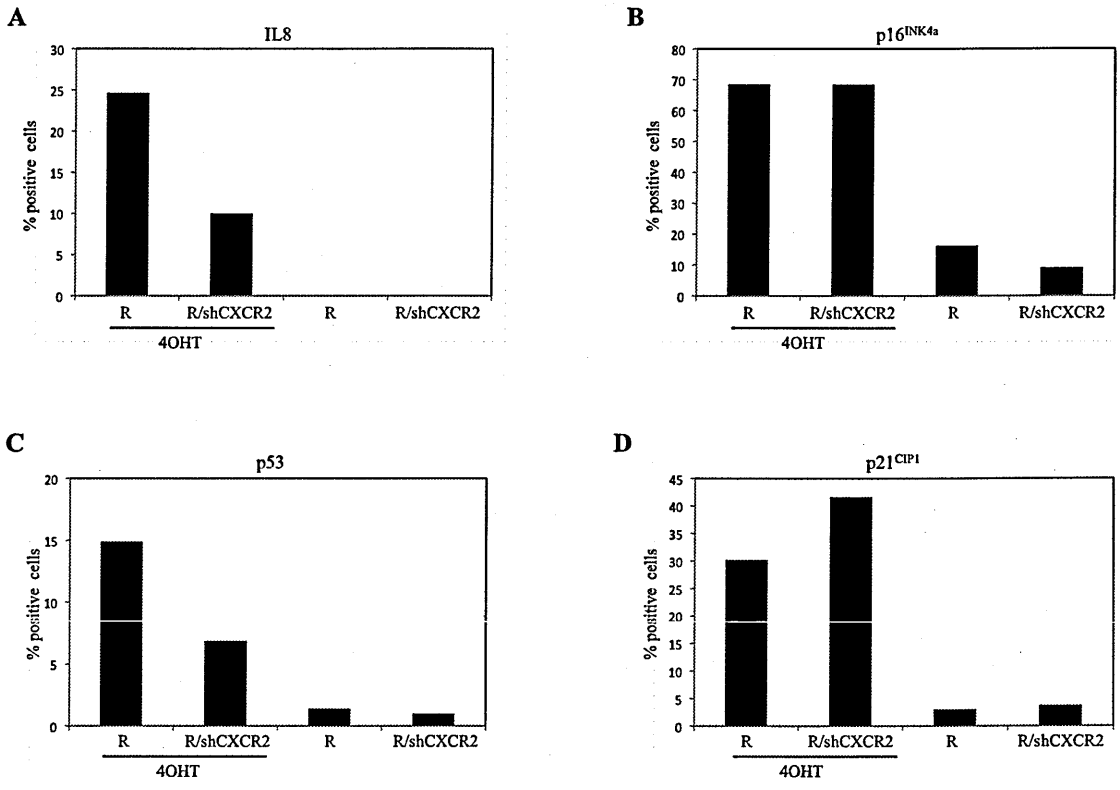

Figure 4.13 Effect of CXCR2 depletion on IL8 and tumour suppressor proteins expression. A-D) Analysis of IL8, $p16^{INK4a}$, p53 and $p21^{CIP1}$ levels by immunofluorescence in H-RAS^{G12V} (R) with or without 4OHT, as a function of CXCR2 knockdown.

As CXCR2 ligand, IL8, is upregulated during senescence, we investigated its involvement in the process. To this end, we knockdown IL8 expression with two independent retroviral shRNAs (#1, #2) which, compared to the control, alleviated senescence in H-RAS^{G12V} treated with 4OHT as shown by enhanced BrdU incorporation (3% vs 8% and 8.5% respectively) (Figure 4.14A-B). To determine whether IL8 depletion affected CXCR2 activation, we analyzed the levels of CXCR2 via immunofluorescence. We observed a decrease of CXCR2 expression when comparing control cells with cells expressing both sh-IL8 (27% vs 13% and 9% respectively), suggesting that sh-IL8 confers growth advantage by restricting CXCR2 activity (Figure 4.14C).

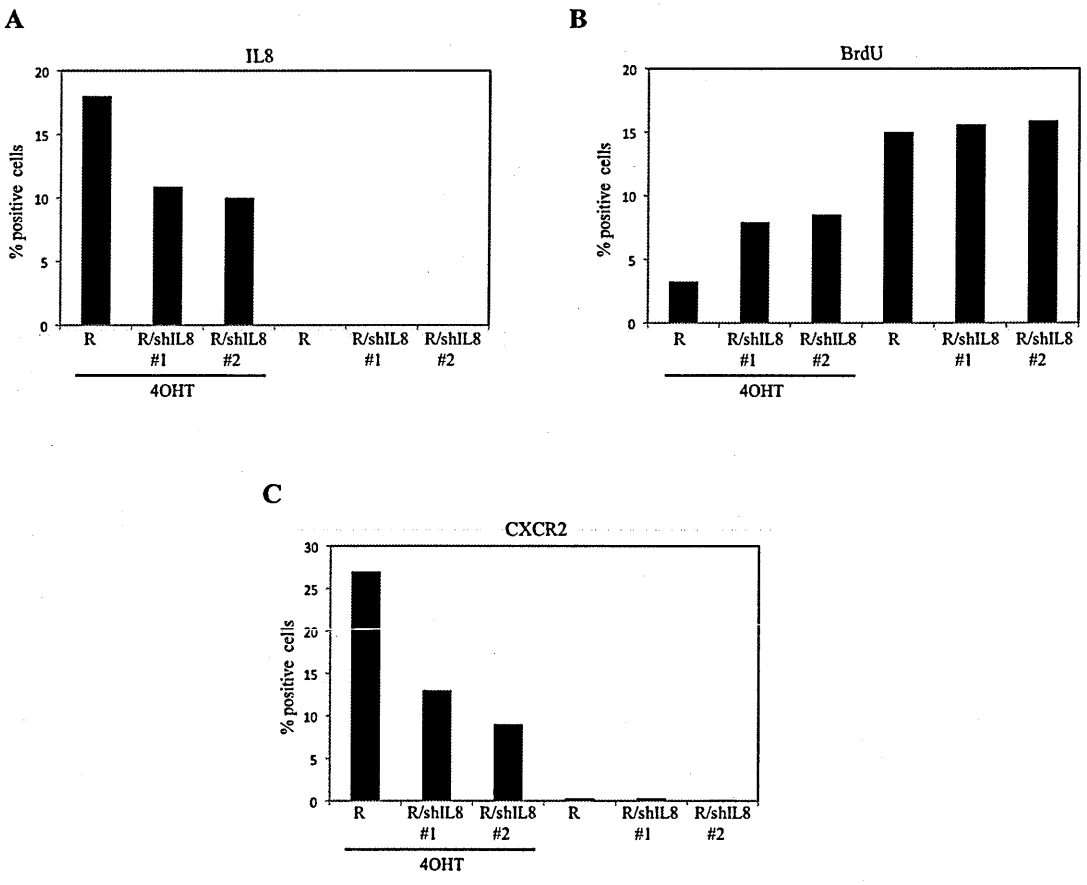

Figure 4.14 Role for CXCR2 ligand in mediating OIS. A) Cells infected with H-RAS^{G12V} (R) were re-transduced with two independent shRNAs targeting IL8 (#1 and #2), selected for integration of the construct and treated with or without 4OHT. The analysis of IL8 expression was performed via immunofluorescence 7 days after adding 4OHT. **B)** Cells infected with the indicated retroviruses and treated with or without 4OHT were analyzed by immunofluorescence and quantified for BrdU incorporation 7 days after adding 4OHT. **C)** Cells infected with the indicated vectors were subjected to CXCR2 immunofluorescence after 7 days 4OHT treatment. The percentage of positive cells is shown.

4.2 Discussion

We have already described in chapter 3 that H-RAS^{G12V} frequently detected in PTC, induces senescence in primary human thyrocytes similarly to the others PTC-associated oncogenes. As tool for a deeper analysis of OIS thyrocytes, here we established and characterized the H-RAS^{G12V} inducible system in our cellular model by transduction of thyrocytes with retroviral vector carrying H-RAS^{G12V} coupled to the ligand binding domain of the estrogen receptor. Activation of oncogene expression led to senescence-associated characteristics in thyrocytes.

In view of the strong evidence that H-RAS^{G12V} mediated senescence in primary thyrocytes through activation of both the pRb and p53 pathways, we assessed the relative contribution of the p16^{INK4a}/pRb and the p53/p21^{CIP1} in the senescence program.

As reported in several studies the critical role of p53 and pRb is not universal across cells types. Some are significantly delayed in their onset upon inactivation of p16^{INK4a} (Ben-Porath and Weinberg, 2005) while for others p53 plays a major role (Serrano et al., 2005), whereas yet in other setting inactivation of both is required to bypass the senescence response (Serrano et al., 1997).

In our experimental setting depletion of p53 by using RNA interfering strategy had not impact on senescence upon oncogenic stress. For instance, no change in cell proliferation, BrdU incorporation or SA-β-Gal activity was observed between p53-intact and p53-null senescent thyrocytes. Interestingly, p53 depletion did not reduce the levels of p21^{CIP1}, suggesting a p53-independent expression of p21^{CIP1}, whereas the expression of p16^{INK4a} was maintained. In light of this specific regulation, we next investigated the involvement of p21^{CIP1} in the OIS program. Indeed, we found that its knock down had no influence in the inhibition of proliferation induced by H-RAS^{G12V}.

It is reasonable to assume that in the absence of p53, the activation of $p16^{INK4a}$/pRb pathway was sufficient for induction and maintenance of OIS as its depletion with retroviral shRNA abrogated the onset of senescence. This was illustrated by increased of cell proliferation and BrdU incorporation, as well as decreased in SA-β-Gal activity. Thus, in our experimental setting $p16^{INK4a}$ seems to play a dominant role supporting a model in which oncogenic $H\text{-}RAS^{G12V}$ acts primarily through the $p16^{INK4a}$/pRb pathway in thyrocytes.

It is important to note that these results are in contrast with our previous findings presented in chapter 3 in which inactivation of $p16^{INK4a}$ with lentiviral shRNA in $BRAF^{V600E}$ transduced thyrocytes was not sufficient to prevent induction of senescence suggesting that the critical role of $p16^{INK4a}$ in the abrogation of senescence may also depend on different genetic context. This is in agreement with models previously proposed by others (Serrano et al., 1997; Michaloglou et al., 2005). Thus, to get more insight into the reported differences (lentiviral $BRAF^{V600E}$ vs retroviral $H\text{-}RAS^{G12V}$) regarding the contribution of $p16^{INK4a}$ we also determined the role of $p16^{INK4a}$ in thyrocytes infected with retroviral vector encoding $BRAF^{V600E}$. Interestingly, we observed the abolishment of OIS by inactivation of $p16^{INK4a}$. In aggregate, the different methods of oncogene delivery resulting in different oncogene accumulation may vary the mechanism of senescence activation and may warrant the different response upon $p16^{INK4a}$ depletion.

In recent years, several groups have demonstrated that cells undergoing senescence produce increased amount of inflammatory cytokines and chemokines that play an essential role in the initiation and maintenance of cellular senescence (Acosta et al., 2008; Kuilman et al., 2008).

We also observed that IL8 and its receptor CXCR2 were upregulated in $H\text{-}RAS^{G12V}$ transduced cells.

This regulation prompted us to examine their roles in OIS. Upon depletion of CXCR2 by shRNA vector, senescent thyrocytes expressing H-RAS^{G12V} were able to bypass OIS in a p53-dependent manner. We also observed a drop of IL8 expression after CXCR2 abrogation, suggesting that the induced IL8 is responsible for the activation of CXCR2 during senescence. Similarly, knock down of IL8 using two independent shRNAs vectors allowed cells to circumvent OIS and resulted in decreased CXCR2 levels.

These findings in harmony with and extend previously model proposed by Gil and co-workers (Acosta et al., 2008) indicate that the activation of chemokine signalling via CXCR2 plays an essential role in execution of cellular senescence.

The inducible OIS model allowed us to get more insight into the molecular mechanisms and players controlling H-RAS^{G12V}-mediating senescence. We will employed this system for further studies regarding the interplay between oncogene-triggered thyrocytes senescence and microenvironment, in particular macrophages with the aim to dissect the macrophage role in early stage of thyroid tumours. In order to investigate the effects of senescent thyrocytes on macrophage differentiation and polarization, purified peripheral blood-derived human monocytes from independent donors will be co-cultured with senescent thyrocytes or exposed to their conditioned medium in the presence of M-CSF and the phenotype and functional activity will be characterized. In particular we will check M1 and M2 associated markers (MHC II, CD206, CD16, MSF), cytokine and chemokine production, functional activities (antigen presenting ability, invasion of Matrigel-coated membranes). We are next interested in determining whether activated macrophages either reinforce senescence in H-RAS^{G12V}-transduced thyrocytes or help them to bypass senescence, thus promoting tumorigenesis. To this end, thyrocytes at different phase of OIS will be co-cultured with different of activated macrophages or exposed to their CM.

The extent of senescence in thyrocytes will be monitored over time by assessing the presence of senescence markers such as SA-β-Gal, SAHFs, $p16^{INK4a}$. Finally, it will be interesting to investigate in human thyroid samples PTMC the presence of the players identified by *in vitro* models including senescent thyrocytes-derived soluble factors and senescent thyrocytes induced infiltrating cells and their specific markers.

4.3 Materials and methods

4.3.1 Cell culture

Human primary thyrocytes and HEK293T packaging cells were described in chapter 2.

4.3.2 Retrovirus production and transduction of target cells

HEK293T were seeded the previous day to reach a confluence of 70-80% the day of transfection. For each plate, 1 ml of serum-free DMEM containing 20 μg of expression plasmid and 10 μg of helper plasmid (gag-pol and VSV-g) was prepared. As transfection reagent, 75 μl of 25 KDa linear polyethylenimine (PEI 1mg/ml) was used. The mixture was incubated at room temperature for 30 minutes and added drop-wise to each plate. Transfection efficiency was monitored the next day by the presence of Cherry fluorescent protein expressed from a reporter plasmid. The day after transfection, the media on the transduced packaging cells was replaced (6ml/plate). In parallel, the target cells, human primary thyrocytes were plated at a density of $1x10^6$ cells per 10cm plate.

After 48 hours, the virus-containing supernatants were collected from packaging cells plates, filtered through 0.45 μm pore-sized acetate filters (Anachem) and supplemented with 4 μg/ml of polybrene (Sigma). The culture media of the target cells was then removed and replaced by the virus-containing supernatant. Infection took place 3 rounds to maximize the efficiency and a period of 3 hours was left between each round for virus production. After 3 rounds cells were refreshed.

Approximately, 2 days after infection, cells were split and subjected to the selection.

4.3.3 Plasmids

Retrovirus encoding H-RAS^{G12V} was cloned via PCR in LXSN neo. Retrovirus encoding shRNAs targeting human p16^{INK4a}, p53, CXCR2 and IL8 were constructed by cloning oligonucleotides in pRetroSuper (pRS) puro.

pMSCV$_{BLAST}$-BRAF^{V600E} was used for retroviral transduction and was kindly provided by Daniel Peeper (NKI, Amsterdam).

The sense shRNA target sequences are as follows:

sh-p16^{INK4a}	GAGGAGGTGCGGGCGCTGC
sh-p53	GTAGATTACCACTGGAGTC
sh-CXCR2	GGACCGTCTACCATCCAA
sh-IL8-1	TTGAACTAACAATCCTAGT
sh-IL8-2	TACAAGATTCCTGGTTAAA

4.4.4 siRNA transfection

Primary thyrocytes were transfected with 30nM siRNA in 96 wells. A 3.5% solution of Hiperfect transfection reagent (QIAGEN) was prepared in serum-free medium and then mixed with the siRNA. The mix was incubated for 30 min at room temperature and then added to the cells. Medium was changed on the following day and cells were fixed for immunofluorescence at day 4 and 5. The Cy3-labeled siGLO cyclophilin B siRNA (Dharmacon) was used to monitor transfection efficiency and as a negative control. A scrambled siRNA (All stars) were included as additional negative controls in the experiments.

4.4.5 BrdU (5-Bromo-2'deoxyuridine) incorporation assay

Cells ($4x10^3$) were plated in 96-well plates in duplicates and subsequently incubated with 5-Bromo-2' deoxyuridine (BrdU, 50 μM, Sigma) for 24 hours. After incubation cells were washed with PBS and fixed for 30 min with 4% (w/v) paraformaldehyde (Sigma). For immunofluorescence staining, cells were first permeabilized for 5 minutes with 0.2 (v/v) Triton X-100 in PBS and incubated for 30 minutes with 1X (blocking solution (0.5% (w/v) BSA, 0.2% (w/v) fish skin gelatin). Treatment with DNase I (0.5U/μL; Sigma) in presence of 1mM $MgCl_2$ was performed simultaneously with anti-BrdU primary antibody (1:500, BD) for 30 minutes. Cells were washed three times with PBS and incubated with Alexa Fluor® 488 mouse secondary antibody (1:500, Invitrogen) for 30 minutes. Cells were washed three times with PBS and incubated with DAPI (Invitrogen, 1.5 μM). Plates were examined using In Cell Analyser and High Content Analysis was performed to discriminate positive BrdU nuclei and total nuclei.

4.4.6 Colony formation assay

Cells were plated at a density of $1x10^5$ and $5x10^4$ per 10-cm dish. After 7 or 15 days cells were washed with PBS and fixed with 0.5% glutaraldehyde (w/v) in PBS for 30 minutes. Finally, plates were stained with 0.2% crystal violet (w/v)

4.4.7 Senescence-associated β-galactosidase (SA-β-gal) assay

Cells were washed once with PBS, fixed with 0.5% glutaraldehyde (w/v), and washed in PBS (pH 6.0) supplemented with 1mM $MgCl_2$. Cells were stained in X-gal solution (1 mg/ml 5-bromo-chloro-3-indolyl-beta-D-galacto-pyranoside [Boehringer], 0.12 mM $K_3Fe[CN]_6$, 1 mM $MgCl_2$ in PBS at pH 6.0) for 7 hours at 37°C. After staining, cells were

washed with PBS and stored at 4°C, in the dark. Images were taken using the Olympus CKX41 inverted fluorescence microscope, supplied with a DP20 digital camera. The percentage of SA-β-gal positive cells were determined upon counting of at least 100 cells.

4.4.8 Immunofluorescence and high content analysis

For immunofluorescence, cells were fixed with 4% PFA (w/v) for 30 min, washed with PBS and permeabilised with 0.2% Triton X-100 (v/v) for 5 minutes. To block unspecific binding of primary antibody, cells were incubated for 30 minutes in blocking solution (0.5% BSA (w/v) and 0.2% fish skin gelatin (v/v) in PBS). Cells were then incubated with the primary antibody, diluted in blocking buffer for 30 minutes at room temperature. Three washes with the blocking buffer for removing unbound primary antibody were performed. Cells were subsequently incubated with the secondary antibody, diluted in blocking buffer for 30 minutes. Cells were washed with PBS three times before adding 3μM DAPI for 30 minutes for nuclear staining.

The antibodies used for immunofluorescence were: anti-p16 (JC8, 1:100, Santa Cruz Biotechnology); anti-p21 (P1484, 1:100, Sigma Aldrich); anti-p53 (DO-1, 1:100, Santa Cruz Biotechnolgy), anti-IL8 (1:100, BD), anti-CXCR2 (1:100, BD), anti-IL6 (1:100, BD). Secondary antibody used was anti-mouse Alexa488-conjugated antibody (1:500, Invitrogen).

Acquisition of immunofluorescence images was performed using the IN Cell Analyzer 1000 automated high-throughput microscope (GE Healthcare) with 10x objective. Image processing was performed using the IN Cell Investigator (v1.7) software (GE Healthcare).

High Content Analysis (HCA) was used for quantification of immunofluorescence images. Two fluorescence images corresponding to DAPI and primary/antibody/Alexa Fluor® 488-

secondary were acquired for each condition. HCA was performed using the IN Cell Investigator (v1.7) software (GE Healthcare). For the analysis, DAPI staining of the nuclei was used to identify nuclear area and number of cells. The nuclei were defined by using top-hat segmentation, specifying a minimum nucleus area of 100 μm^2. To define the cell segmentation, a collar segmentation routine was used with a ratio of 1 μm. To determine the cellular expression of the analysed protein, the average intensity of pixels in the reference channel (Alexa Fluor® 488) within the specified nuclear region (Object Nuclear Intensity) was measured. Each cells was assigned a nuclear intensity value for the specific protein expression and that value was used to set up a threshold filter, which determined high levels (positive) and low levels (negative) expressing cells. The threshold filter used a histogram for data visualisation. In order to set the filter cut-off, expression in the control was measured to define the negative population. Next, the analysis of the positive control was performed to determine the high-expressing population. Once the cut-off was set up, the analysis of the whole experiment was carried out. As a result, the software classified each cell as either positive or negative for the expression of the analysed protein and negative and generated a percentage of both cell population (positive and negative) per well. The mean of the nuclear intensity was also routinely analysed and equivalent results were obtained.

CHAPTER 5

Chapter 5 - Conclusions

Oncogene-induced senescence (OIS) is regarded as an important anti-cancer mechanism that restricts uncontrolled proliferation of cells and prevents neoplastic transformation *in vitro* and *in vivo,* and is recognized as a tumour suppressor mechanism. While its importance is beyond doubt, there are many key questions yet to be answered:

- How do cells decide whether to undergo senescence or apoptosis in response to stress signals?
- How homogenous is this response in different cellular contexts?
- Which features of senescent phenotype are of fundamental importance?
- Which is the relative contribution of OIS to tumour suppression?
- Is senescence a common trait, across different tissue types, at the early stage of tumorigenesis?

In this study we have demonstrated for the first time the involvement of OIS in thyroid carcinogenesis. We found that all the oncogenes activated in thyroid tumours (BRAF, RAS, RET, and TRK) have the potential to drive senescence in human primary thyrocytes. The comparative characterization in their capability to induce senescence in human primary thyrocytes revealed interesting similarities and differences in the phenotypes and pathways regulating this cellular program.

Translating our *in vitro* observations in an *in vivo* setting we found senescent cells at early stages of papillary thyroid tumour namely PTMC, as judged by the presence of OIS markers, whereas their gradual lost was observed during tumour progression suggesting that in thyroid cancer the senescence response may act as an initial barrier that restricts a full blown transformation.

Firstly, it was interesting to detect OIS in human primary thyrocytes with different oncogenes transfected with different methods and thus expressed at different levels.

We also established an OIS inducible system in our cellular model and again upon oncogene activation (H-RAS^{G12V}) cells underwent senescence.

PTC-associated oncogenes triggered senescence by a distinct set of alterations in cellular phenotype, changes in chromatin structure and gene expression. Upon oncogenic stress human primary thyrocytes became large, flat and multinucleated. Moreover, PTC-associated oncogenes drove senescence by increased SA-β-Gal activity, the most widely used senescence marker (Dimri et al., 1995) and by formation of bright, punctate DNA foci through the cell nucleus, the so called SAHF (Narita et al., 2003).

Regardless of the senescence initiating signals, tumour suppressor pathways are critical for initiation and maintenance of the senescent phenotype. These pathways are controlled by the tumour suppressor proteins p53 and pRb (Shay et al., 1991). In our cellular model, PTC-associated oncogenes triggered a strong and persistent induction of p16^{INK4a} and p53, whereas we failed to observe any significant upregulation of p21^{CIP1}, with exception of H-RAS^{G12V} expressing thyrocytes.

In light of this specific regulation, we examined the relative function of p53 and pRb in the initiation of senescence by assessing the outcomes of their inactivation. To this end, we focused on BRAF^{V600E} and inducible H-RAS^{G12V}-driven senescence.

As reported in several studies the critical role of p53 and pRb differs in mouse and human cells. In mouse embryo fibroblasts, disruption of p53 alone is sufficient to prevent senescence (Dirac and Bernards, 2003). Likewise, inactivation of pRb gene together with other members of Rb family such as p107 and p130, but not pRb alone, is sufficient to escape senescence (Dannenberg et al., 2000; Sage et al., 2000).

This implies that both p53 and pRb pathways are required for the induction of senescence. Inactivation of either of these genes in senescent MEFs is enough for proliferation to resume (Dannenberg et al., 2000; Sage et al., 2000). These observations suggested a model of linear signalling, whereby a stress signal activates p53 which in turn activates pRb. Unlike the behaviour of mouse cells, the inactivation of both p53 and pRb is essential to prevent to onset of replicative senescence in human cells (Smogorzewska and de Lange, 2002), whereas disruption of only one of these proteins delays the onset of senescence. This indicates that in human cells, p53 and pRb operate in two parallel pathways.

From the observations made in this study it emerges that suppression of $p16^{INK4a}$ in $BRAF^{V600E}$ lentivirally transduced in human primary thyrocytes did not influence the onset of senescence, whereas cells retrovirally infected with inducible $H\text{-}RAS^{G12V}$ vector bypassed senescence upon disruption of $p16^{INK4a}$. These results are in harmony with models previously proposed by others (Michaloglou et al., 2005; Serrano et al., 1997). To better understand these differences in the pathways executing OIS by $BRAF^{V600E}$ versus $H\text{-}RAS^{G12V}$, we also investigated the role of $p16^{INK4a}$ in human primary thyrocytes transduced with retroviral carrying $BRAF^{V600E}$. Here, it was interesting to discover a strict correlation between $p16^{INK4a}$ expression and cell cycle arrest. Thus, it is possible that different oncogenic levels due to the different oncogene delivery may trigger different responses upon $p16^{INK4a}$ abrogation.

While $p16^{INK4a}$ plays a dominant role in $H\text{-}RAS^{G12V}$ mediated senescence, p53 is not required for the onset of senescence as its inactivation was not sufficient to re-enter the cell cycle.

In the last few years, growing body of evidence suggests that OIS is tightly connected with inflammation.

Cells undergoing senescence display profound changes in their secretome, termed the senescence-associated secretory phenotype (SASP) or senescence-messaging secretome (SMS) (Coppé et al., 2008; Kuilman and Peeper, 2009): they produce a wide range of inflammatory cytokines and growth factors which reinforce senescence (Acosta et al., 2008; Kuilman et al., 2008; Wajapeyee et al., 2008) or promote carcinogenesis. These opposite effects of SASP factors may depend on the cellular context and genetic make-up of target cells.

Among SASP factors IGFBP7 is a secreted protein recently proposed as a mediator of $BRAF^{V600E}$ induced senescence in melanocytes (Wajapeyee et al., 2008).

Firstly, it was important to find out that IGFBP7 is downregulated in a consistent fraction of PTC with respect to normal thyroid. We addressed the functional consequences of IGFBP7 downregulation in PTC-derived NIM1 cell line, in which the expression of IGFBP7 is lacking. We provided evidence that the restoration of IGFBP7 reduced the growth rate, migration, anchorage independent growth of NIM1 cells and all these effects were related to apoptosis. This was also recapitulated *in vivo*: re-expression of IGFBP7 reduced the NIM1 cells capability to induce tumour formation in mouse xenografts. In nutshell, our results suggest that IGFBP7 exerts an oncosuppressor role in thyroid tumour, this in agreement with different human cancer models proposed by others. (Akaogi et al., 1996; Sprenger et al., 1999; Wilson et al., 2002; Burger et al., 2005; Ruan et al., 2006; Chen et al., 2007; Sato et al., 2007).

Given the involvement of IGFBP7 in $BRAF^{V600E}$ mediated senescence in melanocytes by Wajapeyee and colleagues it was of particular interest to determine whether the IGFBP7 expression is changed in $BRAF^{V600E}$ senescent thyrocytes. Surprisingly, we did not detect any significant upregulation of IGFBP7 in response to oncogenic BRAF: we saw a reduction in IGFBP7 levels in $BRAF^{V600E}$ infected cells compared with the controls.

Meanwhile, Scurr and co-workers observed similar IGFBP7 regulation in melanocytes, they also reported that $BRAF^{V600E}$ induced senescence in melanocytes irrespective of the presence of IGFBP7 (Scurr et al., 2010).

Shifting towards others SASP factors, the finding that $H\text{-}RAS^{G12V}$ induces senescence in human primary thyrocytes through activation of inflammatory network including IL8 and its receptor CXCR2 as well as IL6 was exciting. This specific regulation prompted us to explore the requirement for CXCR2 receptor and IL8 in OIS. Upon either CXCR2 or IL8 abrogation senescent thyrocytes expressing $H\text{-}RAS^{G12V}$ were able bypass OIS and to continue proliferating, suggesting that the activation of chemokine signalling via CXCR2 plays an important role for the senescence establishment.

We wished to extend our findings obtained *in vitro* in humans by the analysis of thyroid tumours characterized by different aggressiveness (including PTMC, PTC NOS, PDTC and ATC). It was important to discover that the expression of OIS markers such as $p16^{INK4a}$, $p21^{CIP1}$ and IGFBP7 is upregulated at early stages, and lost during tumour progression. The highest expression of all OIS markers analyzed observed in PTMCs would suggest that OIS may play a role in the generally indolent clinical course of this PTC variant by keeping proliferation under control. Thus, OIS is a mechanism involved in the pathogenesis of thyroid carcinoma by constraining neoplastic transformation.

In sum, in this thesis we have established the role of oncogene-induced senescence in thyroid carcinogenesis *in vitro* and *in vivo*. We have used the oncogene-induced cell system *in vitro* to unravel what mechanisms are important for senescence induction and maintenance. Furthermore, we have tried to use the *in vitro* cell system to identify and study some genes involved in OIS, and to link them to cancer progression.

REFERENCES

References

Acosta JC, O'Loghlen A, Banito A, et al. Chemokine signalling via the CXCR2 receptor reinforces senescence. Cell *133*, 1006-18 (2008).

Adams PD. Remodelling of chromatin structure in senescent cells and its potential impact on tumor suppressor and aging. Gene *397*, 84-93 (2007).

Ahmed S, Yamamoto K, Sato Y, et al. Proteolytic processing of IGFBP-related protein-1 (TAF/angiomodulin/mac25) modulates its biological activity. Biochem Biophys Res Commun *310*, 612-618 (2003).

Airaksinen MS, Titievsky A, and Saarma M. GDNF family neurotrophic factor signalling: four masters, one servant? Mol Cell Neurosci *13*, 313-25 (1999).

Akaogi K, Okabe Y, Sato J, et al. Specific accumulation of tumor-derived adhesion factor in tumor blood vessels and in capillary tube-like structures of cultured vascular endothelial cells. Proc Natl Acad Sci USA *93*, 8384-89 (1996).

Albores-Saavedra J, Henson DE, Glazer E, et al. Changing patterns in the incidence and survival of thyroid cancer with follicular phenotype-papillary, follicular, and anaplastic: a morphological and epidemiological study. Endocr Pathol *18*, 1-7 (2007).

Aldred MA, Huang Y, Liyanarachchi S, Pellegata NS, et al. Papillary and follicular thyroid different microarray expression profiles and can be distinguished by a minimum of five genes. J Clin Oncol *22*, 3531-9 (2004).

Anania MC, Sensi M, Vizioli MG, et al. TIMP3 regulates migration, invasion and in vivo tumorigenicity of thyroid tumor cells. Oncogene *30*, 3011-23 (2011).

Andreozzi F, Melillo RM, Carlomagno F, et al. Protein kinase C alpha activation by RET: evidence for a negative feedback mechanism controlling RET tyrosine kinase. Oncogene *22*, 2942-9 (2003).

Ball DW, Baylin SB, De Bustros AC. Medullary thyroid carcinoma. In: Werner and Ingbar's the Thyroid, 8th ed., 930-43 (2000).

Ball E, Bond J, Franc B, et al. An immunohistochemical study of p16(INK4a) expression in multistep thyroid tumorigenesis. European Journal of Cancer 43, 194-01 (2007).

Bartokova J, Rezaei N, Liontos M, et al. Oncogene-induced senescence is part of the tumorigenesis barrier imposed by DNA damage checkpoints. Nature *444*, 633-37 (2006).

Basolo F, Giannini R, Monaco C, et al. Potent mitogenicity of the RET/PTC3 oncogene correlates with its prevalence in tall-cell variant of papillary thyroid carcinoma. Am J Pathol *160*, 247-54 (2002).

Basolo F, Pisaturo F, Pollina LE, et al. N-ras mutation in poorly differentiated thyroid carcinomas: correlation with bone metastases and inverse correlation to thyroglobulin expression. Thyroid *10*, 19-23 (2000).

Bhattacharyya N. A population-based analysis of survival factors in differentiated and medullary thyroid carcinoma. Otolaryngol Head Neck Surg *128*, 115-23 (2003).

Bierman EL. The effect of donor age on the in vitro life span of cultured human arterial smooth-muscle cells. In Vitro *14*, 951-5 (1978).

Bodnar AG, Ouellette M, Frolkis M, et al. Extension of lifespan by introduction of telomerase into normal human cells. Science *279*, 349-52 (1998).

Bond J, Jones C, Haughton M, et al. Direct evidence from siRNA-directed "knock down" that $p16^{INK4a}$ is required for human fibroblasts senescence and for limiting ras-induced epithelial cell proliferation. Experimental Cell Research *292,* 151-156 (2004).

Bongarzone I, Vigneri P, Mariani L, et al. RET/NTRK1 rearrangements in thyroid gland tumors of the papillary carcinoma family: correlation with clinicopathological features. Clin Cancer Res *4*, 223-8 (1998).

Borrello MG, Alberti L, Fisher A, et al. Induction of a proinflammatory program normal human thyrocytes by the RET/PTC1 oncogene. Proc Natl Acad Sci USA *102*, 14825-30 (2005).

Borrello MG, Bongarzone I, Pierotti MA, et al. Trk and Ret proto-oncogene expression in human neuroblastoma specimens: high frequency of trk expression in non-advanced stages. Int J Cancer *54*, 540-5 (1993).

Braig M, Lee S, Loddenkemper C, et al. Oncogene-induced senescence as an initial barrier in lymphoma development. Nature *436*, 660-65 (2005).

Brzezinski J, Migodzinski A, Toczek A, et al. Patterns of cyclin E, retinoblastoma protein, and $p21^{Cip1/WAF1}$ immunostaining in the oncogenesis of papillary thyroid carcinoma. Clinical Cancer Research *11*, 1037-43 (2005).

Burger AM, Leyland-Jones B, Banerjee K, et al. Essential roles of IGFBP-3 and IGFBP-rP1 in breast cancer. Eur J Cancer *41*, 1515-1527 (2005).

Byrd DA, Sweet DJ, Pante' N, et al. Trp, a large coiled coil protein whose amino terminus is involved in activation of oncogenic kinases, is localized to the cytoplasmic surface of the nuclear pore complex. J Cell Biol *127*, 1515-26 (1994).

Caillou B, Talbot M, Weyemi U, et al. Tumor-associated macrophages (TAMs) form an interconnected cellular supportive network in anaplastic thyroid carcinoma. PLoS One 6, e22567 (2011).

Campisi J. Cellular senescence as a tumor suppressor mechanism. Trends Cell Biol *11*, S27-31 (2001).

Campisi J. Senescent cells, tumor suppression, and organismal aging: Good citizens, bad neighbours. Cell *120*, 513-22 (2005).

Campisi J and d'Adda di Fagagna F. Cellular senescence: when bad things happen to good cells. Nat Rev Mol Cell Biol *8*, 729-40 (2007).

Cesare AJ and Reddel RR. Alternative lengthening of telomerese: models, mechanisms and implications. Nat Rev Genet *11*, 319-30 (2010).

Ciampi R, Knauf JA, Kerler R, et al. Oncogenic AKAP9-BRAF fusion is a novel mechanism of MAPK pathway activation in thyroid cancer. J Clin Invest *115*, 94-101 (2005).

Chen QM, Liu J, and Merrett JB. Apoptosis or senescence-like growth arrest: influence of cell-cycle position of normal human fibroblasts. Biochem J *347*, 543-51 (2000).

Chen Z, Trotman LC, Shaffer D, et al. Crucial role of p53-dependent cellular senescence in suppression of Pten-deficient tumorigenesis. Nature *436*, 725-30 (2005).

Collins K and Mitchell JR. Telomerase in the human organism. Oncogene *21*, 564-79 (2002).

Collado M, Gil J, Efeyan A, et al. Tumor biology: Senescence in premalignant tumors. Nature *436*, 642 (2005).

Coppé JP, Patil CK, Rodier F, et al. Senescence-associated secretory phenotypes reveal cell-nonautonomous functions of oncogenic RAS and the p53 tumor suppressor. PLoS Biol *6*, 2853-68 (2008).

Coppè JP, Kauser K, Campisi J, et al. Secretion of vascular endothelial growth factor by primary human fibroblasts at senescence. J Biol Chem *281*, 29568-74 (2006).

Cristofalo VJ. SA-beta-Gal staining: biomarker or delusion. Exp Gerontol *40*, 836-8 (2005).

Cristofalo VJ and Sharf BB. Cellular senescence and DNA synthesis. Thymidine in corporation as a measure of population age in human diploid cells. Exp Cell Res *76*, 419-27 (1973).

Courtois-Cox S, Genther Williams SM, Reczeck EE, et al. A negative feedback signalling network underlies oncogene-induced senescence. Cancer Cell *10*, 459-72 (2006).

Curcio F, Ambes-Impiombato FS, Perrella G, et al. Long-term culture and functional characterization of follicular cells from adult normal human thyroids. PNAS *91*, 9004-8 (1994).

D'Adda di Fagagna F. Living on break: Cellular senescence as a DNA-damage response. Nat Rev Cancer *8*, 512-222 (2008).

D'Adda di Fagagna F, Reaper PM, Clay-Farrace L, et al. A DNA damage checkpoint response in telomere-initiated senescence. Nature *426*, 194-98 (2003).

Dankort D, Filenova E, Collado M, et al. A new mouse model to explore the initiation, progression, and therapy of $BRAF^{V600E}$-induced lung tumors. Genes Dev *21*, 379-84 (2007).

Davies TF. Making thyroid simple-avoid hyper and hypo! Thyroid *12*, 93 (2002).

Davies H, Bignell GR, Cox C, et al. Mutations of the BRAF gene in human cancer. Nature *417*, 949-54 (2002).

Davies L and Welch HG. Increasing incidence of thyroid cancer in the United Sates, 1973-2002. JAMA *295*, 2164-7 (2006).

DeLellis R, Lloyd R, and Heitz P. Tumors of the thyroid and parathyroid. Pathology and genetics of tumours of endocrine organs (IARC WHO classification of tumours) by The International Agency for Research on Cancer (2004).

Degeorges A, Wang F, Frierson HF Jr, et al. Distribution of IGFBP-rP1 in normal human tissues. J Histochem Cytochem *48*, 747-54 (2000).

Dennenberg JH, van Rossum A, Schuijff L, et al. Ablation of the retinoblastoma gene family deregulates G(1) control causing immortalization and increased cell turnover under growth-restricting conditions. Genes Dev *14*, 3051-64 (2000).

Descamps S, Lebourhis X, Delehedde M, et al. Nerve growth factor is mitogenic for cancerous but not normal human breast epithelial cells. J Biol Chem *273*, 16659-62 (1998).

Dhillon AS and Kolch W. Oncogenic B-RAF mutations: crystal clear at last. Cancer Cell *5*, 303-4 (2004).

Dhomen N, Reis-Filho JS, Da Rocha Dias S, et al. Oncogenic Braf induces melonocyte senescence and melanoma in mice. Cancer Cell *15*, 294-03 (2009).

Di Micco R, Fumagalli M, Cicalese A, et al. Oncogene-induced senescence is a DNA damage response triggered by DNA hyper-replication. Nature *444*, 638-42 (2006).

Dimri GP, Itahana K, Acosta M, et al. Regulation of a senescence checkpoint response by the E2F1 transcription factor and p14(ARF) tumor suppressor. Mol Cell Biol *20*, 273-85 (2000).

Dimri GP, Lee X, Basile G, et al. A biomarker that identifies senescent human cells in culture and in aging skin in vivo. Proc Natl Acad Sci USA *92*, 9363-67 (1995).

Dirac AM and Bernards R. Reversal of senescence in mouse fibroblasts through lentiviral suppression of p53. J Biol Chem *278*, 11731-34 (2003).

Donehower LA, Harvey M, Slagle BL, et al. Mice deficient for p53 are developmentally normal but susceptible to spontaneous tumours. Nature *356*, 251-21 (1992).

Dwight T, Thoppe SR, Foukakis T, et al. Involvement of the PAX8/peroxisome proliferator-activated receptor gamma rearrangement in follicular thyroid tumors. J Clin Endocrinol Metab *88*, 4440-5 (2003).

Efeyan A, Ortega-Molina A, Velasco-Miguel S, et al. Induction of p53-dependent senescence by the MDM2 antagonist nutlin-3a in mouse cells of fibroblast origin. Cancer Res *67*, 7350-7 (2007).

Eng C, Clayton D, Schuffenecker I, et al. The relationship between RET proto-oncogene mutations and disease phetotype in multiple endocrine neoplasia type 2. International RET mutation consortium analysis. JAMA *276*, 1575-9 (1996).

Fagin JA. Challenging dogma in thyroid cancer molecular genetics-role of RET/PTC and BRAF in tumour initiation. J Clin Endocrinol Metab *89*, 4264-6 (2004).

Ferrario C, Lavagni P, Gariboldi M, et al. Metallothionein 1G acts as an oncosupressor in papillary thyroid carcinoma. Lab Invest *88*, 474-81 (2008).

Ferru A, Fromont G, Gibelin H, et al. The status of CDKN2A alpha (p16INK4a) and beta (p14ARF) transcripts in thyroid tumour progression. British Journal of Cancer *95*, 1670-77 (2006).

Foreman Ke and Tang J. Molecular mechanisms of replicative senescence in endothelial cells. Exp Gerentol *38*, 1251-57 (2003).

Frasca F, Nucera C, Pellegriti G, et al. BRAF(V600E) mutation and the biology of papillary thyroid cancer. Endocr Relat Cancer *15*, 191-205 (2008).

Frattini M, Ferrario C, Bressan P, et al. Alternative mutations of BRAF, RET and NTRK1 are associated with similar but distinct gene expression patterns in papillary thyroid cancer. Oncogene *23*, 7436-40 (2004).

Gao CF, Xie Q, Su YL, et al. Proliferation and invasion: plasticity in tumor cells. PNAS *102*, 10528-33 (2005).

Garcia-Rostan G, Zhao H, Camp RL, et al. Ras mutations are associated with aggressive tumor phenotypes and poor prognosis in thyroid cancer. J Clin Oncol *21*, 3226-35 (2003).

Giordano TJ, Kuick R, Thomas DG, et al. Molecular classification of papillary thyroid carcinoma : distinct BRAF, RAS, and RET/PTC mutation-specific gene expression profiles discovered by DNA microarray analysis. Oncogene *24*, 6646-56 (2005).

Greco A, Fusetti L, Miranda C, et al. Role of the TFG N-terminus and coiled-coil domain in the transforming activity of the thyroid TRK-T3 oncogene. Oncogene *16*, 809-16 (1998).

Greco A, Mariani C, Miranda C, et al. Characterization of the NTRK1 genomic region involved in chromosomal rearrangements generating TRK oncogenes. Genomic *2*, 397-400 (1993).

Greco A, Mariani C, Miranda C, et al. The DNA rearrangement that generates the TRK-T3 oncogene involves a novel gene on chromosome 3 whose product has a potential coiled-coil domain. Mol Cell Biol *15*, 6118-27 (1995).

Greco A, Miranda C, Pagliardini S, et al. Chromosome 1 rearrangements involving the genes TPR and NTRK1 produce structurally different thyroid-specific TRK oncogenes. Genes Chromosomes Cancer *19*, 112-23 (1997).

Greco A, Pierotti MA, Bongarzone I, et al. TRK-T1 is a novel oncogene formed by the fusion of TPR and TRK genes in human papillary thyroid carcinomas. Oncogene *7*, 237-42 (1992).

Grieco M, Santoro M, Berlingieri MT, et al. PTC is a novel form of the ret proto-oncogene and is frequently detected in vivo in human thyroid papillary carcinomas. Cells *60*, 557-63 (1990).

Grodski S, Brown T, Sidhu S, et al. Increasing incidence of thyroid cancer is due to increased pathologic detection. Surgery *144*, 1038-43 (2008).

Guignat L, Bidart JM, Nocera M, et al. Chromogranin A and the alpha-subunit of glycoprotein hormones in medullary thyroid carcinoma and phaeochromocytoma. Br J Cancer *84*, 808-12 (2001).

Ha L, Ichikawa T, Anver M, et al. ARF functions as a melanoma tumor suppressor by inducing p53-independent senescence. PNAS *104*,10968-73 (2007).

Hag M and Harmer C. Differentiated thyroid carcinoma with distant metastases at presentation: prognostic factors and outcome. Clin Endocrinol *63*, 87-93 (2005).

Hampel B, Malisan F, Niederegger H, et al. Differential regulation of apoptotic cell death in senescent human cells. Exp Gerontol *39*, 1713-21 (2004).

Hansford JR and Mulligan LM. Multiple endocrine neoplasia type 2 and RET: from neoplasia to neurogenesis. J Med Genet *37*, 817-27 (2000).

Harley CB, Futcher AB, and Greider CW. Telomerase shorten during ageing of human fibroblasts. Nature *345*, 458-60 (1990).

Hay ID, Hutchinson ME, Gonzalez-Losada T, et al. Papillary thyroid microcarcinoma: a study of 900 cases observed in a 60-years period. Surgery *144*, 980-87 (2000).

Hayflick L. The limited in vitro lifetime of human diploid cell strains. Exp Cell Res *37*, 614-36 (1965).

He H, Jazdzewski K, Li W, et al. The role of microRNA genes in papillary thyroid carcinoma. Proc Natl Acad Sci USA *102*, 19075-80 (2005).

Hedinger C, Williams ED, and Sobin LH. Histological typing of thyroid tumours. In: International classification of tumours, 2nd ed. Berlin: Springer-Verlag (1988).
Hinoue T, Weisenberger DJ, Pan F, et al. Analysis of the association between CIMP and BRAF in colorectal cancer by DNA methylation profiling. PLoS One *4*, e8357 (2009).

Hu S, Liu D, Tufano RP, et al. Association of aberrant methylation of tumour suppressor genes with tumour aggressiveness and BRAF mutation in papillary thyroid cancer. Int J Cancer *119*, 2322-39 (2006).

Huang SC, Torres-Cruz J, Pack SD, et al. Amplification and overexpression of mutant RET in multiple endocrine neoplasia type 2-associated with medullary thyroid carcinoma. J Clin Endocrinol Metab *88*, 459-63 (2003).

Huang Y, Prasad M, Lemon WJ, et al. Gene expression in papillary thyroid carcinoma reveals highly consistent profiles. Proc Natl Acad Sci USA *98*, 15044-15049 (2001).

Hundahl SA, Fleming ID, Fremgen AM, et al. A National Cancer Data Base report on 53.856 cases of thyroid carcinoma treated in the U.S., 1985-1995. Cancer *83*, 2638-48 (1998).

Ikenoue T, Hikiba Y, Kanai F, et al. Functional analysis of mutations within the kinase activation segment of B-Raf in human colorectal tumors. Cancer Res *63*, 8132-7 (2003).

Indo Y, Tsuruta M, Hayashida Y, et al. Mutations in the TRKA/NFG receptor gene in patients with congenital insensitivity to pain with anhidrosis. Nat Genet *13*, 485-8 (1996).

Ishizaka Y, Itoh F, Tahira T, et al. Human ret proto-oncogene mapped to chromosome 10q11.2. Oncogene *4*, 1519-21 (1989).

Iwashita T, Murakimi H, Asai N, et al. Mechanism of ret dysfunction by Hirschsprung mutations affecting its extracellular domain. Hum Mol Genet *5*, 1577-80 (1996).

Jackson JG and Pereira-Smith OM. p53 is preferentially recruited to the promoters of growth arrest genes p21 and GADD45 during replicative senescence of normal human fibroblasts. Cancer Res *66*, 8356-60 (2006).

Jarbaz B, Wiench M, Fujarewicz K, et al. Gene expression profile of papillary thyroid cancer: sources of variability and diagnostic implications. Cancer Res *65*, 1587-97 (2005).

Jones CJ, Kipling D, Morris M, et al. Evidence for a telomere-independent "Clock" limiting RAS oncogene-driven proliferation of human thyroid epithelial cells. Molecular and Cellular Biology *20*, 5690-99 (2000).

Kanemitsu N, Kato MV, Miki T, et al. Characterization of the promoter of the murine mac25 gene. Biochem Biophys Res Commun *279*, 251-257 (2000).

Kaplan DR and Miller FD. Neurotrophin signal transduction in the nervous system. Curr Opin Neurobiol *3*, 381-91 (2000).

Kato MV. A secreted tumor-suppressor, mac25, with activin-binding activity. Mol med *6*, 126-35 (2000).

Kim TY, Kim WB, Song JY, et al. The BRAF mutation is not associated with poor prognostic factors in Korean patients with conventional papillary thyroid microcarcinoma. Clin Endocrinol *63*, 588–93 (2005).

Kimura ET, Nikiforova MN, Zhu Z, et al. High prevalence of BRAF mutations in thyroid cancer: genetic evidence for constitutive activation of the RET/PTC-RAS-BRAF signaling pathway in papillary thyroid carcinoma. Cancer Res *63*, 1454-57 (2003).

Kitahara CM, Platz EA, Freeman LE, et al. Obesity and thyroid cancer risk among U.S. men and women: a pooled analysis of five prospective studies. Cancer Epidemiol Biomarkers Prev *20*, 462-72 (2011).

Knauf JA, Ma X, Smith EP, et al. Targeted expression of $BRAF^{V600E}$ in thyroid cells of transgenic mice results in papillary thyroid cancers that undergo dedifferentiation. Cancer Res *65*, 4238-45 (2005).

Kondo T, Nakazawa T, Murata S, et al. Enhanced B-RAF protein expression is independent of V600E mutant status in thyroid carcinomas. Hum Pathol *12*, 1810-8 (2007).

Kortlever RM, Higgins PJ, and Bernards R. Plasminogen activator inhibitor-1 is a critical downstream target of p53 in the induction of replicative senescence. Nat Cell Biol *8*, 877-84 (2006).

Kouvaraki MA, Shapiro SE, Perrier ND, et al. RET proto-oncogene: a review and update genotype-phenotype correlations in hereditary medullary thyroid cancer and associated endocrine tumors. Thyroid *15*, 531-44 (2005).

Krizhanovsky V, Yon M, Dickins RA, et al. Senescence of activated stellate cells limits liver fibrosis. Cell *134*, 657-67 (2008).

Krtolica A, Parrinello S, Lockett S, et al. Senescent fibroblasts promote epithelial cell growth and tumorigenesis: A link between cancer and aging. Proc Natl Acad Sci *98*, 12072-77 (2001).

Kuilman T, Michaloglou C, Vredeveld LCW, et al. Oncogene-induced senescence relayed by an interleukin-dependent inflammatory network. Cell *133*, 1019-31 (2008).

Kuilman T and Peeper DS. Senescence-messaging secretome: SMS-ing cellular stress. Nat Rev Cancer *9*, 81-94 (2009).

Kumamoto K, Spillare EA, Fujita K, et al. Nutlin-3a activates p53 to both down-regulate inhibitor of growth 2 and up-regulate mir-34a, mir-34b, and mir34c expression, and induce senescence. Cancer Res *68*, 3193-203 (2008).

Land H, Parada LF, and Weinberg RA. Tumorigenic conversion of primary embryo fibroblasts requires at least two cooperating oncogenes. Nature *304*, 596-02 (1983).

Latini FR, Hemerly JP, Oler G, et al. Re-expression of ABI3-binding protein suppresses thyroid growth by promoting senescence and inhibiting invasion. Endocr Relat Cancer *15*, 787-99 (2008).

La Vecchia C, Bosetti C, Lucchini F, et al. Cancer mortality in Europe, 2000-2004, and an overview of trends since 1975. Ann Oncol *21*, 1323-60 (2010).

Lee BY, Han Ja, Im JS, et al. Senescence-associated beta-galactosidase is lysosomal beta-galactosidase. Aging Cell *5*, 187-95 (2006).

Lee MH, Lee SE, Kim DW, et al. Mitochondrial localization and regulation of $BRAF^{V600E}$ in thyroid cancer: a clinically used RAF inhibitor is unable to block the mitochondrial activities of $BRAF^{V600E}$. J Clin Endocrinol Metab *96*, E19-30 (2011).

Leicht DT, Balan V, Kaplun A, et al. Raf kinases: functions, regulation and role in human cancer. Biochim Biophys Acta *1773*, 1196-212 (2007).

Lin AW, Barradas M, Stone JC, et al. Premature senescence involving p53 and p16 is activated in response to constitutive MEK/MAPK mitogenic signalling. Genes Dev *12*, 3008-19 (1998).

Lin J, Lai M, Huang Q, et al. Methylation patterns of IGFBP7 in colon cancer cell lines are associated with levels of gene expression. J Pathol *212*, 83-90 (2007).

Lowe SW, Copero E, and Evan G. Intrinsic tumour suppression. Nature *432*, 307-15 (2004).

Lupi C, Giannini R, Ugolini C, et al. Association of $BRAF^{V600E}$ mutation with poor clinicopathological outcomes in 500 consecutive cases of papillary thyroid carcinoma. J Clin Endocrinol Metab *92*, 4085-90 (2007).

Mallette FA, Goumont-Leclerc MF, and Ferbeyre G. The DNA damage signalling pathway is a critical mediator of oncogene-induced senescence. Genes Dev *21*, 43-48 (2007).

Malumbres M and Barbacid M. Cell cycle, CDKs and cancer: a changing paradigm. Nat Rev Cancer *9*, 153-66 (2009).

Manenti G, Pilotti S, Re FC, et al. Selective activation of ras oncogenes in follicular and undifferentiated thyroid carcinomas. Eur J Cancer *30A*, 987-93 (1994).

Marcotte R, Chen JM, Huard S, et al. c-Myc creates an activation loop by transcriptionally repressing its own functional inhibitor, hMad4, in young fibroblasts, a loop lost in replicatively senescent fibroblasts. J Cell Biochem *96*, 1071-85 (2005).

Martin-Zanca D, Mitra G, Long LK, et al. Molecular characterization of the human Trk oncogene. Cold Spring Harb Symp Quant Biol *2*, 983-92 (1986).

Mason DX, Jackson T, and Lin AW. Molecular signature of oncogenic ras-induced senescence. Oncogene *23*, 9238-46 (2004).

Masutomi K, Yu EY, Khurts S, et al. Telomerase maintains telomere structure in normal human cells. Cell *114*, 241-53 (2003).

McIever B, Hay ID, Giuffrida DF, et al. Anaplastic thyroid carcinoma: a 50-year experience at a single institution. Surgery *130*, 1028-34 (2001).

McKay MM and Morrison DK. Integrating signals from RTKs to ERK/MAPK. Oncogene *26*, 3113-21 (2007).

Melillo RM, Castellone MD, Guarino V, et al. The RET/PTC-RAS-BRAF linear signaling cascade mediates the motile and mitogenic phenotype of thyroid cancer cells. J Clin Invest *115*, 1068-81 (2005).

Mettler FA Jr, Gus'kova AK, and Gusev I. Health effect in those with acute radiation sickness from the Chernobyl accident. Health Phys *93*, 462-9 (2007).

Michaloglou C, Vredeveld LCW, Soengas MS, et al. BRAFE600-associated senescence-like cell cycle arrest of human naevi. Nature *436*, 720-24 (2005).

Minimino T, Miyauchi H, Yoshida T, et al. Endothelial cell senescence in human atherosclerosis: Role of telomere in endothelial dysfunction. Circulation *105*, 1541-44 (2002).

Miranda C, Minoletti F, Greco A, et al. Refined localization of the human TPR gene to chromosome 1q25 by in situ hybridization. Genomics *23*, 714-5 (1994).

Moley JF and DeBenedetti MK. Patterns of nodal metastases in palpable medullary thyroid carcinoma: recommendations for extent of node dissection. Ann Surg *229*, 880-7 (1999).

Motoi N, Sakamoto A, Yamochi T, et al. Role of ras mutation in the progression of thyroid carcinoma of follicular epithelial origin. Pathol Res Pract, *196*, 1-7 (2000).

Nakagawara A, Arima M, Azar CG, et al. Inverse relationship between trk expression and N-myc amplification in human neuroblastomas. Cancer Res *52*, 1364-8 (1992).

Namba H, Rubin SA, and Fagin JA. Point mutations of RAS oncogenes are an early event in thyroid tumorigenesis. Mol Endocrinol *4*, 1474-79 (1990)

Narita M, Nunez S, Heard E, et al. Rb-mediated heterochromatin formation and silencing of E2F target genes during cellular senescence. Cell *113*, 703-16 (2003).

Neumann AA and Reddel RR. Telomere maintenance and cancer-look, no telomerase. Nat Rev Cancer *2*, 879-84 (2002).

Newbold RF and Overell RW. Fibroblast immortality is a prerequisite for transformation by EJ c-H-ras oncogene. Nature *304*, 648-51 (1983).

Niccoli-Sire P, Murat A, Rohmer V, et al. Familial medullary thyroid carcinoma with noncysteine ret mutations: phenotype-genotype relationship in a large series of patients. J Clin Endocrinol Metab *86*, 3746-53 (2001).

Nickoloff BJ, Lingen MW, Chang BD, et al. Tumor suppressor maspin is up-regulated during keratinocyte senescence, exerting a paracrine antiangiogenic activity. Cancer Res *9*, 2956-61 (2004).

Nikiforov YE. RET/PTC rearrangement in thyroid tumors. Endocr Pathol *13*, 3-16 (2002).

Nikiforov YE. Radiation-induced thyroid cancer: what we have learned from Chernobyl. Endocr Pathol *17*, 307-17 (2006).

Nikiforov YE and Nikiforova MN. Molecular genetics and diagnosis of thyroid cancer. Nat Rev Endocrinol *7*, 569-80 (2011).

Nikiforova MN and Nikiforov YE. Molecular genetics of thyroid cancer: implications for diagnosis, treatment and prognosis. Expert Rev Mol Diagn *8*, 83-95 (2008).

Nikiforova MN, Stringer JR, Blough R, et al. Proximity of chromosomal loci that participate in radiation-induced rearrangements in human cells. Science *290*, 138-41 (2000).

Olovnikov AM. Principle of marginotomy in template synthesis of polynucleotides. Dokl Akad Nauk SSSR *201*, 1496-99 (1971).

Okayasu I. The Relationship of Lymphocytic Thyroiditis to the Development of Thyroid Carcinoma. Endocr Pathol *3*, 225-230 (1997).

Pang JH and Chen KY. Global change of gene expression at late G1/S boundary may occur in human IMR-90 diploid fibroblasts during senescence. J Cell Physiol *160*, 531-8 (1994).

Pallante P, Federico A, Berlingieri MT, et al. Loss of the CBX7 gene expression correlates with a highly malignant phenotype in thyroid cancer. Cancer Res *68*, 6770-78 (2008).

Pasini B, Hofstra RM, Yin L, et al. The physical map of the human RET proto-oncogene. Oncogene *11*, 1737-43 (1995).

Pierotti MA, Bongarzone I, Borrello MG, et al. Cytogenetics and molecular genetics of the carcinomas arising from the thyroid epithelial follicular cells. Genes Chrom Cancer *16*, 1-14 (1996).

Pilotti S, Collini P, Mariani L, et al. Insular carcinoma: a distinct de novo entity among follicular carcinomas of the thyroid gland. Am J Surg Pathol *12*, 1466-73 (1997).

Price JS, Waters JG, Darrah C, et al. The role of chondrocyte senescence in osteoarthritis. Aging Cell *1*, 57-65 (2002).

Pollak MN, Schernhammer ES, and Hankinson SE. Insulin-like growth factors and neoplasia. Nat Rev Cancer *4*, 505-18 (2004).

Powell DR, Russell J, Nibu K, et al. The RET/PTC3 oncogene: metastatic solid-type papillary carcinomas in murine thyroids. Cancer Res *58*, 5523-28 (1998).

Puxeddu E, Moretti S, Giannico A, et al. RET/PTC activation does not influence clinical and pathological features of adult papillary thyroid carcinomas. Eur J Endocrinol *148*, 505-13 (2003).

Raman M, Chen W, and Cobb MH. Differential regulation and properties of MAPKs. Oncogene *26*, 3100-12 (2007).

Rebbaa A, Zheng X, Chou PM, et al. Caspase inhibition switches doxorubicin-induced apoptosis to senescence. Oncogene *22*, 2805-11 (2003).

Ren JL, Pan JS, Lu YP, et al. Inflammatory signaling and cellular senescence. Cellular Signalling *21*, 378-83 (2009).

Reuther GW, Lambert QT, Caligiuri MA, et al. Identification and characterization of an activating TrkA deletion mutation in acute myeloid leukemia. Mol Cell Biol *23*, 8655-66 (2000).

Rheinwald JG and Green H. Serial cultivation of strains of human epidermal keratinocytes: the formation of keratinizing colonies from single cells. Cell *6*, 331-43 (1975).

Roberson RS, Kussick SJ, Vallieres E, et al. Escape from therapy-induced accelerated cellular senescence in p53-null lung cancer cells and in human lung cancers. Cancer Res *65*, 2795-803 (2005).

Roccato E, Miranda C, Raho G, et al. Analysis of SHP-1-mediated down-regulation of the TRK-T3 oncoprotein identifies Trk-fused gene (TGF) as a novel SHP-1-interacting protein. J Biol Chem *280*, 3382-9 (2005).

Rodier F, Coppé JP, Patil CK, et al. Persistent DNA damage signalling triggers senescence-associated inflammatory cytokine secretion. Nat Cell Biol *11*, 973-79 (2009).

Rosai J, Carcangiu ML, and De Lellis R. Tumors of the thyroid gland. Atlas of tumor pathology *3*, 207–45 (1992).

Ruan W, Xu E, Xu F, et al. IGFBP7 plays a potential tumor suppressor role in colorectal carcinogenesis. Cancer Biol Ther *6*, 354-359 (2007).

Russell JP, Powell DJ, Cunnane M, et al. The TRK-T1 fusion protein induces neoplastic transformation of thyroid epithelium. Oncogene *19*, 5729-35 (2000).

Ryder M, Ghossein RA, Ricarte-Filho JC, et al. Increased density of tumor-associated macrophages is associated with decreased survival in advanced thyroid cancer. Endocr Relat Cancer *15*, 1069-74 (2008).

Saenko V, Rogounovitch T, Shimizu-Yoshida Y, et al. Novel tumorigenic rearrangement, Delta rfp/ret, in a papillary thyroid carcinoma from externally irradiated patient. Mutat Res *527*, 81-90 (2003).

Sage J, Mulligan GJ, Attardi LD, et al. Targeted disruption of the three Rb-related genes leads to loss G(1) control and immortalization. Genes Dev *14*, 3037-50 (2000).

Sakorafas GH, Giotakis J, and Stafyla V. Papillary thyroid microcarcinoma: a surgical perpective. Cancer Treat Rev *31*, 423-38 (2005).

Samaan NA, Schultz PN, Hickey RC, et al. The results of various modalities of treatment of well differentiated thyroid carcinomas: a retrospective review of 1599 patients. J Clin Endocrinol Metab *75*, 714-20 (1992).

Santoro M, Chiappetta G, Cerrato A, et al. Development of thyroid papillary carcinomas secondary to tissue-specific expression of the RET/PTC1 oncogene in transgenic mice. Oncogene *12*, 1821-6 (1996).

Santoro M, Melillo RM, Carlomagno F, et al. Molecular mechanisms of RET activation in human cancer. Ann NY Acad Sci *963*, 116-21 (2002).

Santoro M, Melillo RM, Carlomagno F, et al. Minireview: RET: normal and abnormal fuctions. Endocrinology *145*, 5448-51 (2004).

Santoro M, Melillo RM, and Fusco A. RET/PTC activation in papillary thyroid carcinoma: European Journal of Endocrinology Prize Lecture. Eur J Endocrinol *155*, 645-53 (2006).

Santoro M, Sabino N, Ishizaka Y, et al. Involvement of RET oncogene in human tumours: specificity of RET activation to thyroid tumours. Br J Cancer *68*, 460-4 (1993).

Sato Y, Chen Z and Miyazaki K. Strong suppression of tumor growth by insulin-like growth factor-binding protein-related protein 1/tumor-derived cell adhesion factor/mac25. Cancer Sci *98*, 1055-1063 (2007).

Scarpino S, Stoppacciaro A, Ballerini F, et al. Papillary carcinoma of the thyroid: hepatocyte growth factor (HGF) stimulates tumor cells to release chemokines active in recruiting dendritic cells. Am J Pathol *156*, 831-7 (2000).

Schimitt CA, Fridman JS, Yang M, et al. A senescence program controlled by p53 and $p6^{INK4a}$ contributes to the outcome of cancer therapy. Cell *109*, 335-46 (2002).

Schrama D, Kneitz H, Willmes C, et al. Lack of correlation between IGFBP7 expression and BRAF mutational status in melanoma. J Invest Dermatol *130*, 897 (2010).

Scurr LL, Pupo GM, Becker TM, et al. IGFBP7 is not required for B-RAF-induced melanocyte senescence. Cell *141*, 717-727 (2010).

Seluanov A, Gorbunova V, Falcovitz A, et al. Change of the death pathway in senescent human fibroblasts in response to DNA damage is caused by an inability to stabilize p53. Mol Cell Biol *21*, 1552-64 (2001).

Serrano M, Lin AW, McCurrach ME, et al. Oncogenic ras provokes premature cell senescence associated with accumulation of p53 and $p16^{INK4a}$. Cell *88*, 593-602 (1997).

Seshandri T, and Campisi J. Repression of c-fos transcription and an altered genetic program in senescent human fibroblasts. Science *247*, 205-9 (1990).

Severino J, Allen RG, Balin S, et al. Is beta-galactosidase staining a marker of senescence in vitro and in vivo? Exp Cell Res *257*, 162-71 (2000).

Shay JW, Pereira-Smith OM, and Wright WE. A role for both RB and p53 in the regulation of human cellular senescence. Exp Cell Res *196,* 33-39 (1991).

Shay JW, Wright WE, and Werbin H. Loss of telomeric DNA during aging may predispose cells to cancer. Int J Oncol *3*, 559-63 (1993).

Shelton DN, Chang E, Whittier Ps, et al. Microarray analysis of replicative senescence. Curr Biol *9*, 939-45 (1999).

Sherman SI. Thyroid carcinoma. Lancet *361*, 501-11 (2003).

Sherr CJ, and McCormick F. The RB and p53 pathways in cancer. Cancer Cell *2*, 103-12 (2002).

Sherr CJ, and Roberts JM. CDK inhibitors: positive and negative regulators of G1-phase progression. Genes Dev *13*, 1501-12 (1999).

Smogorzewska A, and de Lange T. Different telomere damage signalling pathways in human and mouse cells. EMBO J *4*, 4338-48 (2002).

Sobrinho-Simoes M. Poorly differentiated carcinomas of the thyroid. Endocr Pathol *7*, 99-102 (1996).

Sobrinho-Simoes M, Eloy C, Magalhaes J, et al. Follicular thyroid carcinoma. Mod Pathol *2*, S10-8 (2011).

Sobrinho-Simoes M, Maximo V, Castro IV, et al. Hurthle (oncocytic) cell tumors of thyroid: etiopathogenesis, diagnosis and clinical significance. Int J Surg Pathol *13*, 29-35 (2005).

Sprenger CC, Damon SE, Hwa V, et al. Insulin-like growth factor binding protein-related protein 1 (IGFBP-rP1) is a potential tumour suppressor protein for prostate cancer. Cancer Res *59*, 2370-75 (1999).

Stewart CE, and Rotwein P. Growth, differentiation, and survival: multiple physiological functions for insulin-like growth factors. Physiol Rev *76*, 1005-26 (1996).

Suarez HG, du Villard JA, Severino M, et al. Presence of mutations in all three ras genes in human thyroid tumors. Oncogene *5*, 565-70 (1990).

Sugg SL, Ezzat S, Rosen IB, et al. Distinct multiple RET/PTC gene rearrangements in multifocal papillary thyroid neoplasia. J Clin Endocrinol Metab *83*, 4116-22 (1998).

Suziki H, Igarashi S, Nojima M, et al. IGFBP7 is a p53-responsive gene specifically silenced in colorectal cancer with CpG island methylator phenotype. Carcinogenesis *31*, 342-49 (2010).

Takai H, Smogorzewska A, and de Lange T. DNA damage foci at dysfunctional telomeres. Curr Biol *13*, 1549-56 (2003).

Tallini G and Asa SL. Ret oncogene activation in papillary thyroid carcinoma. Adv Anat Pathol *8*, 345-54 (2001).

Tallini G, Santoro M, Helie M, et al. RET/PTC oncogene activation defines a subset of papillary thyroid carcinomas lacking evidence of progression to poorly differentiated or undifferentiated tumor phenotypes. Clin Cancer Res *4*, 287-94 (1998).

Tassin J, Malaise E, and Courtois Y. Human lens cells have an in vitro proliferative capacity inversely proportional to the donor age. Exp Cell Res *123*, 388-92 (1979).

Taylor RC, Cullen SP, and Martin SJ. Apoptosis: controlled demolition at the cellular level. Nat Rev Mol Cell Biol *9*, 231-41 (2008).

te Poele RH, Okorokov AL, Jardine L, et al. DNA damage is able to induce senescence in tumor cells in vitro and in vivo. Cancer Res *62*, 1876-83 (2002).

Tice RR, Schneider EL, Kram D, et al. Cytokinetic analysis of the impaired proliferative response of peripheral lymphocytes from aged humans to phytohemagglutinin. J Exp Med *149*, 1029-41 (1979).

Trougakos IP, Saridaki A, Panayotou G, et al. Identification of differentially expressed proteins in senescent human embryonic fibroblasts. Mech Ageing Dev *127*, 88-92 (2006).

Trovisco V, Soares P, Soares R, et al. A new BRAF gene mutation detected in a case of a solid variant of papillary thyroid carcinoma. Hum Pathol *36*, 694-7 (2005).

Tuveson DA, Weber BL, and Herlyn M. BRAF as a potential therapeutic target melanoma and other malignancies. Cancer Cell *4*, 95-8 (2003).

Ugolini C, Basolo F, Proietti A, et al. Lymphocyte and immature dendritic cell infiltrates in differentiated, poorly differentiated and undifferentiated thyroid carcinoma. Thyroid *17*, 389-93 (2007).

Vasko V, Espinosa AV, Scouten W, et al. Gene expression and functional evidence of epithelial-to-mesenchymal transition in papillary thyroid carcinoma invasion. Proc Natl Acad Sci USA *104*, 2803-08 (2007).

Ventura A, Kirsch DG, Mclaughlin ME, et al. Restoration of p53 function leads to tumour regression in vivo. Nature *445*, 661-65 (2007).

Verdun RE and Karlseder J. The DNA damage machinery and homologous recombination pathway act consecutively to protect human telomeres. Cell *127*, 709-20 Cell (2006).

Vitagliano D, Portella G, Troncone G, et al. Thyroid targeting of N-ras (Gln61Lys) oncogene in transgenic mice results in follicular tumors that progress to poorly differentiated carcinomas. Oncogene *25*, 5467-74 (2006).

Vizioli MG, Sensi M, Miranda C, et al. IGFBP7: an oncosuppressor gene in thyroid carcinogenesis. Oncogene *29*, 3835-44 (2010).

Vizioli MG, Possik PA, Tarantino E, et al. Evidence of Oncogene-induced senescence in thyroid carcinogenesis. Endocrine-Related Cancer *18*, 743-57 (2011).

Wajapeyee N, Serra RW, Zhu X, et al. Oncogenic BRAF induces senescence and apoptosis through pathways mediated by the secreted protein IGFBP7. Cell *132*, 363-74 (2008).

Wajapeyee N, Kapoor V, Mahalingam M, et al. Efficacy of IGFBP7 for treatment of metastatic melanoma and other cancers in mouse models and human cell lines. Mol Cancer Ther *8*, 3009-14 (2009).

Watson JD. Origin of concatemeric T7 DNA. Nat New Biol *239*, 197-01 (1972).

Weeraratna AT, Darymple SL, Lamb JC, et al. Pan-trk inhibition decreases metastasis and enhances host survival in experimental models as a result of its selective induction of apoptosis of prostate cancer cells. Clin Cancer Res *7*, 2237-45 (2001).

Weinberg RA. The molecular basis of oncogenes and tumor suppressor genes. Ann NY Acad Sci *758*, 331-8 (1995).

Williams D. Cancer after nuclear fallout: lessons from the Chernobyl accident. Nat Rev Cancer *2*, 543-9 (2002).

Wilton SD, Eyre H, Akkari PA, et al. Assignment of the human a-tropomyosin gene TPM3 to 1q22-->q23 by fluorescence in situ hybridisation. Cytogenet Cell Genet *68*, 122-4 (1995).

Wilson HM, Birnbaum RS, Poot M, et al. Insulin-like growth factor binding protein-related protein 1 inhibits proliferation of MCF-7 breast cancer cells via senescence-like mechanism. Cell Growth Differ *13*, 205-213 (2002).

Wu CH, van Riggelen J, Yetil A, et al. Cellular senescence is an important mechanism of tumor regression upon c-Myc inactivation. Proc Natl Acad Sci *104*, 13028-33 (2007).

Xing M. BRAF mutation in papillary thyroid cancer: pathogenic role, molecular bases, and clinical implications. Endocr Rev *28*, 742-62 (2007).

Xing M. Gene methylation in thyroid carcinogenesis. Endocrinology *148*, 948-53 (2007).

Xue W, Zender L, Miething C, et al. Senescence and tumour clearance is triggered by p53 restoration in murine liver carcinomas. Nature 445, 656-60 (2007).

Yamanaka Y, Wilson EM, Rosenfeld RG, et al. Inhibition of insulin receptor by insulin-like growth factor binding proteins. J Biol Chem *49*, 30729-34 (1997).

Yang TT, Namba N, Hara T, et al. p53 induced by ionizing radiation mediates DNA end-jointing activity, but not apoptosis of thyroid cells. Oncogene *14*, 1511-1519 (1997).

Zapf J. Physiological role of the insulin-like growth factor binding proteins. Eur J Endocrinol *132*, 645-54 (1995).

Zhang R, Poustovoitov MV, Ye X, et al. Formation of MacroH2A-containing senescence associated heterochromatin foci and senescence driven by ASF1a and HIRA. Dev Cell *8*, 19-30 (2005).

Zhang BH and Guan KL. Activation of B-Raf kinase requires phosphorylation of the conserved residues Thr598 and Ser601. EMBO J *19*, 5429-39 (2000).

Zeki K, Nakano Y, Inokuchi N, et al. Autocrine stimulation of interleukin-1 in the growth of human thyroid carcinoma cell line NIM1. J Clin Endocrinol Metab *76*, 127-33 (1993).

Publications

Parts of the work presented here have been published as fallow:

Vizioli MG, Possik PA, Tarantino E, et al. Evidence of Oncogene-induced senescence in thyroid carcinogenesis. Endocrine-Related Cancer *18*, 743-57 (2011).

Vizioli MG, Sensi M, Miranda C, et al. IGFBP7: an oncosuppressor gene in thyroid carcinogenesis. Oncogene *29*, 3835-44 (2010).

Others publications:

Anania MC, Sensi M, Radaelli E, Miranda C, **Vizioli MG**, et al. TIMP3 regulates migration, invasion and in vivo tumorigenicity of thyroid tumor cells. Oncogene *30*, 3011-23 (2011).

Miranda C, Fumagalli T, Anania MC, **Vizioli MG**, et al. Role of STAT3 in In Vitro Transformation Triggered by TRK Oncogenes. PLoS ONE *5*, e9446 (2010).

Collaborators contribution

Chapter 2

Maria Luisa Sensi (*Human Tumours Immunobiology Unit, Department of Experimental Oncology and Molecular Medicine, IRCCS Foundation-Istituto Nazionale dei Tumori, Milan, Italy*) performed statistical analysis of the array data;
Loredana Cleris (*Chemoprevention Unit, Department of Experimental Oncology and Molecular Medicine, IRCCS Foundation-Istituto Nazionale dei Tumori, Milan, Italy*) carried out the *in vivo* experiments.

Chapter 3

Patricia A Possik (*Division of Molecular Genetics, The Netherlands Cancer Institute, Amsterdam, The Netherland*) contributed to design and carry out $BRAF^{V600E}$ experiments;
Eva Tarantino (*Department of Pathology IRCCS Foundation-Istituto Nazionale dei Tumori, Milan, Italy*) carried out immunohistochemical (IHC) experiments;
Silvana Pilotti (*Department of Pathology IRCCS Foundation-Istituto Nazionale dei Tumori, Milan, Italy*) contributed to select the thyroid tumour samples and to analyze IHC data.

Acknowledgements

At the end of my PhD program, I would like to say thank you to all those who have contributed to this project .

First of all, I would like to thank my director of studies Dr. Angela Greco, for giving me the opportunity to work on this exciting project and for guiding me through the ups and downs. I hope you are proud of me.

I would also like to thank Dr. Jesus Gil and Prof. Daniel Peeper for giving me the opportunity to work in their lab over my last two years of the PhD. I have really enjoyed the time I spent at the MRC-CSC in London and at the NKI in Amsterdam, interacting within exciting scientific environments, learning new techniques and getting to know such lovely people.

Thank you Patricia for your collaboration in this project, it was a great pleasure working with you in Amsterdam. I thoroughly enjoyed designing experiments and trying out new ideas with you. Thank you for all your help, patience, cheerfulness and friendship. Saudade!

Thank you Joaninha, all Cell Proliferation group and the guys of the "csckids group" who spiced up my year in London. Thanks for all the good times in and out of the lab.

I would also like to thank my colleagues from Molecular Mechanisms Lab, Pathology Department and Animal facility. I am grateful for receiving your support.

I would also like to thank all my friends in Milan and Modena who supported me outside working hours and helped me recharge my batteries. A special thanks to Alastair (Piggy), Aurora, Luisa, Lisa, Andrea, Maria Chiara, Nunzia, Daniele, Chiara, Katia, Luca. Thank you for helping me unwind, for all the laughs, advice, talks and lovely dinner parties. Your company couldn't have been better !

Finally, I would like to say a special thank you to my family, my mum, my dad and my brother Nicola as well for supporting and encouraging me every day with their love and trust. Thank you for being there for me, always !!